การหาปริมาณรังสีในผู้ป่วยจากการตรวจเพทซีทีด้วยฟลูออรีน-18 ฟลูออโรดิออกซีกลูโคส

นายกิติวัฒน์ คำวัน

วิทยานิพนธ์นี้เป็นส่วนหนึ่งของการศึกษาตามหลักสูตรปริญญาวิทยาศาสตรมหาบัณฑิต
สาขาวิชาฉายาเวชศาสตร์ ภาควิชารังสีวิทยา
คณะแพทยศาสตร์ จุฬาลงกรณ์มหาวิทยาลัย
ปีการศึกษา 2550

THE DETERMINATION OF PATIENT DOSE FROM ^{18}F-FDG PET/CT EXAMINATIONS

Mr.Kitiwat Khamwan

A Thesis Submitted in Partial Fulfillment of the Requirements
for the Degree of Master of Science Program in Medical Imaging
Department of Radiology
Faculty of Medicine
Chulalongkorn University
Academic Year 2007

Thesis Title	THE DETERMINATION OF PATIENT DOSE FROM ^{18}F-FDG PET/CT EXAMINATIONS
By	Mr.Kitiwat Khamwan
Field of Study	Medical Imaging
Thesis Advisor	Associate Professor Anchali Krisanachinda, Ph.D.

Accepted by the Faculty of Medicine, Chulalongkorn University in Partial Fulfillment of the Requirements for the Master's Degree

.....Dean of the Faculty of Medicine
(Associate Professor Adisorn Patradul, M.D.)

THESIS COMMITTEE

.....Chairman
(Associate Professor Tawatchai Chaiwatanarat, M.D.)

.....Thesis Advisor
(Associate Professor Anchali Krisanachinda, Ph.D.)

.....External Member
(Professor Franco Milano, Ph.D.)

.....Member
(Associate Professor Supatporn Tepmongkol, M.D.)

.....Member
(Associate Professor Somrat Lertmaharit, M.Sc., M.Med.Stat)

กิติวัฒน์ คำวัน : การหาปริมาณรังสีในผู้ป่วยจากการตรวจเพทซีทีด้วยฟลูออรีน-18 ฟลูออโรดิออกซีกลูโคส. (THE DETERMINATION OF PATIENT DOSE FROM ^{18}F-FDG PET/CT EXAMINATIONS)
อ.ที่ปรึกษา: รศ.ดร.อัญชลี กฤษณจินดา, 93 หน้า

ในปัจจุบันการตรวจวินิจฉัยโรคด้วยเพทซีที ได้เข้ามามีบทบาทสูงทางการแพทย์ แต่อย่างไรก็ตามผู้ป่วยที่เข้ารับการตรวจดังกล่าวอาจได้รับปริมาณรังสีมากกว่าการตรวจด้วยเอกซเรย์คอมพิวเตอร์หรือเพทสแกนเพียงอย่างใดอย่างหนึ่ง วัตถุประสงค์ของการศึกษาวิจัยนี้เพื่อหาปริมาณรังสีเฉลี่ยและปัจจัยที่มีผลต่อปริมาณรังสีที่ผู้ป่วยได้รับจากการตรวจเพทซีที ด้วยการฉีดสารฟลูออรีน-18 ฟลูออโรดิออกซีกลูโคส โดยได้ทำการศึกษาในผู้ป่วยที่สงสัยว่ามีการแพร่กระจายของมะเร็งที่เข้าทำการตรวจเพทซีที ณ โรงพยาบาลจุฬาลงกรณ์ จำนวน 35 ราย ซึ่งในส่วนของปริมาณรังสีที่ผู้ป่วยได้รับจากการฉีดสารเภสัชรังสีนั้น อวัยวะที่ทำการศึกษา ได้แก่ ตับ ไต กระเพาะอาหาร กระเพาะปัสสาวะ ลำไส้ใหญ่ ต่อมไทรอยด์ อวัยวะสืบพันธุ์ ปอด ผิวหนัง ไขกระดูก ผิวกระดูก เต้านม และม้าม โดยใช้วิธีคำนวณตามหลักวิธีการ MIRD (Medical Internal Radiation Dosimetry) และใช้โปรแกรมมอนติคาร์โล ซิมูเลชั่น วินโดส เวอร์ชั่น 2.1 a ทำการคำนวณหาค่าปริมาณรังสียังผลที่ผู้ป่วยได้รับจากเอกซเรย์คอมพิวเตอร์

จากผลการศึกษาพบว่า กระเพาะปัสสาวะเป็นอวัยวะที่ได้รับรังสีดูดกลืนสูงสุด จากการฉีดสารฟลูออรีน-18 ฟลูออโรดิออกซีกลูโคส โดยมีค่าเฉลี่ยเท่ากับ 63.72±9.41 ไมโครเกรย์ต่อเมกะเบเคอเรล (95 % CI: 60.49-66.95) และที่อวัยวะสืบพันธุ์ ปริมาณรังสีดูดกลืนเฉลี่ยที่ได้รับเท่ากับ 11.46±3.78 ไมโครเกรย์ต่อเมกะเบเคอเรล ค่าเฉลี่ยของ dose coefficient เท่ากับ 15.56±1.52 ไมโครซีเวิร์ตต่อเมกะเบเคอเรล ความแรงของสารรังสีของฟลูออรีน-18 ฟลูออโรดิออกซีกลูโคสที่ฉีดให้ผู้ป่วย มีค่าเฉลี่ยเท่ากับ 312 เมกะเบเคอเรล และปริมาณรังสียังผลที่ผู้ป่วยได้รับทั่วทั้งร่างกายจากเพทสแกนมีค่าเฉลี่ยเท่ากับ 4.82±0.5 มิลลิซีเวิร์ต โดยมีค่าอยู่ในช่วงระหว่าง 3.81 ถึง 5.81 มิลลิซีเวิร์ต ในส่วนของปริมาณรังสียังผลที่ผู้ป่วยได้รับจากเอกซเรย์คอมพิวเตอร์ มีค่าเฉลี่ยเท่ากับ 14.45±2.82 มิลลิซีเวิร์ต โดยมีค่าอยู่ในช่วงระหว่าง 10.04 ถึง 21.98 มิลลิซีเวิร์ต เมื่อทำการรวมปริมาณรังสียังผลจากทั้งเพทสแกนและเอกซเรย์คอมพิวเตอร์แล้ว ค่าปริมาณรังสียังผลที่ผู้ป่วยได้รับมีค่าเฉลี่ยเท่ากับ 19.27±2.93 มิลลิซีเวิร์ต โดยมีค่าอยู่ในช่วงระหว่าง 14.27 ถึง 26.95 มิลลิซีเวิร์ต และจากการศึกษาความสัมพันธ์ระหว่างปริมาณรังสีที่ผู้ป่วยได้รับกับปัจจัยต่างๆ พบว่า ปัจจัยที่มีความสัมพันธ์ต่อปริมาณรังสีประกอบด้วย ความแรงของสารรังสี น้ำหนักของอวัยวะ ดัชนีมวลกายของผู้ป่วย ค่าเอ็มเอเอส และความยาวของการสแกน โดยความแรงของรังสีมีความสัมพันธ์สูงกับปริมาณรังสีที่ผู้ป่วยได้รับจากการตรวจเพทสแกน ที่ค่า r เท่ากับ 0.720 (p-value < 0.01) ในส่วนค่าเอ็มเอเอสและดัชนีมวลกายของผู้ป่วยมีความสัมพันธ์สูงกับปริมาณรังสีที่ผู้ป่วยได้รับจากการตรวจเอกซเรย์คอมพิวเตอร์ ที่ค่า r เท่ากับ 0.980 และ 0.866 (p-value < 0.01) ตามลำดับ ประโยชน์จากการศึกษาวิจัยนี้เป็นการรายงานถึงข้อมูลขั้นพื้นฐานของปริมาณรังสีเฉลี่ยที่ผู้ป่วยได้รับจากการตรวจเพทซีทีในประเทศไทย เพื่อเป็นข้อมูลอ้างอิงและประโยชน์ต่อผู้ที่เข้ารับการตรวจในอนาคตข้างหน้า

ภาควิชา รังสีวิทยา ลายมือชื่อนิสิต .....
สาขาวิชา ฟิสิกส์การแพทย์ ลายมือชื่ออาจารย์ที่ปรึกษา .....
ปีการศึกษา 2550

4974706630: MAJOR MEDICAL IMAGING

KEYWORDS: ^{18}F-FDG / MIRD/ PATIENT DOSE / PET/CT

KITIWAT KHAMWAN: THE DETERMINATION OF PATIENT DOSE FROM ^{18}F-FDG PET/CT EXAMINATIONS. THESIS ADVISOR: ASSOC. PROF. ANCHALI KRISANACHINDA, PH.D., 93 pp.

The development of PET/CT scan has received great attention in the medical diagnostic study. However, whole-body PET/CT examinations increase patient exposure compared to an individual CT or PET examination. The purpose of this study is to investigate the patient doses and factors affecting from the administration of fluorine-18-fluorodeoxyglucose (^{18}F-FDG) and the CT scan. Thirty-five patients with aged ranged from 28 years to 60 years (mean ± SD, 44±10), underwent whole-body PET/CT examinations at King Chulalongkorn Memorial Hospital, with suspected of cancer spreading to other organs. Internal dose at the target organs included liver, kidneys, stomach, urinary bladder, colon, thyroid gland, gonads, lungs, skin, bone marrow, bone surface, breast and spleen, were calculated using the MIRD (Medical Internal Radiation Dosimetry) method. The effective dose from CT scan was calculated using Monte Carlo simulation, WinDose program version 2.1a.

The results show the organ receiving the highest absorbed doses was the urinary bladder of 63.72±9.41 μGy/MBq (95 % CI: 60.49-66.95). The critical organ such as gonads received average absorbed dose of 11.46±3.78 μGy/MBq. Average dose coefficient from administration of ^{18}F-FDG of 15.56±1.52 μSv/MBq. Average ^{18}F-FDG activities of 312 MBq was administered, resulted the average whole-body effective doses from PET scan of 4.82±0.5 mSv, ranged from 3.81 and 5.81 mSv. The average whole-body effective dose from the CT scan was 14.45±2.82 mSv, ranged from 10.04 and 21.98 mSv. The average effective dose for patients undergoing whole-body ^{18}F-FDG PET/CT examinations was 19.27±2.92 mSv, ranged from 14.27 and 26.95 mSv. Factors influenced the patient dose in this study were the activity of ^{18}F-FDG, the mass of organs, patient BMI, mAs and scan length. The patient dose is mostly dependent on the activity of ^{18}F-FDG with the correlation, r = 0.720 (*p-value* < 0.01) from PET scan, and dependent on mAs and patient BMI with the correlation 0.980 and 0.866 (*p-value* < 0.01), respectively, for CT scan. The benefits of this study are the records of patient dose and related information for ^{18}F-FDG PET/CT in Thai patient in the future.

Department Radiology Student's signature Kitiwat K.
Field of study Medical Imaging Advisor's signature Anchali Kris
Academic year 2007

ACKNOWLEDGEMENTS

The success of this thesis depends on the contributions of many people. In particular, I wish to express gratitude and deepest appreciation to Associate Professor Dr.Anchali Krisanachinda, Department of Radiology, Faculty of Medicine, Chulalongkorn University, my major advisor, for her supervision, guidance, encouragement and invaluable advice during the whole study. I wish to express gratitude and appreciation to Mr.Panya Pasawang, Section of Nuclear Medicine, King Chulalongkorn Memorial Hospital, Thai Red Cross Society, my co-advisor for his help in the experiment, assistance and suggestion for this work. I would like to greatly thank Radiological Technologist, Nuclear Medicine Clinician and staffs at PET/CT centre, Section of Nuclear Medicine, King Chulalongkorn Memorial Hospital, Thai Red Cross Society, especially, Mr.Tanawat Suntrapornpol, Mr.Chatchai Nawigachevin, Associate Professor Tawatchai Chaiwatanarat, M.D. and Associate Professor Supatporn Tepmongkol, M.D. for their helps and suggestions in this research. I would like to deeply thank Associate Professor Sivalee Suriyapee, Head of Physicist at Division of Radiation Oncology, Department of Radiology, Faculty of Medicine, Chulalongkorn University and Professor Franco Milano, University of Florence, Italy, for their comments and suggestions in this work. I would like to thank Associate Professor Somrat Lertmaharit, Department of Preventive and Social Medicine, Faculty of Medicine, Chulalongkorn University for her advice and comment with statistical and analysis in this research. I also thank Professor Kwan-Hoong Ng, Department of Biomedical Imaging, University of Malaya, Malaysia, Assistance Professor Dr.Napapong Pongnapong and Miss Woranut Iampa, Department of Radiological Technology, Faculty of Medical Technology, Mahidol University for WinDose, Monte Carlo simulation program. And I also thank for all teachers, lecturers and staffs in the Master of Science Program in Medical Imaging, Faculty of Medicine, Chulalongkorn University, for their unlimited teaching throughout whole study in Medical Imaging.

Finally, I also express my gratefulness to every member in my family for their financial supports, valuable encouragement, entire care during the course study.

CONTENTS

Page

Page

Page

Page

Page

LIST OF TABLES

Table **Page**

LIST OF FIGURES

Figure **Page**

LIST OF ABBREVIATIONS

Abbreviation	Terms
≈	Approximate
%	Percent
2D	Two dimension
3D	Three dimension
AEC	Automatic exposure control
BGO	Bismuth germanium oxide
BMI	Body mass index
^{11}C	Carbon-11
Ci	Curies
cm^3	Cubic centimeter
cps	Count per second
CT	Computed Tomography
CTDI	Computed Tomography Dose Index
D	Absorbed dose
ED	Effective dose
EDE	Effective dose equivalent
e.g.	For example
^{18}F	Fluorine-18
FDG	Fluorodeoxyglucose
FOV	Field of view
FWHM	Full width at half-maximum
FWTM	Full width at tenth maximum
g	Gram

Abbreviation	Terms
^{68}Ga	Gallium-68
^{68}Ge	Germanium-68
Gy	Gray
GSO	Gadolinium oxyorthosilicate
hr	Hour
HU	Hounsfield units
ICRP	International Commission on Radiological Protection
IEC	International Electric Commission
J	Joules
keV	Kiloelectronvoltage
kg	Kilogram
kVp	Kilovoltage peak
LOR	Line of response
LSO	Lutetium oxyorthosilicate
mA	Milliampere
MBq	Megabecquerel
MeV	Megaelectronvolt
MIRD	Medical Internal Radiation Dosimetry
m	Mass of target organ
mL	Milliliter
mm	Millimeter
NaI(Tl)	Sodium iodide thallium activated
NECR	Noise-equivalent count-rate
NEMA	National Electrical Manufacturers Association

Abbreviation	**Terms**
ns	Nanosecond
^{18}O	Oxygen-18
PC	Personal computer
PET	Positron Emission Tomography
PMTs	Photomultiplier tubes
QF	Quality factor
R	Random counting rate
^{82}Rb	Rubidium-82
r_h	Source region
r_k	Target region
S	Scatter counting rate
SPECT	Single Photon Emission Computed Tomography
SUVs	Standardized uptake values
Sv	Sievert
T	Trues counting rate
Tl	Thallium
μ	Micron
W_T	Tissue weighting factor
Z	Atomic number

CHAPTER 1

INTRODUCTION

1.1 Background and rationale

As the anatomic localization of functional abnormalities seen on PET scan is limited by the spatial resolution, whereas, the CT image lacks of functional information and diagnostic accuracy in assessing tumor stages. This situation is changed dramatically by combining two established modalities between PET and CT to the first PET/CT scanner in 1998 [1], to address these problems. These modalities provide a medical imaging with the capability to acquire accurately aligned anatomy and functional images of a patient within single examination. While CT scan provides anatomical detail, such as size, location of the tumor and mass, PET scan provides metabolic detail, cellular activity of the tumor and mass. Combined PET/CT is more accurate than PET and CT alone. The availability of this technology has realized of combined imaging to appropriate with separate devices, such as the use of CT for attenuation correction of PET images, the convenience for both physician and patient of a single scan for both modalities, and increased confidence in study interpretation that originates from having coregistered anatomy and function available immediately after scan.

The most commonly used positron-emitting radiopharmaceutical in clinical imaging for PET is the glucose analog Fluorine-18 –2-fluoro-2-deoxy-D-glucose (^{18}F-FDG). Many tumor cells use large amounts of glucose as an energy source and possess increased expression of glucose transporters and increased hexokinase activity. Glucose transporters transfer glucose and fluorodeoxyglucose into the cell, where they are phosphorylated by hexokinase. ^{18}F-FDG is essentially trapped within the cell in proportion to the rate of glucose metabolism. This allows sufficient time to imaging its distribution in normal and abnormal bodily tissues. ^{18}F-FDG is formed through radiochemical synthesis from cyclotron-produced ^{18}F. ^{18}F decays to stable ^{18}O by positron emission with a half-life of approximately110 minutes [2].

Since the introduction of the first PET/CT prototype was over 9 years ago, several thousand cancer patients had been scanned on combined PET/CT scans. Whole-body PET/CT examinations may be incurred an increased patient exposure compared with an individual CT or PET examination, internal exposure from positron emitter radiopharmaceuticals and external exposure from CT [3]. Therefore, patient referral for PET/CT studies must be justified in each case to avoid repeated exposure or overexposure of radiation to patients. Besides justification, optimization is the second general principle in radiological protection.

The first PET/CT system, LSO PET/CT HI-REZ, CTI/Siemens Medical System had been installed in August 2006, at Department of Radiology, King Chulalongkorn Memorial Hospital, Thai Red Cross Society. Cancer patients of over 200 cases referred to PET/CT examination for whole-body scan, was administered with ^{18}F-FDG. Thus, the average patient dose in PET and CT procedures, correlated factors of radiopharmaceutical activity, mass of organs, scan length and patient body mass index are being investigated.

1.2 Research objectives

1. To evaluate patient dose from ^{18}F-FDG PET/CT examinations at King Chulalongkorn Memorial Hospital.

2. To study the correlated factors affecting the patient dose from ^{18}F-FDG PET/CT examinations.

1.3 Definitions [4]

Algorithm
Image reconstruction from the measured raw data.

Annihilation
Spontaneous conversion of a particle and its anti-particle into radiation. e.g. positron and electron into two gamma-ray photons of energy 511 keV.

Becquerel
Measure unit of radioactivity, corresponding to one disintegration per second.

Computed Tomography
A technique for constructing images of the structures at a particular depth within the body - done by taking several x-ray images at different angles and then using a computer to reconstruct and analyze the resulting images.

Cyclotron
Device in which positively charged particles are accelerate in a spiral path in a vacuum between poles of a magnet, energy being provided by a high frequency voltage across the vacuum.

Dose, Absorbed dose
The amount of energy deposited in any substance by ionizing radiation per unit mass of the substance. It is expressed numerically in rads (traditional units) or Grays (SI units).

Effective half-life
The time required for the amount of a radionuclide deposited in a living organism to be diminished 50 percent as a result of the combined action of radioactive decay and biological elimination.

External dose
Radiation exposure from a source outside the body.

Fluorodeoxyglucose

A glucose analog used for differentiating malignant neoplasm from benign lesions, staging malignant neoplasm, differentiating severely hypoperfused.

Gray

The international system (SI) unit of radiation dose expressed in terms of absorbed energy per unit mass of tissue. The gray is the unit of absorbed dose and has replaced the rad. 1 Gray = 1 Joule/kilogram and also equals 100 rad.

Internal dose

Radiation exposure from a source inside the body.

Positron

A positively charged particle having the same mass and magnitude of charge as the electron and constituting the antiparticle of the electron.

Positron Emission Tomography

A modality generates images depicting the distributions of positron-emitting nuclides in patients.

rad

The original unit developed for expressing absorbed dose, which is the amount of energy from any type of ionizing radiation, such as alpha, beta, gamma, neutrons, etc, deposited in any medium. A dose of one rad is equivalent to the absorption of 100 ergs per gram of absorbing tissue. The rad has been replaced by the Gray in the SI system of units (1 Gray = 100 rad).

Reference man

A person assumed to have the anatomical and physiological characteristics of an average individual. These assumed characteristics are used in calculations assessing internal dose, also may be called "Standard Man".

Sievert

The international system (SI) unit for dose equivalent equal to 1 Joule/kilogram. The sievert has replaced the rem. 1 sievert is equivalent to 100 rem.

Tissue weighting factor

A multiplier that is used for converting the equivalent dose to a specific organ or tissue into what is called the “effective dose”. The goal of this process was to develop a method for expressing the dose to a portion of the body in terms of an equivalent dose to the whole body that would carry with it an equivalent risk in terms of the associated fatal cancer probability. It applies only to the stochastic effects of radiation.

CHAPTER 2

REVIEW OF RELATED LITERATURES

2.1 Theory

Over the past 25 years, PET (Positron Emission Tomography) imaging has developed from the research techniques to the mainstream clinical imaging tool. Through positron-emitting radionuclide labeling, PET allows the in-vivo imaging of physiologically and pathologically important molecules containing basic organic chemical elements such as carbon, hydrogen, and oxygen. Such data provide molecular and/or metabolic information essential to the diagnosis and evaluation of disease and thus to the effective management of patient care.

2.1.1 Basic positron physics [5]

Positron-emitting radionuclides are most commonly produced by cyclotrons by bombarding a stable element with protons, or deuterons. The produced radionuclides have an excess of protons and decay by the emission of positrons.

When a positron is emitting, it travels for a short distance from its site of origin, gradually losing energy to the tissue through which it moves. When most of its kinetic energy has been lost, the positron reacts with a resident electron in an annihilation reaction. This reaction generates two 511-keV gamma photons, which are emitted in opposite directions at about 180 degrees from each other. In a PET scanner, these photons interact with the detector ring at opposite site, which defines a line along which the annihilation reaction occurred and permits localization of the reaction. By using many such events, an imaging can be reconstructed.

It is noted that the site of origin of the positron and the site of the annihilation reaction occur at slightly different locations. Furthermore, the positrons are not all emitted with the same energy, therefore, the distance the positron travels before annihilation varies for each specific radionuclide. For example the positrons from fluorine-18 (^{18}F) energy 640 keV and carbon-11 (^{11}C) energy 960 keV have a range in water of about 1 to 1.5 mm and 2.5 mm in tissue, whereas rubidium 82 (^{82}Rb) energy 3.15 MeV has a range of about 10 mm in water and 16 mm in tissue before annihilation. The positron travels a distance before annihilation causes some uncertainty in determining the original location of the positron (range related uncertainty). Further, the two resultant annihilation photons may actually be emitted up to +/- 0.25 degrees from the theoretical 180 degrees. This variation in emission angle (noncolinearity) also generates some uncertainty in the original location of the annihilation reaction. Both of these issues contribute to fundamental degradation of spatial resolution in any PET detector system as shown in figure 2.1.

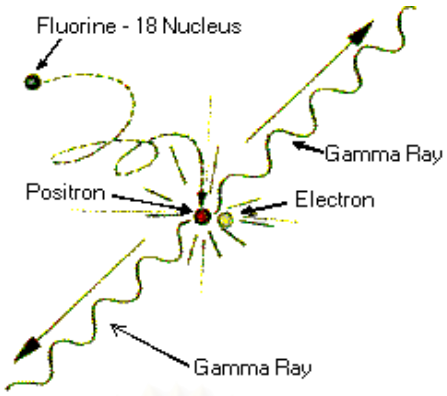

Figure 2.1 Positron emission and annihilation

2.1.2 PET instrumentation

2.1.2.1 Overview of PET scan [5]

The PET scan contains multiple rings of detectors of scintillation crystals coupled with photomultiplier tubes (PMTs). The advantage is that two photons detected in close temporal proximity by two opposed detectors in the ring are likely to be from a single annihilation event. Such a simultaneous detection event is called a *coincidence.* The simultaneous detection of two photons provides localizing information in that the annihilation event can be assumed to have occurred somewhere on a line between the two detectors, the line of response, or LOR. Many coincidence events recorded by the PET scanner constitute a raw data set representing projections of the distribution of the positron radiopharmaceutical in the body. These data are then reconstructed by using a filtered back projection algorithm or an iterative algorithm to produce cross-sectional images.

As photons travel at the speed of light, PET cameras require very fast electronics to determine if two detected photons were likely produced by a single annihilation event. In a PET scanner, each annihilation photon reaching a detector generates a single electronic pulse in the detector. For this photon to be accepted and used in the PET image, it must be in a specific energy range, ideally approaching 511 keV, and be paired with another photon reaching another detector simultaneously. Coincidence circuitry connecting the many detectors in the ring determines whether two such single pulses fall within a short *coincidence time window,* typically 6 to 12 nanoseconds. If so, they are deemed to constitute a coincidence event and are recorded in the resultant image. The actual coincidence time is typically about 1 nanosecond. However, the time window for coincidence detection varies with different camera systems and depends in large part on the speed of the electronic circuitry and detector crystal type. It is about 12 nanoseconds for bismuth germanium oxide (BGO), 8 nanoseconds for gadolinium oxyorthosilicate (GSO) and sodium iodide (NaI), and 6 nanoseconds for lutetium oxyorthosilicate (LSO) detectors. Because the energy resolution of the various crystal detectors is not precise, photons within a broad energy range, 250 to 600 keV, are counted as valid annihilation photons.

2.1.2.2 Types of coincidence events [6]

Events detected by PET scanners include true, scattered, and random coincidence as shown in figure 2.2, providing both annihilation photons are actually detected and fall within the coincidence window. True coincidences are those that result when both 511-keV photons from an annihilation reaction are detected within the coincidence time window, neither photon having undergone any form of interaction before reaching the detector. These true coincidence events provide the desired information for constructing accurate images of the distribution of a PET radiopharmaceutical in clinical imaging.

A scattered coincidence is one in which at least one of the detected photons has undergone at least one Compton scattering event prior to detection. Since the direction of the photon is changed during the Compton scattering process, it is likely that the resulting coincidence event will be assigned to the wrong LOR. Scattered coincidences add a background to the true coincidence distribution, which changes slowly with position, decreasing contrast and causing the isotope concentrations to be overestimated. They also add statistical noise to the signal. The number of scattered events detected depends on the volume and attenuation characteristics of the object being imaged, and on the geometry of the camera.

Random coincidences occur when two photons not arising from the same annihilation event are incident on the detectors within the coincidence time window of the system. The number of random coincidences in a given LOR is closely linked to the rate of single events measured by the detectors joined by that LOR and the rate of random coincidences increase roughly with the square of the activity in the FOV. As with scattered events, the number of random coincidences detected also depends on the volume and attenuation characteristics of the object being imaged, and on the geometry of the camera. The distribution of random coincidences is fairly uniform across the FOV, and will cause isotope concentrations to be overestimated if not corrected for. Random coincidences also add statistical noise to the data.

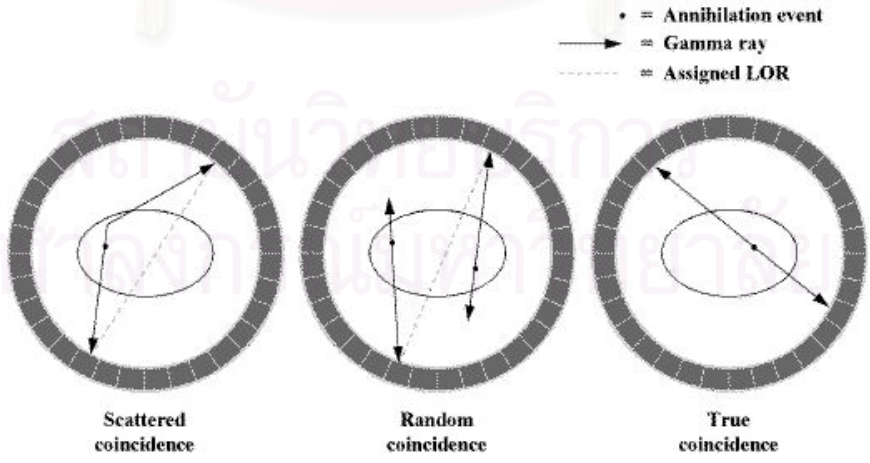

Figure 2.2 Types of coincidences in PET images

There are a number of methods available to reduce the image degrading of scattered coincidences. Most scattered photons are not detected because they are absorbed in tissue of the body, are scattered away from the detector rings, or have lost significant energy during Compton scattering. These lower-energy scattered events can be rejected by using an energy window designed to exclude photons of certain energies. The success of such rejection depends on the energy resolution characteristics of the detectors being used. Because crystal detectors have only a finite energy resolution, if one were to measure only photons approaching 511 keV and exclude scattered photons of slightly different energies, a large number of true events would also be excluded, there by either reducing image statistics or increasing image acquisition times unacceptably. Therefore, a rather broad energy window is used that allows some scattered events to be recorded as true events.

2.1.2.3 PET scintillation detectors

All PET detector systems use the principle of scintillation whereby the photon interacting with a crystal produces a flash of light, which is then detected and localized by photomultiplier tubes (PMTs) coupled to the scintillation crystal. The ideal PET crystal detector would have

1. High stopping power for 511-keV photons providing high efficiency and optimum spatial resolution
2. Fast, intense light output with rapid decay of the light for decreased system dead time
3. Good energy resolution for accurate scatter rejection.

Stopping power is best for crystalline materials with high density and high effective atomic number (Z). There are several types of crystalline detector materials used for PET imaging. These include sodium iodide (NaI), bismuth germanium oxide (BGO), gadolinium oxyorthosilicate (GSO) and lutetium oxyorthosilicate (LSO). Some characteristics of these are shown in table 2.1 and table 2.2.

From these tables it is evidence that BGO has the poorest energy resolution, whereas NaI has the best energy resolution as a result of the highest light output. The energy resolution of BGO crystals requires that a wide energy window, 250 to 600 keV, be used to avoid rejecting true events and reducing the detected count rate. The use of a wide energy window means that a BGO detector system will accept more scattered events than will the other systems with better energy resolution. NaI(Tl) systems use a narrower energy window than do BGO, LSO or GSO systems.

Table 2.1 Physical properties of various types of PET scintillation detectors [5]

Crystal	Ralative light output* (%)	Decay time (ns)	Density (g-cm-3)	Effective atomic number	Energy resolution at 511 keV
NaI(Tl)	100	230	3.7	51	8
BGO	15	300	7.1	75	12
LSO	75	40	7.4	65	10
GSO	25	60	6.7	59	9

* Light output depends on cerium concentration and read-out device (PMT or APD)
All crystal emits light with wavelengths ranging from 410 to 480 nm

Table 2.2 Relative properties of various crystalline detector materials [5]

Crystal	Stopping power (511-keV photons)	Light yield	Decay time	Energy resolution
NaI(Tl)	low	high	long	high
BGO	high	low	long	low
LSO	intermediate	intermediate	short	intermediate
GSO	intermediate	low	short	intermediate

The light signal produced by scintillation detectors is not discrete in time but occurs over a short time interval, scintillation decay time about 10 to 300 nanoseconds, which includes the period over which the light fades to background. Along with the speed of processing electronics, this decay time is an important determinant of system dead time. Dead time is the brief period during with a crystal-PMT detector is busy producing and recording a scintillation event and having the scintillation light decay so that the next distinct scintillation can be recognized and recorded. During this time additional arriving events cannot be processed and are lost. This limits the rate at which events may be detected. High count rate capability of PET instruments is particularly important in three-dimensional acquisitions and in setting requiring high activities of very short-lived radionuclide, such as oxygen 15. Currently count rate capabilities are about 500,000 counts/second.

The relatively long decay times of both BGO and NaI(Tl) crystals limit count rate capability. The shorter decay time of light output for LSO crystals can reduce scan time for comparable images to about half of the time required for BGO systems. LSO crystal probably has the best combination of properties for optimizing PET imaging, especially in three-dimensional imaging systems, without septa, with the potential for very high count rates.

2.1.2.4 PET detector geometry [5]

The PET scanners are multidetector full ring, circular or polygonal, systems that axially surround the patient. These cameras have multiple adjacent detector rings that significantly increase the axial FOV of the patient. A larger FOV allows more counts to be detected for a standardized administered radiopharmaceutical dose and a fixed scan time by allowing more time at each table position.

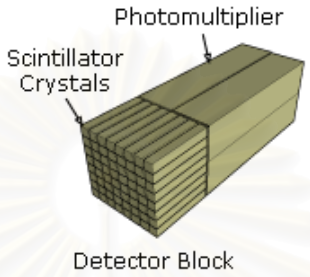

Figure 2.3 PET scintillation block detector

Table 2.3 Properties of a typical PET camera

Characteristic	PET scanner
Radionuclides imaged	PET only
Detector array	Ring (usually 18-32)
Detector (crystal material)	Sodium iodide (NaI) curved Bismuth germinate (BGO) Lutetium oxyorthosilicate (LSO) Gadolinium oxyorthosilicate (GSO)
Crystal number and size	Block detectors contain 10,000-20,000 small crystals (4 x 4 x 30 mm) with 36-46 crystals per block
Counting rate	High
Algorithm for location	Specific detector
Acquisition	2 or 3 dimensional
Spatial resolution	High (5-6 mm)
Coincidence window	6-12 nanoseconds
Energy window	350-650 keV
System sensitivity (cps/Bq/mL)	25-35%
Axial resolution FWHM (mm) at 10 mm	5.5-7

FWHM = full width at half-maximum

The most common detector arrangement used in PET camera consists of rings of individual detector modules of small crystal arrays or cut block scintillation crystals coupled with photomultiplier tubes. In crystal arrays, multiple separate very small scintillation crystals are grouped together in blocks, often arranged in 6x6 or 8x8 blocks, 36 to 64 crystals per detector block. This concept is more economically achieved by using a single crystalline block onto which deep channels have been cut, forming a matrix (8x8 or 64 elements) on the face of the block. The channels in the crystal are filled with opaque material so that the light from scintillation events cannot spread between sections, but travels only toward the PMTs. This achieves the effect of multiple small crystalline detectors as in figure 2.3.

Many blocks are then assembled to form a crystal ring as in figure 2.4. The light from each block is collected by PMTs servicing the entire block of crystals. Even though the number of PMTs per block is far less than the number of individual crystal elements, it is still possible to attribute each light pulse to a particular crystal for localization by comparing pulse heights in each of the PMTs. Most full multi-ring PET scanners have 10,000-20,000 crystals arranged in about 200 to 400 blocks and with about 500 to 1000 PMTs. For multi-crystal PET cameras, the intrinsic spatial resolution is a function of crystal size; thus, the small sizes of the crystal faces allowed by block design permits optimization of intrinsic resolution. Further, a large number of small independent detectors in a PET system significantly reduces dead time count losses and allows camera operation at higher rates.

Figure 2.4 Ring designs of PET cameras

With ring detectors of any sort, resolution varies with location in the FOV. As an annihilation event gets closer to the edge of the FOV, more image blurring occurs because the path of an annihilation photon may traverse more than one detector element and is capable of producing scintillation in any of them.

Alternative detector arrangements to the small “multi-crystal” complete ring design have been available. These include a hexagonal array or a ring of large curved thallium-doped sodium iodide, crystals, and dual opposed arcs of small detectors that rotate around the axis of the patient to acquire data. There are advantages and disadvantages to these alternative configurations. Because septa are not typically use with these systems, only three-dimensional imaging is employed.

2.1.2.4.1 Full ring [6]

With few exceptions, as in figure 2.5A, PET scanners are full-ring systems-that is, scintillation detectors cover a full 360° around the volume to be imaged. Advantages offered by this particular configuration are (a) optimal system sensitivity, which is necessary to obtain high counting statistics to achieve the needed physical detector resolution; (b) reduction of image artifacts due to tracer, organ, or patient motion; and (c) absence of moving components, which would require further calibrations and would introduce additional variables to be considered.

2.1.2.4.2 Partial ring

Two opposed curved matrices constituted by BGO crystal blocks (11 tangentially x 3 axially) with a reciprocal 15° angular shift rotate, supported by a slip ring technology at 30 rpm, as shown in figure 2.5B. The 2 block banks are not perfectly opposed to increase the transverse FOV during detector rotation. Compared with full-ring systems, this category is characterized by lower overall sensitivity. Using this dedicated scanner, only 3D acquisition is possible.

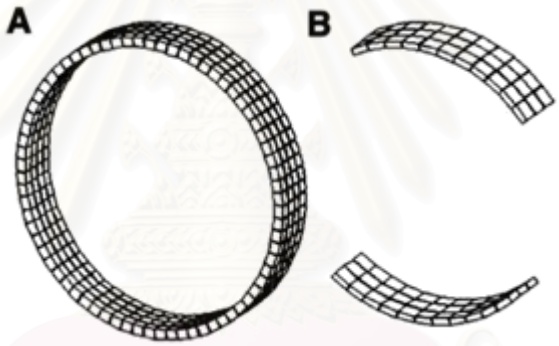

Figure 2.5 Graphic representation of full-ring (A) and partial-ring (B) of PET scanner.

2.1.2.5 Attenuation correction [5]

Attenuation is the loss of true events through photon absorption in the body or by scattering out of the detector FOV. Attenuation problems are significantly worse with PET imaging than with single-photon emission computed tomography (SPECT). Even though the energy of the annihilation photons is greater than for single-photon imaging, with PET, two photons must escape the patient to be detected and the mean photon path is longer, increasing the likelihood of attenuation. In a larger person, the loss of counts due to attenuation can excess 50% to 95%.

Loss of counts through attenuation increases image noise, artifacts, and distortion. Significant artifacts may occur on whole-body PET images obtained without attenuation correction. These include (1) distortions of areas of high activity, such as the bladder, due to variable attenuation in different directions, (2) a prominent body surface edge and (3) apparently high count rates in tissue of low attenuation, such as the lungs. As a result, attenuation correction of these images is necessary before the true amount of radionuclide present at various locations in the body can be accurately determined. This is true both for accurate qualitative assessment of activity

distribution on regional or whole-body images and for precise quantitative measurements of tracer uptake, such as standardized uptake values (SUVs).

Methods of attenuation correction include (1) calculated correction, based on body contour assumptions and used primarily for imaging the head/brain where attenuation is relatively uniform; and (2) measured correction using actual transmission data, used for imaging the chest, abdomen, pelvis, and whole body where attenuation is variable. Transmission attenuation correction is performed by acquiring a map of body density and correcting for absorption in the various tissues. The amount of positron-emitting radionuclide at a specific location can then be determined. Once the correction is performed, the information is reconstructed into cross-sectional images.

One method to obtain a transmission attenuation map of the body is to use an orbiting long-lived radioactive source outside the patient, typically a rod of 120 to 370 MBq, of germanium-68 (^{68}Ge)/gallium-68 (^{68}Ga) with a half-life of 9 months, or 185 to 740 MBq of cesium-137 (^{137}Cs) with a half-life of 30 years, and measure transmission through the patient by using the same system ring detectors used for primary position imaging. In a ^{68}Ge/^{68}Ga transmission source, the ^{68}Ge decays to ^{68}Ga, which then decays by positron emission. In general, performing the transmission scan with either of these radionuclides can take 20 to 25 minutes and account for up to 40% of total scanning time.

In PET/CT scanners, x-rays from the computed tomography (CT) scan are used for attenuation correction and for providing localizing anatomic information. Because the x-rays used are less than 511-keV, the transmission data are adjusted to construct an attenuation map appropriate for annihilation photons. Attenuation maps can be obtained much more quickly with a PET/CT scanner than with external radionuclide sources, and the quality of the attenuation maps is improved. However, because the attenuation map obtained with CT was obtained much more quickly than is PET scan, artifacts in regions of moving structures such as the diaphragm may occur.

Attenuation is more likely when the annihilation reaction occurs in the center of the patient and less likely when the event occurs at the edge of the body. Thus, in a non-attenuation-corrected image, there is less activity at the skin surface. Typically both attenuation corrected and non-attenuation corrected images are provided for interpretation. Images without attenuation correction can be recognized by the surface of the body and the lungs appearing to contain considerably increased activity. On attenuation corrected images, the lungs have less activity than do structures nearer the surface and appear photopenic. Some lesions located near the surface of the body are more obvious on the uncorrected images, but most will be seen on the corrected images. A misalignment artifact can occur when a patient move in between the transmission and emission scans. This can result in overcorrection on one side of the body and undercorrection on the other. In addition, an artifact may occur as a result of the bladder filling with radionuclide during the PET scan acquisition. This results in a hot area appearing around the bladder on the attenuation corrected images but not on the non-attenuation-corrected images.

2.1.3 PET image acquisition and processing [6]

PET systems are most commonly used in a whole-body scanning mode. This usually entails obtaining sequential segmental views of the body by moving the scanning table stepwise to acquire multiple contiguous views. There is a need to overlap the views to get uniform counting statistics, because in multiple detector ring systems, the detector rings at the edge of the FOV have less sensitivity than do those in the middle. A whole-body scan usually extends from the base of the brain to the mid-thigh using a two or three-dimensional acquisition. Depending on the size of the patient and the scanner overlapping images are usually obtain every 15 to 20 cm for several minutes per position.

2.1.3.1 2D and 3D images acquisition

Imaging with lead septa is called two-dimensional or slice imaging, there are thin lead or tungsten septa between the detectors and the adjacent rings of detectors such that each ring of detectors accepts coincidences only between detectors in the same ring or in closely adjacent rings as shown in figure 2.6A. This defines a single plane, eliminating out-of-plane scatter. Although sensitivity is reduced, image quality is enhanced. Two-dimensional imaging is usually performed when imaging small portions of the body or obese patient, when using respiratory gating or short scan times with high activity, or when obtaining higher resolution or accurate quantification.

When three-dimensional acquisition is performed, septa are not present or are retracted. This allows acquisition of a large volume defined by the FOV with coincidences recorded between the multiple detector rings in any combination as shown in figure 2.6B. Sensitivity is about 5 to 10 times higher than with two-dimensional acquisition due to absence of the septa and the increased FOV of each crystal. However, although the number of recorded true coincidences is increased, out-of-plane scatter and random events are also considerably increased reducing image contrast and quality, compared with two-dimensional imaging, three-dimensional acquisitions increase sensitivity of the system by fivefold or more. However, because both true coincidence and scatter rates are increased, better temporal and energy resolutions are needed to accurately eliminate scatter and random events.

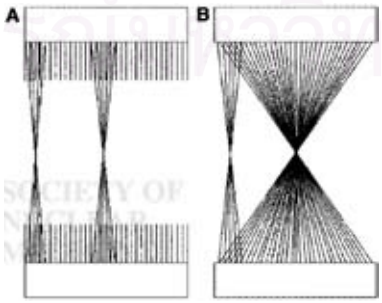

Figure 2.6 Comparison between 2D (A) and 3D (B) acquisition modality. Septa removal causes significant sensitivity improvement when moving radioactive sources toward center of FOV

2.1.3.2 Filtered backprojection

This method provides accurate estimation of 2D radiotracer distribution when projection data are noise free. The basic principles are to perform the Fourier transform of angular projections, apply the ramp filter in the frequency domain, uniformly distribute the filtered data over the reconstructed matrix, and then antitransform. This method is simple to implement and fast in performing sections reconstruction. However, the ramp filter used to eliminate the star artifact and improve spatial resolution also amplifies the noise component, which is particularly important at low counting statistics. To compensate for these effects, low-pass smoothing filters are applied to cutoff frequencies higher than a certain limit, thereby producing more blurred images and worsening spatial resolution.

2.1.3.3 Iterative algorithms

Iterative algorithms are based on the attempt to maximize or minimize a target function determined by the particular algorithm used. The target is reached through several analytic processes called iterations. A major advantage of this type of algorithm is the possibility of incorporating different a priori information, such as noise component, attenuation, or characteristics of detector nonuniformity, for more accurate image reconstruction; however, it must be pointed out that inclusion of additional parameters means increase in processing times.

2.1.3.4 Sinograms

PET raw data was acquired directly into sinogram as shown in figure 2.7. In the sinogram, the LORs associated with each coincidence detection is plotted as a function of angle of orientation versus the shortest distance between the LORs and the center of the gantry. There is a separate sinogram for each slice containing the projection data across all projection angles. These data can be reorganized into projection views where each image represents the projection data for all slices. A particular pixel in the transverse image plots into half of a sine wave in the sinogram. Conversely, each pixel in the sinogram corresponds to a particular LORs or detector pair. Events associated with particular detectors are plotted on diagonals across the sinogram. Thus, the sinogram of a uniform source can be used for scanner quality control.

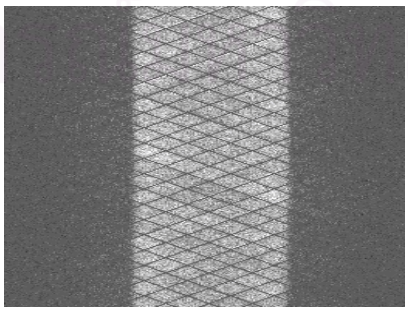

Figure 2.7 Sinograms images

2.1.4 PET performance parameters [7]

As with any medical imaging devices, PET systems are judged on the basis of their quantifiable performance parameters and by the clinical utility of the images they produce. The standard numerical specifications that enter into image characterization are spatial resolution, sensitivity, and ability to reject scattered radiation; count rate limit; and overall image quality. The National Electrical Manufacturers Association (NEMA) has worked with the user community to define methods and techniques to measure and quantify the important parameters for gamma cameras and PET cameras fairly and reproducibly. The document is "NU1-2001 Performance Measurements of Scintillation Cameras". For PET cameras, it is "NU 2-2001 Performance Measurements of Positron Emission Tomographs".

2.1.4.1 Spatial resolution

The spatial resolution of a system represents its ability to distinguish between 2 points of radioactivity in an image. The purpose of the measurement of spatial resolution is to characterize the widths of the point spread function (PSF) in the reconstructed image of compact radioactive sources. The width of the PSF is reported as the full width at half maximum (FWHM) and full width at tenth maximum (FWTM)

Spatial resolution in PET scanners is, in large part, a function of detector size, which smaller detectors increasing the resolving capability of the system. Because of inherent physical limitations on positron localization imposed by their movement from the site of their emission (range) and the noncolinearity of annihilation photons, submillimeter resolution, such as possible with magnetic resonance imaging (MRI), is not achieved. The ultimate limit of spatial resolution when using ^{18}F-fluorodeoxyglucose (^{18}F-FDG) is about 1 mm. However, the practical spatial resolution for clinical imaging is about 4 to 6 mm.

2.1.4.2 Sensitivity

The sensitivity is defined as the recorded true coincidence rate divided by the activity concentration. Sensitivity of a PET camera is determined by multiple factors, including, but not limited to, scanner geometry, crystal efficiency, and photon attenuation tissue. Most photons emitted from the patient, 98% to 99%, are not detected because they are emitted in all directions from the patient and the detector rings cover only a fraction of the patient's body surface. And when attenuation by absorption or scatter is considered, current systems record substantially less than 0.1% of the true events. However, PET scanners typically image in three-dimensional mode, their efficiency for detecting emitted radiation is still considerably greater than that for SPECT imaging. Further, the sensitivity of PET is such that picomolar concentration of PET radiopharmaceuticals can be detected.

2.1.4.3 Scattered photons and random counts

In single-photon planar nuclear medicine, SPECT and PET cross-sectional imaging, photons that enter the detector after having been scattered in the patient degrade image quality. Rejection of scattered radiation is primary accomplished by gamma energy windowing.

PET has adopted additional maneuvers, as with the lead or tungsten septa of 2D and 3D systems. In PET, moreover, the average number of photon scattered uniformly in the image is estimated and removed, a correction that improves contrast at the cost of adding noise.

With PET cameras it is possible for two unrelated photons to arrive at opposing detectors within the coincidence time window. This event, referred to as a *random*, lowers image quality. The random's rate for any two opposing detector elements is given by R = S1 x S2 x τ, where S1 and S2 are individual counting rates for the two detector elements and τ is the length of the coincidence time window. PET cameras estimate the average random's rate and remove it from the final image; this, as with scatter, improves image contrast but adds noise to the corrected image. The coincidence time windows for BGO, LSO, and GSO are typically about 13, 6, and 6 nanoseconds, respectively.

2.1.4.4 Contrast and noise

Evaluation of PET performance based on images from simple phantom is of questionable value, but such tests are nevertheless commonplace. For SPECT cameras, the phantom typically contains "cold" spheres ranging from 31 mm to 9 mm in diameter, and cold rod from 19 mm to 4.8 mm in diameter, and these may provide a rough indication of the status of uniformity corrections, contrast, scatter, and spatial resolution.

For PET, NEMA has defined a test using anthropomorphic phantom containing air and materials that resemble spheres of various diameters. The hot spheres have a target-to-background or contrast ratio is either 4:1 or 8:1 between the hot spheres and phantom background. Standard calculations provide measures of noise, image contrast and scatter, and attenuation correction accuracy.

To facilitate the comparison of PET scanning technique, a figure-of-merit known as noise-equivalent count-rate (NECR) has been defined as:

$$NECR = \frac{T^2}{(T + S + R)} \qquad [2.1]$$

Where T = trues counting rate, S = scatter counting rate, R = randoms counting rate, and (T+S+R) = prompts or total counting rate. The NECR is a measure of the increased image noise due to the subtraction of scatter and randoms from the initial image.

2.1.5 Florine-18-fluorodeoxyglucose (^{18}F-FDG) [5]

The most commonly used positron-emitting radiopharmaceutical in clinical imaging is the glucose analog ^{18}F-FDG. The structure of ^{18}F-FDG is shown in figure 2.8. ^{18}F-FDG is formed through radiochemical synthesis from cyclotron-produced ^{18}F. ^{18}F decays to stable ^{18}O by positron emission with a half-life of 109.77 minutes. Many tumor cells use large amounts of glucose as an energy source and possess increased expression of glucose transporters (especially GLUTI) and increased hexokinase activity (especially HK2). Glucose transporters transfer glucose and fluorodeoxyglucose into the cells, where they are phosphorylated by hexokinases. The rate-limiting step in this process is at the hexokinase level and not at glucose transport. Although phosphorylated glucose can be further metabolized, phosphorylated FDG cannot be rapidly metabolized and ^{18}F-FDG is essentially trapped within the cell in proportion to the rate of glucose metabolism. This allows sufficient time to image its distribution in normal and abnormal bodily tissues. A notable exception to the trapping of phosphorylated FDG is the liver, in which an abundance of phosphotases causes enhanced dephosphorylation of FDG-6-phosphate, which accelerates its washout from that organ.

Although ^{18}F-FDG reaches a plateau of accumulation in tumors at about 45 minutes after injection, the tumor-to-background ratio is best at 2 to 3 hours. Highest activity levels at 2 hours are seen in the brain, heart and urinary system.

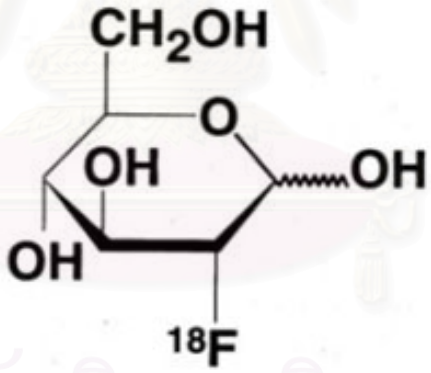

Figure 2.8 2-fluoro-2-deoxy-D-glucose structures

2.1.6 Computed Tomography [8]

2.1.6.1 CT principles

The principles of CT are conceptually simple. Physically, X-rays can traverse a cross-section of an object along straight lines, attenuated by the object, and detected outside it. During CT scanning, the cross-section is probed with X-rays from various directions; attenuated signals are recorded and converted to projections of the linear attenuation coefficient distribution of the cross-section. These X-ray shadows are directly related to the Fourier transform of the cross-section, and can be processed to reconstruct the cross-section.

The measured attenuations of the X-rays passing through the patient are converted into pixels and converted into CT numbers, measured by Hounsfield units (HU).The 3D CT images are obtained from 2D transverse slices which show anatomical information in terms of tissue densities (HU). Because we cannot see the difference between 2000 different shades of grey it would be pointless to produce an image which covered the whole range of Hounsfield numbers. In order to produce a useful image of the area of interest a system of windowing and levels is used.

The available grey scale is spread over the chosen range of Hounsfield numbers. The window defines the upper and lower limits of this range. To produce an image which shows up most major structures a large window is used. For more detailed information about tissues with very similar density a small window is used. The smaller the window the more detailed the image but the range of tissue density that is seen is reduced. The level is the Hounsfield number at the centre of the window. This is chosen so that the window covers the type of tissue of interested. To image dense tissues a high level of window setting is used and to image low density tissues a low level window setting is used. Multi-slice detector geometries allow whole-body imaging, reduces scanning times, which the patient discomfort is reduced and movement artifacts in images are minimized. To enhance some structures with similar tissue density values, contrast media is used.

2.1.6.2 Factors influence radiation dose from CT [8]

a. Beam energy

The energy of the x-ray beam has a direct influence on patient radiation dose. This is selected by the operator, when the kilovolt peak is chosen for the scan. However, it is also influenced by the filtration selected for the scan. When all other technical parameters are held constant and the kilovolt peak is increased on a single-detector CT scanner.

b. Photon influence

The photon influence, as influenced by the tube current–time product, milliampere-seconds (mAs), also has a direct influence on patient radiation dose. As one might expect, the radiation dose is directly proportional to the mAs value.

c. Helical pitch

For helical scans, the pitch parameter, defined as table distance traveled in one 360° rotation/total collimated width of the x-ray beam, has a direct influence on patient radiation dose. This is essentially because as pitch increases, the time that any one point in space spends in the x-ray beam is decreased, causing the reduction in radiation dose.

d. X-ray beam collimation

The collimation of the x-ray beam will both directly and indirectly influence the patient radiation dose. For a single section with all other technical parameters held constant, more x-ray photons will be transmitted when the collimator setting is wider, wider x-ray beam for a thicker section. However, exposure and absorbed radiation dose are defined on a per unit mass basis. The thicker section has more photons available but also more mass being irradiated than a thinner section, thus indicating that the radiation dose for thick and thin sections may be close to equivalent, the difference might be attributed to the higher scatter expected in the thicker section.

2.1.7 PET/CT principles

The PET images offer a great functional contrast but don't provide too good anatomical resolution. On the other hand, the CT images provide a very good anatomical representation but it is difficult to find out functional information. The combination of PET and CT in a single device provides simultaneous structural and biochemical information (fused images) under almost identical conditions, minimizing the temporal and spatial differences between the two imaging modalities as show in figure 2.9.

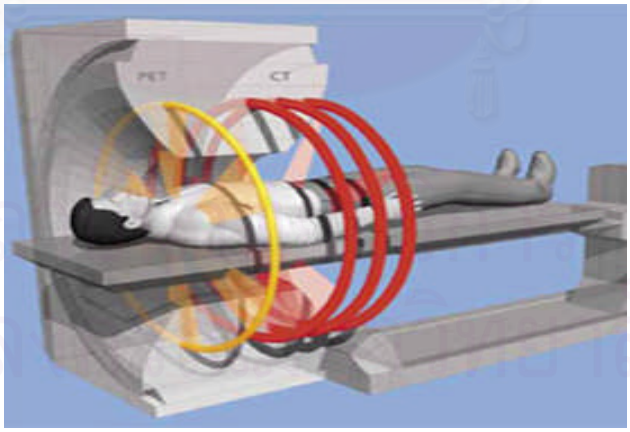

Figure 2.9 PET/CT scan

2.1.7.1 Basic components of a PET/CT system

Among the advantages that having this two modalities together offers we can find that the patient stays on the same table for both acquisitions minimizing any intrinsic spatial misalignment; the total examination of PET is notably reduced; because of the transmission scan is being done by the CT reducing the costs of maintenance and of replacing the radioactive source available in the standard PET scanners. The examination starts with the injection of the radionuclide. After an optional uptake time the patient is positioned as comfortable as possible on the table of the PET/CT scanner. Normally a CT-topogram follows. Then the table moves into the start position of the PET system and the emission scan is initiated. By the time the emission PET scan is completed the CT transmission images have been already reconstructed and available for the attenuation and scatter corrections of the emission data. The total time for the images to be ready for diagnostics is restricted to the reconstruction time, which is more or less the time taken to have enough counts for each bed position of the PET acquisition.

2.1.7.2 PET/CT imaging [5]

Interpretation of PET scans has often been hampered by difficulty in determining the anatomic location of an area of increased activity. The exact location of the activity can greatly affect whether it is considered abnormal, a normal variant, or simply physiologic. For example, increased activity in a ureter or the bowel is likely normal, whereas increased activity in a lymph node is more often abnormal. Accurate localization also gives a better indication of possible causes of abnormal activity. For example, the likely etiologies may be somewhat different if the activity is in the skeleton rather than adjacent soft tissue. Software efforts to fuse CT images with either SPECT or PET data obtained at substantially difference times are often hampered by a number of problems, such as difference in patient positioning and internal change in organ position due to variations in breathing patterns and physiology, especially in the abdomen, between examinations. Thus, a single instrument that can acquire both PET and CT data sequentially on the same table and at close to the same time is desirable.

The addition of CT to PET instruments yields several distinct advantages, depending on the CT protocols used. These include more efficient and accurate attenuation correction, shorter imaging time, more precise anatomic localization of lesions, and acquisition of diagnostic CT and PET scans in one effort. PET/CT scans produce more accurate result than does CT or PET alone or side-by-side visual correlation of PET and CT scans. The primary improvement is a reduction of equivocal interpretations. Given current trends, PET/CT is likely to become the preferred technique in most clinical setting to generate images that contain both anatomic and physiologic information.

Early PET/CT scanners were two separate machines operated by different sets of software at separate consoles. Such scanners used a CT device that obtained basic anatomic and attenuation data but without sufficient spatial resolution to provide diagnostic quality images. Current PET/CT scanners appear to be a single machine, but most are simply a CT and PET scanner placed together within a single

cover. The patient table transverses the bore of both machines. These systems obtain diagnostic quality studies with four to sixty-four slices CT devices.

The current PET/CT scanners can produce good whole-body fused or coregistered PET/CT images as shown in figure 2.10, in less than 30 minutes. When fusing the data, matching CT and PET images is possible to within a few millimeters. However, there may still be slight differences due to the limited spatial resolution of the PET scanner as well as patient movement and/or differences in positioning occurring between the CT scan and completion of the PET scan. PET images are acquired over minutes and CT images are acquired over seconds, there are still some minor alignment problems related to the position of the diaphragm.

In addition to providing precise anatomic localization, the CT scan data are also used to perform PET attenuation correction, eliminating the need and additional time for transmission scans using ^{68}Ge or ^{137}Cs sources. The CT transmission images have less noise than do those from radionuclide sources, resulting in attenuation-corrected PET images with less noise. SUV values obtained on attenuation-corrected images using either CT or radioisotopic methods are generally comparable. However, the lower energy used in the CT scan allows more artifacts from high-density materials. Very high density, contrast on the CT scan can cause overestimation of tissue ^{18}F-FDG concentration, producing areas of apparent increased activity. A similar effect occurs if there are significant metallic objects in the patient.

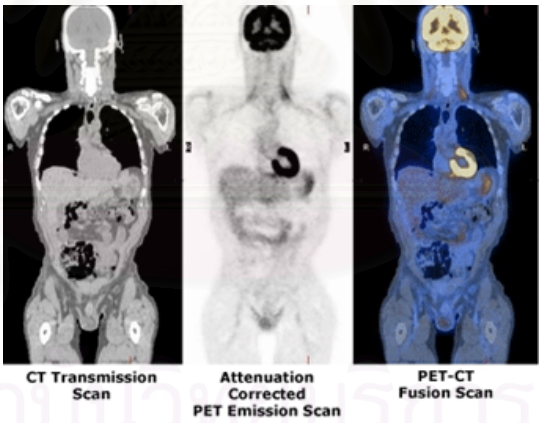

Figure 2.10 PET/CT imaging

2.1.8 Medical Internal Radiation Dosimetry (MIRD)

To ensure the safe use of radioactivity labeled drugs in medical practice, it is necessary to determine the radiation dose received by the patient. Because these radiation doses are received from radioactive materials within the body, they are normally referred to as internal doses. Unlike radiation doses received from external sources such as an x-ray machine, internal doses can never be directly measured; rather, they are calculated from standardized assumptions and procedures. Although several methodologies exist to calculate internal doses, the schema developed by the

Medical Internal Radiation Dosimetry (MIRD) Committee of the Society of Nuclear Medicine is normally used to calculate doses from radiopharmaceuticals [9].

The MIRD formalism takes into account variables associated with the deposition of ionizing radiation energy and those associated with the biologic system for which the dose is being calculated. Although some of the variables are known with a relatively high degree of accuracy, others are best estimates or simplified assumptions that, taken together, provide an estimate of the dose to the average adult, adolescent, child, and fetus.

2.1.8.1 Basic concepts of MIRD [10]

Radioactivity is the property of some nuclides that results in spontaneous transition from one nuclear state to another. The nuclear transition rate (nuclear transition per unit time) is designated as *activity*. Radiations are usually emitted when nucleus undergoes a nuclear transition. Radiations vary widely in energies and absorption properties, but all can give rise to ionization when absorbed in matter. Thus, they are called ionizing radiations. The energy absorbed from ionizing radiation per unit mass of any materials is called *absorbed dose*, designated by the symbol *D*.

Absorbed dose is defined as:

$$D = \frac{d\varepsilon}{dm} \qquad [2.2]$$

Where $d\varepsilon$ is the mean energy imparted by ionizing radiation to matter of mass dm. The units of absorbed dose are typically erg/g or J/kg. The special units are rad in older unit (100 erg/g) or the Gray (Gy) (1 J/kg = 100 rad = 10^4 erg/g). Dose equivalent (H) is the absorbed dose multiplied by a “quality factor” (Q), the latter accounting for the effectiveness of different types of radiation in causing biological effects:

$$H = DQ \qquad [2.3]$$

Because the quality factor is in principle dimensionless, the pure units of this quantity are the same as absorbed dose (i.e. erg/g or J/kg). However, the special units have unique names, specifically, the rem and sievert (Sv). Values for the quality factor have changed as new information about radiation effectiveness has become available. Current values, recommended by the International Commission on Radiological Protection (ICRP 1979), are given in Table 2.4.

Table 2.4 Quality factors recommended in ICRP 30

Particle or photon	Quality factor
Alpha particles	20
Beta particles (+/-)	1
Gamma rays	1
X-rays	1

The quantity dose equivalent was originally derived for use in radiation protection programs. The development of the effective dose equivalent (EDE) by the ICRP in 1979, and the effective dose (ED), in 1991, however, allowed nonuniform internal doses to be expressed as a single value, representing an equivalent whole body dose.

In 1977, the International Commission on Radiological Protection (ICRP) introduced the parameter *effective dose equivalent*, which is a weighted sum of the individual organ absorbed doses. The *tissue weighting factor* for each organ was defined as the ratio between the absorbed dose delivered to the whole body, which would confer a certain probability of cancer induction, and the absorbed dose in a single organ (H_T), which would confer the same probability of cancer induction in that organ. For example, a dose of 0.12 Gray to the whole body confers some probability of cancer induction; a dose of 1 Gray to the lungs results in the same numerical probability of lung cancer induction; thus, the tissue weighting factor for lung is set equal to 0.12.

The product of the tissue weighting factor W_T and the absorbed dose equivalent in an organ is called the organ effective dose equivalent; the sum of organ effective dose equivalents is called the effective dose equivalent H_E and is calculated as follows:

$$H_E = \Sigma_T W_T H_T \qquad [2.4]$$

(The ICRP uses the symbol H_T for the absorbed dose in an organ or tissue, which is the same quantity as D in the MIRD formalism.)

Tissue weighting factors recommended in ICRP 60 [11] for calculation of the effective dose equivalent are given in table 2.5.

Table 2.5 Tissue weighting factors

Organ	Weighting factor
Gonads	0.20
Red Bone Marrow	0.12
Colon	0.12
Breast	0.05
Bladder	0.05
Esophagus	0.05
Liver	0.05
Lung	0.12
Skin	0.01
Thyroid	0.05
Bone Surface	0.01
Remaining tissue	0.05

2.1.8.2 MIRD equation [10]

Depending upon the identified of the radionuclide, particles or rays of characteristic energy and abundance will be given off at a rate dependent upon the amount of activity present. The quantities needed for equation are the *fraction of emitted energy* which is absorbed within the target. This quantity is most often called the "absorbed fraction" and is represented by the symbol Ø. For photons, some of the emitted energy will escape objects of the size and composition of interest to internal dosimetry, mostly soft tissue organs with diameter of the order of centimeters. For electrons and beta particles, most energy is usually considered to be absorbed, so we usually set the absorbed fraction to 1.0. Electron, beta particles [12], are usually grouped into a class of radiations referred to as *nonpenetrating* emissions while X- and γ-rays are called *penetrating* radiations. An absorbed fraction property in various organs was illustrated in figure 2.11.

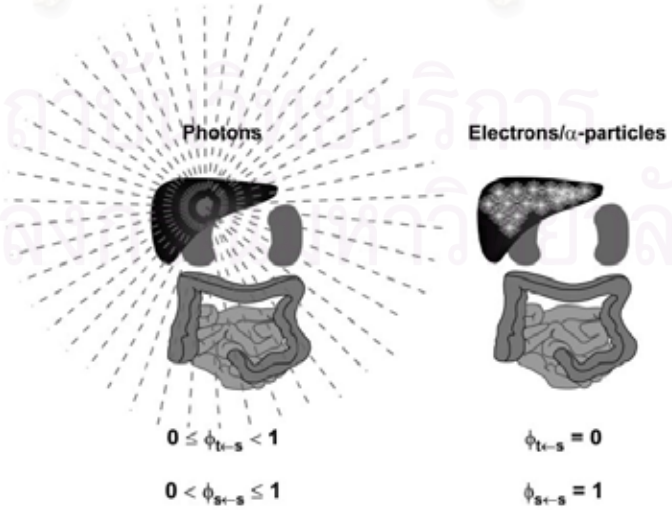

Figure 2.11 Different absorption properties of photons versus electron

So, the fraction absorbed depends on:

(1) the distance between the source and target organs
(2) the composition of the tissue between the source and target organs
(3) the penetrating ability of the radiation.

We can show a generic equation for the absorbed dose in as [10]:

$$D = \frac{k\tilde{A}\sum_i n_i E_i \phi_i}{m} \qquad [2.5]$$

D	is absorbed dose (rad or Gy)
$\tilde{A}$	is cumulated activity (μCi-hr or MBq-sec)
n	is number of radiations with energy E emitted per nuclear transition
E	is energy per radiation (MeV)
$Ø$	is absorbed fraction
m	is mass of target region (g or kg)
k	is proportionality constant (rad-g/μCi-hr-MeV or Gy-kg/MBq-s-MeV)
i	is number of emitted radiations

The cumulative activity (Ã), or number of transitions, is represented by the shade area under the curve as shown in figure 2.12.

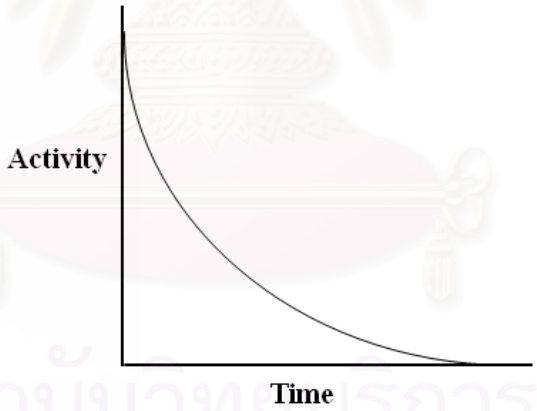

Figure 2.12 Cumulative activity

The cumulative activity depends on two factors: the amount of activity administered to the patient (A_0) and the life time of the radioactive within the body or organ of interest. So, characteristics of both physical and biological factors had affected cumulative activity [13].

The units used for this quantity are μCi-hr, recall that 1 μCi-hr is equivalent to 1.33×10^8 disintegrations. If activity is in units of Bq and time is in units of seconds, cumulated activity will have units of Bq-sec.

The residence time (τ) of a radionuclide in a source can be used instead of cumulative activity in estimating the absorbed dose to a target. The residence time is defined as follows:

$$\tau = \frac{\tilde{A}}{A_0} \qquad [2.6]$$

Therefore, the residence time can be thought of as a "mean" or "effective" life of the administered activity A_0 in the source organ. It is important to remember that residence time accounts for both physical decay and biologic removal.

2.1.8.3 The MIRD system

The equation for absorbed dose in MIRD system, Loevinger et al. 1988, [14] is deceptively simply:

$$D = \tilde{A}S \qquad [2.7]$$

The cumulated activity is there; all other terms must be lumped in the factor S, and so they are:

$$S = \frac{k\sum_i n_i E_i \phi_i}{m} \qquad [2.8]$$

$$D = \tilde{A}\frac{k\sum_i n_i E_i \phi_i}{m} \qquad [2.9]$$

In the MIRD equation, the factor k is 2.13, which gives doses in rad, from activity in microcuries, mass in gram, and energy in MeV. The MIRD system was developed primarily for use in estimating radiation doses received by patients from administered radiopharmaceuticals; it is not intended to be applied to a system of dose limitation for workers.

2.1.8.4 S factor [15]

The S factor is the dose to the target organ per unit of cumulative activity in a specified source organ, rad/μCi-hr. It is determined by a number of factors, including, the mass of the target organ, the type and amount of ionizing radiation emitted per disintegration, and the fraction of the emitted radiation energy that reaches and is absorbed by the target organ. Each S factor is specific to a particular source organ, target organ combination. Usually, the S factor is provided in tabular form for most common diagnostic and therapeutic radionuclides. The MIRD committee has not yet published S factors in SI units, however, this conversion is anticipated.

Once the rules for defining absorbed fractions have been determined, the S-value for any radionuclide and a given source-target combination may be

calculated using the energies and branching fractions, the absorbed fraction, and the target organ mass. Therefore, in MIRD Pamphlet No. 11 [16], these S-values are tabulated for the 117 radionuclides and 20 source and target regions defined in the phantom. If one can estimate the cumulated activity for all important source organs, absorbed doses for any defined target organs may be estimated simply as [10]:

$$D(r_k \leftarrow r_h) = \sum_h \tilde{A}_h \quad S\ (r_k \leftarrow r_h) \qquad [2.10]$$

Where r_h represents a source region and r_k represents a target region.

This equation reduces the entire dose equation to a two-step calculation, per source organ, once the integrals of the time-activity curves are known. Often determination of this latter quantity is the most difficult in a dosimetry analysis. The absorbed doses calculated using this equation are defined for a model of a standard size, 70 kg, with a uniform activity distribution in each source region. This simple equation is quite powerful, but understanding of its underlying assumptions is essential to its proper application.

2.1.8.5 Whole-body dose and effective dose equivalent

The calculated absorbed doses have single target organ, and depending on the biokinetics of the administered radiopharmaceutical. The individual organ dose can range over several orders of magnitude. Consequently, a single parameter that relates to the radiation dose delivered to the body as a whole is needed to evaluate and compare the radiation risks of different procedures. Historically, the parameter used for this function is the *whole-body dose* or *total-body dose*. This quantity is defined as the total radiation energy absorbed in the body divided by the mass of the body, which is taken as 70 kg for the reference man. The whole-body dose is calculated in the MIRD schema by using the published S factor for the combination of whole body as source organ and whole body as target organ. The ratio of whole-body dose to the highest single organ absorbed dose varies from nearly unity for radiopharmaceuticals that tend to be uniformly distributed in the body.

2.1.8.6 The MIRDOSE software [17]

A computer program called MIRDOSE has been developed and is distributed by the Radiation Internal Dose Information Center. The program contains tables of the S factors for the common radionuclide; the user must provide the biokinetic data in the form of residence times for the source organs. The program then generates tables of organ doses per unit administered activity in both traditional and SI units, rad/mCi and mGy/MBq.

2.2 Review of related literatures

Brix G, et al [3], investigated radiation exposure of patients undergoing whole-body ^{18}F-FDG PET/CT examinations at 4 hospitals equipped with different tomographs. They reviewed whole-body PET/CT acquisition protocols used between September 2003 and May 2004 in 4 Germany university hospitals and estimated patient dose by using dose coefficients for ^{18}F-FDG for internal dose and from thermoluminescent measurements performed on an anthropomorphic whole-body phantom for CT dose. Average ^{18}F-FDG activities of 300 MBq (hospital 2) and 370 MBq (hospital 1, 3, 4) were administered and the acquisition time for the whole-body ^{18}F-FDG PET scans was less than 45 minutes at all sites. The effective dose for patients undergoing high quality whole-body ^{18}F-FDG PET/CT examinations at the four university hospitals participating in this study was about 25 mSv.

Table 2.6 Summary of radiation exposure of patient from ^{18}F-FDG PET/CT examinations at 4 German Hospitals from Brix G et al.

Hospital	Type Scan	Effective dose (mSv)	
		Per scan	Per examination
H1	Topogram	0.8	
	Diagnostic CT with CA*	18.6	
	PET, 370 MBq ^{18}F-FDG	7.0	26.4
H2	Topogram	0.1	
	Low-dose CT	4.5	
	PET, 300 MBq ^{18}F-FDG	5.7	
	Diagnostic CT with CA	14.1	24.4
H3	Topogram	0.2	
	Diagnostic CT with CA	17.6	
	PET, 370 MBq ^{18}F-FDG	7.0	24.8
H4	Topogram	0.2	
	Low-dose CT	2.4	
	PET, 370 MBq ^{18}F-FDG	7.0	
	Diagnostic CT with CA	14.1	23.7

* CA - Oncology patient.

Hays MT, et al [2], estimated absorbed dose from a bolus intravenous administration of ^{18}F-FDG. They concluded that the whole-body residence time in the ICRP publication, 2.13 h, is similar to their report, 2.38 h, residence times for some source organs are notably different. This MIRD report found a brain residence time of 0.23 h, which was higher than the ICRP value of 0.15 h, resulting in a correspondingly greater dose to the brain (0.046 mGy/MBq vs. 0.028 mGy/MBq). For the liver, Health Physics 2003 gave the dose as 0.011mGy/MBq, whereas their report listed the mean liver dose as 0.034 mGy/MBq. This difference reflects the observed specific liver uptake found in the human studies that form the basis of this MIRD dose-estimate report, whereas the ICRP authors assumed that the human liver had no specific ^{18}F-FDG uptake.

Kim JH, et al [18], had developed a mathematical phantom model for calculating internal radionuclide dosimetry base on the basic data from the Korean reference adult male, and have also derived paired-organ and other selected inter-organ photon-specific absorbed fractions (SAFs) for this model. Monte Carlo method was applied for the calculation of SAFs. The calculated data were compared against the data of MIRD Pamphlet No. 5 and ORNL TM-8381 report, which are based on the existing data of the ICRP-23 reference man. As a result, SAFs were indicated to be higher in the phantom based on Korean reference adult male than in the data of MIRD 5 and ORNL. This is considered to be so mainly because of the differences in accordance with the photon energy emitted from the source organ of the thyroid glands are estimated to have a connection with the materials composing a medium and the range of photon. Also, the result of calculating SAFs in the adrenals, lungs and kidneys, which are separated into two parts although of the same physiological function, indicated that, if an organ is paired, each of these organ parts serves as an independent source organ and that differences are noted in SAFs according to the region in which these organs are located, that is, to the left or right of the region.

Mejia AA, et al [19], reported the estimation of absorbed doses due to the intravenous administration of fluorine-18-fluorodeoxyglucose in positron emission tomography in normal volunteers. The time activity curves were obtained for seven organs (brain, heart, kidney, liver, lung, pancreas, and spleen) by using dynamic PET scans and for bladder content by using a single detector. Absorbed dose were calculated by the MIRD method using the absorbed dose per unit of cumulated activity, transformed for the Japanese physics and the organ masses of Japanese reference man. The study showed that the bladder wall and the heart were organ receiving higher dose of 0.12 and 0.045 mGy/MBq, respectively. The brain received a dose of 0.029 mGy/MBq and other organs received doses between 0.01 and 0.03 mGy/MBq. Their results concerning the bladder wall agree with other results and also confirmed that the absorbed dose to this organ can be reduced to half of that for the 2 hours void time if the patient void at 1 hour after injection. Although, the absorbed doses estimated in this wok cannot be directly compared to other published data since there is organ weight/total body weight variance in Japanese versus European and American adults, the values reported here are in the range of other published results on the dosimetry of this radiopharmaceutical.

CHAPTER 3

RESEARCH METHODOLOGY

3.1 Research design

This research is designed as a cross sectional study to estimate patient dose from PET/CT scans administered ^{18}F-FDG. The procedures are as the following steps as by in figure 3.1.

3.2. Research design model

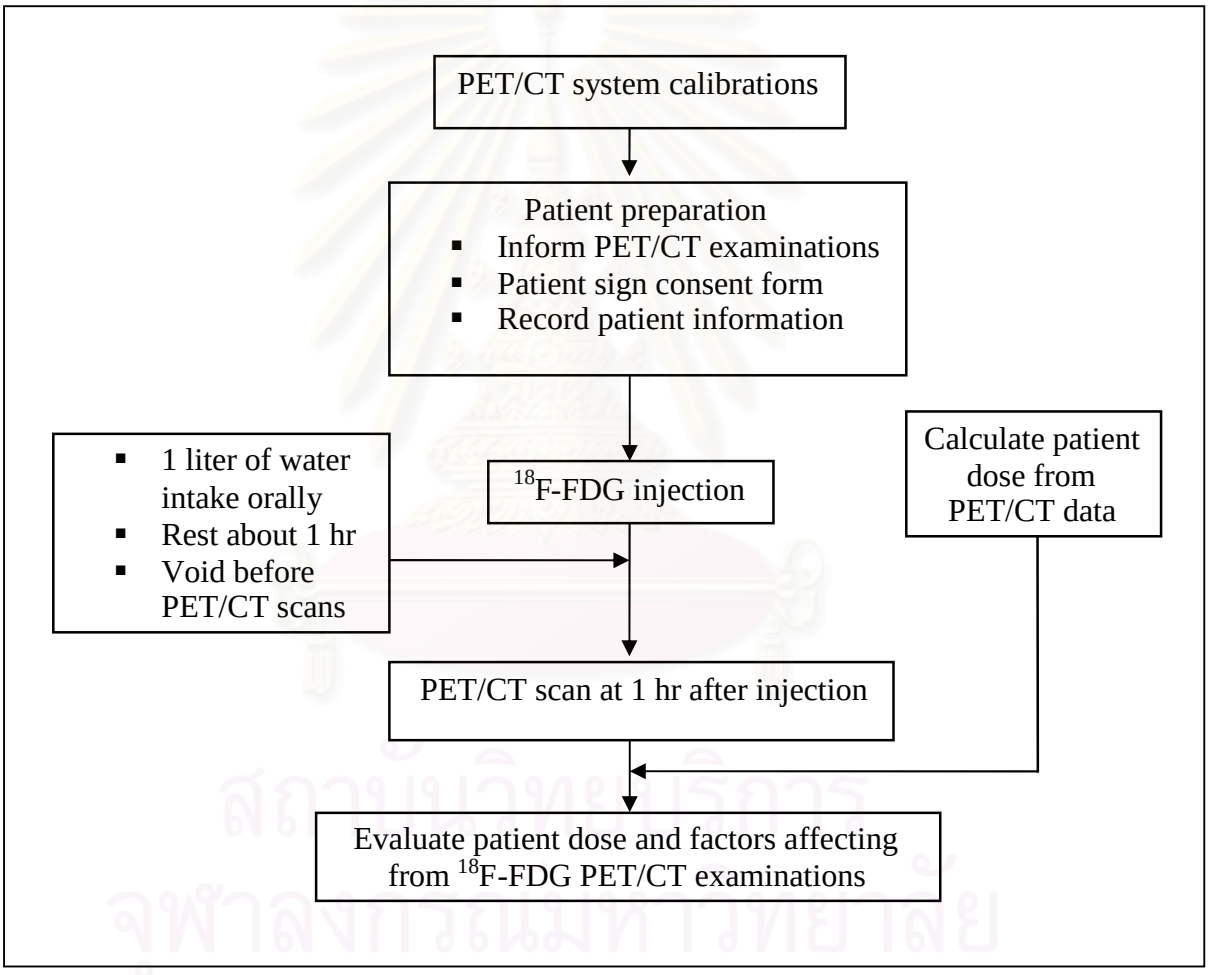

Figure 3.1 Research design model

3.3 Conceptual framework

There are four parameters influencing the patient dose from PET/CT scan. The activity of ^{18}F-FDG and mass of organ influences the internal dose. The scan length and patient body mass index influences the dose from CT scan, or external dose. The conceptual framework of this study is shown in figure 3.2.

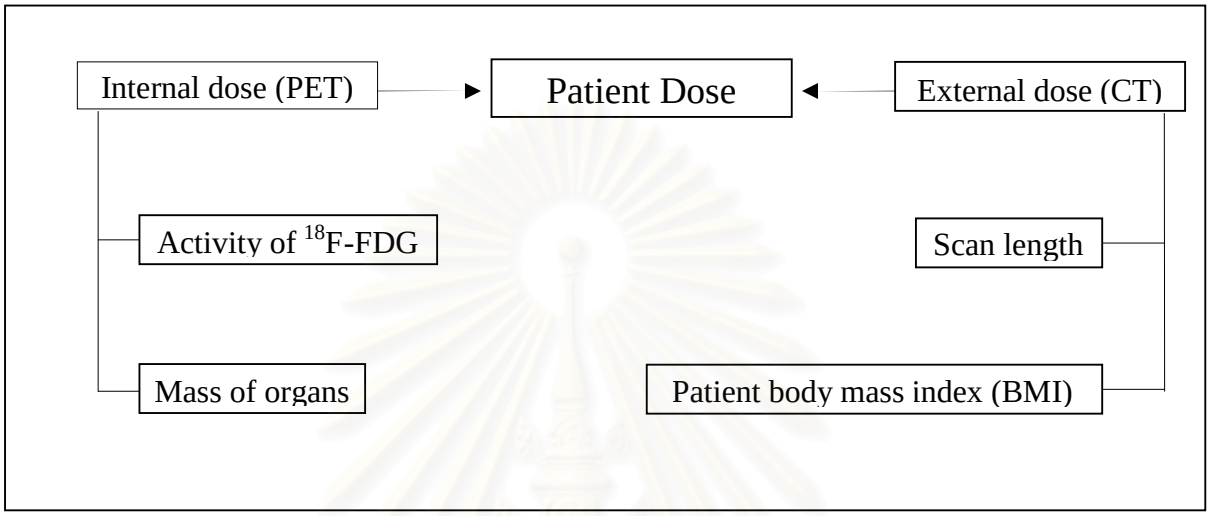

Figure 3.2 Conceptual framework

3.4 Research question

3.4.1 Primary research question:

What is the patient dose from ^{18}F-FDG PET/CT examinations at King Chulalongkorn Memorial Hospital?

3.4.2 Secondary research question:

What are factors affecting the patient doses in PET/CT examinations?

3.5 Key words

- ^{18}F-FDG
- MIRD
- Patient dose
- PET/CT

3.6 The sample

3.6.1 Target population: All patients who were requested for PET/CT examinations at King Chulalongkorn Memorial Hospital.

3.6.2 Sample population: The patients who were requested for PET/CT examinations at King Chulalongkorn Memorial Hospital, and met the eligible criteria.

3.6.3 Eligible criteria:

3.6.3.1 Inclusion criteria:

- Oncology patients

- Whole body scan

3.6.3.2 Exclusion criteria:

- Pregnant patients

- Patient age>60 years

3.6.4 Sample size determination

Sample size, n, is calculated from continuous data to estimate the population based on the formula with 90 % confidence interval (CI):

$$n = \frac{z_{\alpha}^{2}\sigma^{2}}{d^{2}} \qquad [3.1]$$

$$\frac{2.6896 \times 24.01}{2.1025} = 31$$

n is sample size
σ^2 is variance of data (24.01)
d is acceptable error (1.45)
Z_{α} is 90 % CI = 1.64 from table ($\alpha = 0.10$)

The sample size (n) for 90 % confidence interval is 31

3.7 Materials

3.7.1 Positron Emission Tomography/Computed Tomography [20]

The PET/CT system as shown in figure 3.3 is manufactured by Siemens Medical Solutions, Model Biograph Sensation 16. The system integrates a PET scan, with a 16 multi-slice CT scan using the *syngo* multimodality computer platform. PET scan, consist of arrays of lutetium oxyorthosilicate (LSO) crystal detector, dimension 4x4x20 mm, crystal per block are 169 crystals, total detector of LSO are 144 blocks, total number of detectors are 24,336 detectors, covering an axial field of view 162 mm, and transaxial field of view 585 mm. For CT scan, it is able to simultaneously collect data, this 16-row data collection is accomplished via a 24-row detector. The maximum scan FOV is 500 mm. Bore diameter is 700 mm. Three kVp settings are available at 80, 120 and 140 kVp. The tube current ranges from 28 to 500 mA. The automatic exposure control (AEC) protocol to minimize acquisition system efficiency is available.

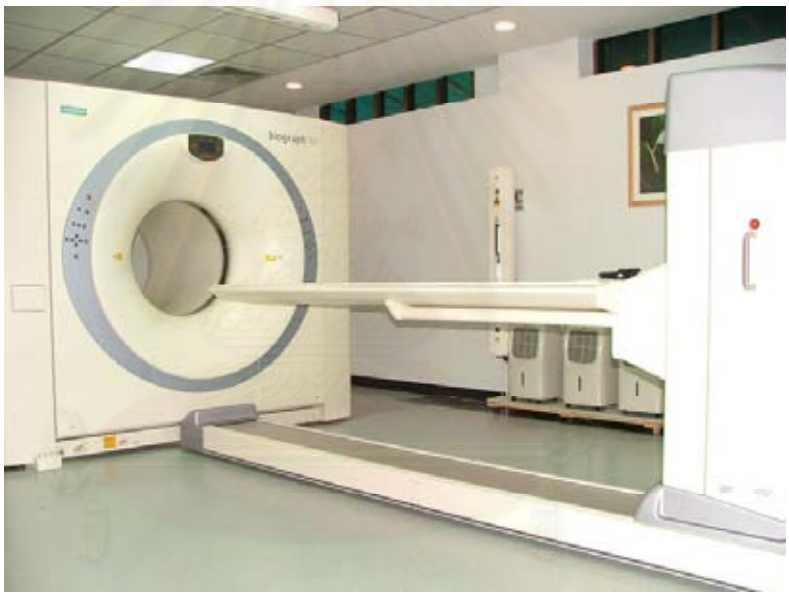

Figure 3.3 PET/CT system

3.7.2 Fluorine-18-fluorodeoxyglucose (^{18}F-FDG)

Fluorine-18 is a cyclotron produce positron emission prepared by radiochemical synthesis. The structure of ^{18}F-FDG is shown in figure 2.8. ^{18}F decays to stable ^{18}O by positron emission with a half-life of 109.77 minutes.

3.7.3 Monte Carlo simulation program [21]

The WinDose program version 2.1a, as shown in figure 3.4, is the PC program for estimating organ dose and effective dose values in computed tomography. The calculations are based on the Monte-Carlo simulations for anthropomorphic phantoms which were obtained earlier by the GSF – National Research Center for Environment and Health, Nurnberg, Germany. The exposure factors were entered into the WinDose spreadsheet, along with CTDI in air which the measurements made with the pencil ionization chamber. The spreadsheet used these data and table of normalized organ doses to estimate the organ dose by matching with the manufacturer CT machine. This program was implemented under Windows 95 to operate on any standard PC or laptop PC at arbitrary sites. It was written in C++ and offers a user-friendly graphical user interface.

Figure 3.4 WinDose program

3.7.4 The pencil ionization chamber [22]

A 100 mm long pencil ionization chamber: DCT 10-RS S/N 1057 is shown in figure 3.5. It has 4.9 cm^3 active volumes, 100 mm total active length, 8.0 mm inner diameter of outer electrode, and 1.0 mm diameter of inner electrode. It is used with an electrometer during the measurement.

Figure 3.5 The pencil ionization chamber

3.7.5 The electrometer [22]

An electrometer: RTI Electronics AB Type SOLIDOSE 400 Electrometer S/N 4103 [23] is shown in figure 3.6, has the leakage within 4×10^{-15} Ampere, for 80 – 150 kV radiation quality, and the calibration factor $N_{D,K}$ equal to 24.2 mGy·cm/nC (120 kV/HWD 4.05 mm Al).

Figure 3.6 The electrometer

3.7.6 Accessories

- Drinking water 1 liter/patient
- Consent form
- Case record form

3.8 Methods

This study is carried out as the following:

3.8.1 PET/CT daily QC [APPENDIX D]

The daily quality control program for CT and PET is regularly performed using water phantom for the study of CT image quality, kVp calibration, pixel noise and CT number values. The Ge/Ga-68 phantom is used for PET daily QC, to check chi-square value, for detector for response, or performance of detectors. Two-bed test is checking the match-registration between PET and CT scan.

3.8.2 Patients

The study was investigated in 7 male and 28 female patients with age range 28-60 years (mean±SD, 44±10), who underwent ^{18}F-FDG PET/CT examinations at King Chulalongkorn Memorial Hospital. The patient is informed about the objective of the study. The written consent was obtained form the patients before PET/CT examinations [APPENDIX C]. Record patient information such as patient identification number, height, weight, injected activity and time in case record form [APPENDIX B]. The injected activity of ^{18}F-FDG is 4.75 MBq per kilogram. The patient is encouraged to drink 1 liter of water and rest at patient's waiting room. The patients urinated before the examination.

3.8.3 PET/CT procedure

Whole-body PET/CT scan was obtained at 1 hour after administration of ^{18}F-FDG. A segmented emission scan was acquired for 3 minutes per bed position, and 6 to 8 bed positions per patient, from the base of skull to the upper thigh. Scanning was performed in the caudocranial direction. Three sequential whole-body emission scans were acquired at 1, 2 and 3 hour after injection to investigate the residence time of various organs. For CT scan, the parameters such as tube voltage (kVp), collimation, slice width, and pitch factor were fixing in all patients, except mAs parameter using the automatic exposure control (AEC) mode, as in table 3.1. The acquisition time for the whole-body scan is about 30 minutes per patients. The image was reconstructed in axial view and reformation to coronal and saggittal planes.

Table 3.1 CT scan parameters for whole-body PET/CT scan.

kVp	Collimation (mm)	Slice width (mm)	Pitch factor
120	16 x 1.5	5	0.75

3.8.4 Data analysis

3.8.4.1 Internal dose

The internal dose calculation is carried out according to MIRD equation as 3.2 [10].

$$D = \frac{k\tilde{A}\sum_i n_i E_i \phi_i}{m} \qquad [3.2]$$

D is absorbed dose (rad or Gy)
$\tilde{A}$ is cumulated activity (μCi-hr or MBq-sec)
n is number of radiations with energy E emitted per nuclear transition
E is energy per radiation (MeV)
$Ø$ is absorbed fraction
m is mass of target region (g or kg)
k is proportionality constant (rad-g/μCi-hr-MeV or Gy-kg/MBq-s-MeV)

Calculation the time-activity curves or cumulative activity

To measure SUV values, the region of interest was drawn within the boundaries of organ. For each time interval of the scan, data from each ROI in SUV was assessed to unit of total organ activity as the following equation:

$$\text{Organ activity(MBq)} = \frac{\text{SUV x Administered activity(MBq) x Organ weight(g)}}{\text{Body weight(g)}} \qquad [3.3]$$

The SUV (Standardized uptake value) is determined by using the PET syngo software on the attenuation-corrected images, by placing ROI over the portion of the organ with greatest ^{18}F-FDG uptake. The target organs are the liver, spleen, kidneys, lungs, bone marrow, bone surface, testes, ovaries, colon, skin, thyroid, urinary bladder wall, stomach and breast. Plot time activity curves using total organ activity in target organ at 1, 2 and 3 hours after injection as the following equation 3.3. Cumulative activities in target organs were obtained by integral area under time activity curves in thirteen target organs as shown in figure 3.7.

Integrated activity under curve using MATLAB program, version 7.5.0 with the following command:

```
>> % Cumulative activity in target organ
>> clc
>> y=textread('target organ.txt');
>> % Scale X value for 0.5
>> x=(0:5:time to integral);
>> plot(x,y,'-')
>> Area=trapz(x,y)
```

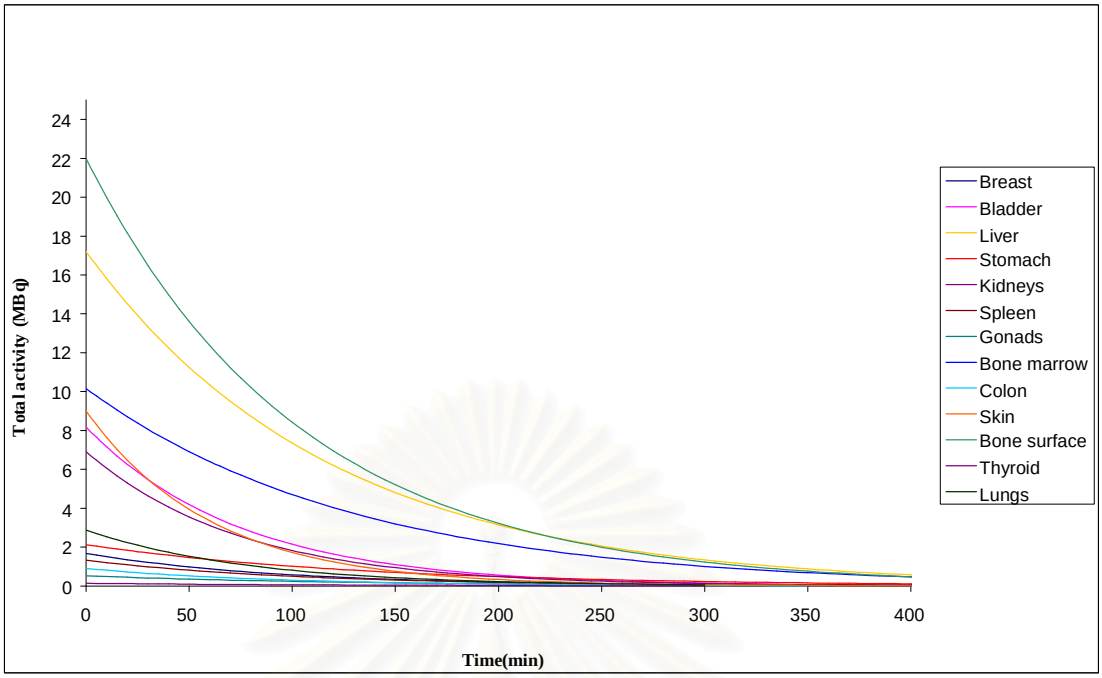

Figure 3.7 Cumulative activities in target organs

Determine the residence time (τ) in target organs as the following equation:

$$\tau = \frac{\tilde{A}}{A_0} \qquad [3.4]$$

Where $\tilde{A}$ is the cumulative activity in target organ, and A_0 is the activity administered to the patients. Therefore, the residence time is related to the characteristics of both the physical and biological removal in target organs.

Radiation dosimetry

Absorbed dose in target organs is calculated according to the MIRD method as in the equation 3.2. Using S factor and the specific absorbed fraction following dose factor for ^{18}F [10], for Thai patient, derived from the ratio of the organ weight in the MIRD reference man [23], multiplied by the organ residence time and multiplied by the activity of ^{18}F-FDG administered to the patient. The effective dose of the organ is determined using weighting factor provided by ICRP publication 60 [11].

The total-body effective dose (E) was determined by formalism [3]:

$$E = A \cdot \Gamma_E^{FDG} \qquad [3.5]$$

Where Γ_E^{FDG} is the dose coefficient (μSv/MBq), and, A is the activity (MBq) administered to the patients.

The dose coefficient (μSv/MBq) is determined by sum the results of absorbed dose multiplied by tissue weighting factor in thirteen target organs as the following table 3.2.

Table 3.2 The dose coefficient (μSv/MBq) to determine the total body effective dose.

Target organ	Absorbed dose (μGy/MBq)	Tissue weighting factor	Dose coefficient (μSv/MBq)
Liver		0.05	
Kidneys		0.05	
Lungs		0.12	
Urinary bladder		0.05	
Stomach		0.12	
Spleen		0.05	
Gonads		0.20	
Bone marrow		0.12	
Colon		0.12	
Bone surface		0.01	
Skin		0.01	
Thyroid		0.05	
Breast		0.05	

3.8.4.2 External dose

For CT scan, the external dose is calculated by using WinDose program as the following:

Input data and parameters

When WinDose is started, the input screen will be shown in figure 3.8. Enter the parameters for the interested scan, the type of scan, conventional or spiral and the sex of the patient. The scan range should be specified, cranial and caudal positions, scan length, table increment or pitch and the number of slices or rotations. In the section “scan parameters”, tube voltage, effective energy, the mAs product and the slice thickness can be selected.

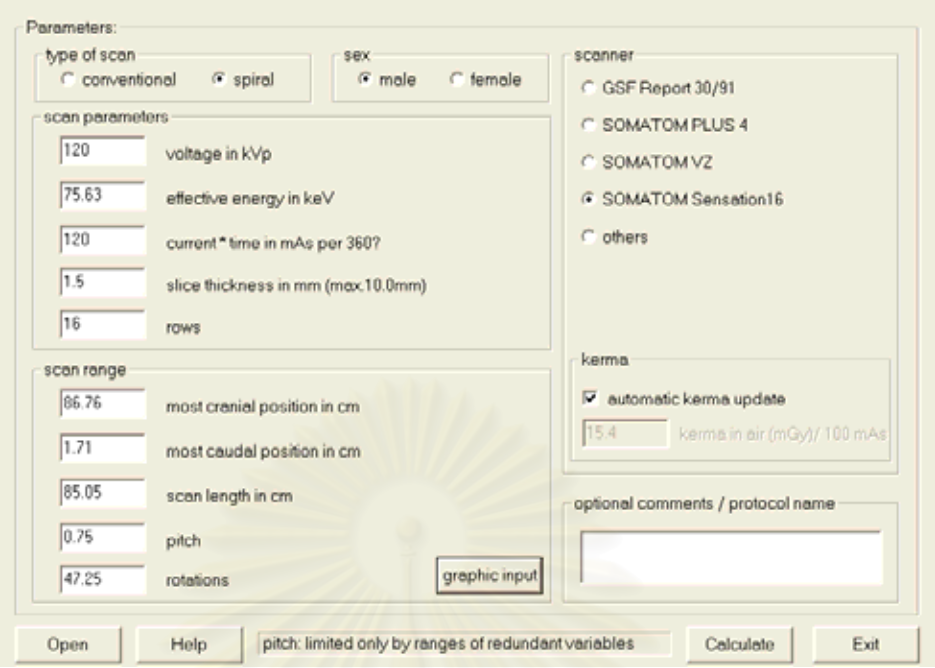

Figure 3.8 WinDose input screen

Kerma data is obtained by the measurements on the scanner or, from the specifications by the manufacturer. WinDose offers an automatic update of kerma. In this study we use the pencil ionization chamber, model DCT 10-RS S/N 1057, 4.9 cm^3 active volume, to measure air kerma [8]. The 100 mm long pencil ionization chamber was placed in air at the center. Exposure techniques used for air kerma measurements were set by the following parameters as table 3.3.

Table 3.3 CTDI in air parameters measurements

Interface	Input
Entry	Head first
Position	Supine
Scan type	Axial
Slice Thickness	10 mm
Tilt	0 degrees
mA	100
kV	120
Rotation speed	1 second
Scan length	100 mm

Output parameters

The available WinDose result screens are shown in figure 3.9 and 3.10. Dose values for the major organs are listed together with a summary of the selected scan parameters and scan range. Click the “Graphical display” button provide an optional graphical representation of the scanned region, the organ positions and the calculated organ doses with a schematic drawing of a male or female patient, respectively. The calculation of effective dose values is carried out according to both ICRP 26 and 60 using the respective tissue weighting factors [24], [11].The resulting effective dose value is also specified in units of natural background radiation per year to give an indication of the orders of magnitude involved.

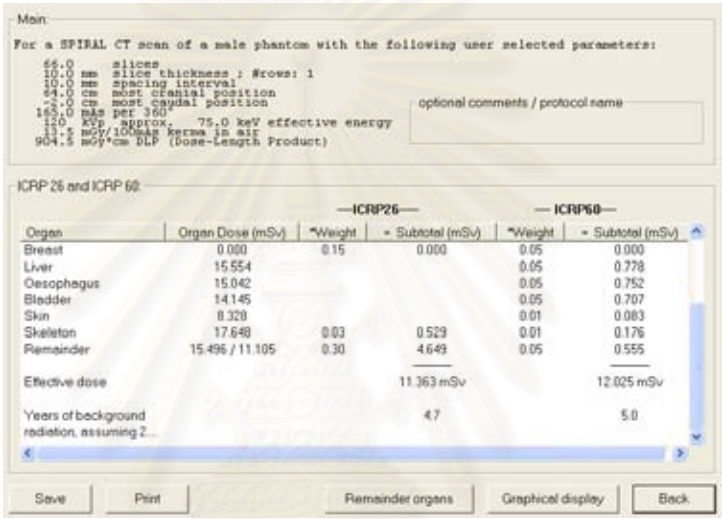

Figure 3.9 WinDose output screen

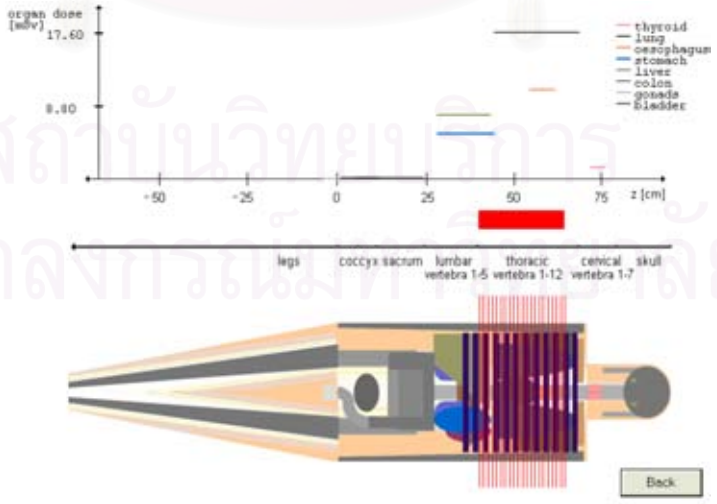

Figure 3.10 WinDose output screen with a graphical presentation of the anatomical scan range, organ ranges and dose levels

Sum the effective dose from both CT and PET scan, and evaluate the correlate factors affecting patient dose from PET/CT examinations.

3.9 Statistical analysis

The study involves the comparison and correlation of the data from independent and dependent variables. Bivariate analysis is chosen for analyzing each independent variables and dependent variable.

Independent variables: Patient body mass index (BMI), Scan length, Patient weight, Activity ^{18}F-FDG.

Dependent variable : Patient dose

Data analysis was done using SPSS program.

3.10 Ethical consideration

This research covers the determination of the average patient dose and its factors affecting PET/CT examinations. ^{18}F-FDG will be administered to patients by intravenous injection. The ethical was approved by Ethics Committee of Faculty of Medicine, Chulalongkorn University.

3.11 Expected benefits

Patient dose from PET/CT examinations at King Chulalongkorn Memorial Hospital.

Factors affecting patient dose from PET/CT examinations.

CHAPTER 4

RESULTS

4.1 The quality control of PET/CT system

The daily quality control program for CT and PET is regularly performed. The quality control of PET/CT system was evaluated with the following topics:

- CT image quality
- kVp calibration
- Pixel noise
- CT number value
- Chi-square value
- Two bed test
- Trues coincidence
- Random coincidence
- Single coincidence
- PET temperature

The results of quality control from July 2007 to December 2007 are shown in APPENDIX D.

4.2 External dose

4.2.1 Measurement of computed tomography dose index

Table 4.1 Computed tomography dose index in air

Method	CTDI in air (mGy/100 mAs)
Measurement	14.83
WinDose	15.40

Table 4.1 shows the CTDI in air values measured from Biograph 16. The mean CTDI measured in air indicates 14.83 mGy. The CTDI in air from WinDose program shows the higher value than the measurement. The difference for CTDI in air between measured and WinDose is 3.70 percent. The CTDI in air from measurement will be used in this study.

4.2.2 The effective dose from Monte Carlo simulation

The summary of effective dose from CT scan calculated using Monte Carlo simulation, WinDose program is presented in table 4.2.

Table 4.2 Summary of patient data including the effective dose from CT scan using Monte Carlo simulation

	Min	Max	Mean ± SD
Patient weight (kg)	40	70	53.34 ± 8.12
Patient height (cm)	149	178	160 ± 7.71
Body Mass Index (kg/m^2)	15.42	28.14	21.12 ± 3.05
Scan length (mm)	759	992	856 ± 71.64
mAs	75	173	112 ± 21.68
Effective dose (mSv)	10.04	21.98	14.45 ± 2.82

The patient information and results of effective dose for 35 patients from CT scan using WinDose, Monte Carlo simulation technique is presented in table 4.3.

The patients have age ranged from 28 to 60 years (mean ± SD, 44 ± 10). Seven cases were male and 28 cases were female. Patient height ranged from 149 cm to 178 cm (mean ± SD, 160 ± 7.71), Patient weight ranged from 40 kg to 70 kg (mean ± SD, 53.34 ± 8.12). Patient BMI ranged from 15.42 kg/m^2 to 28.14 kg/m^2 (mean ± SD, 21.12 ± 3.05). The mAs ranged from 75 to 173 (mean ± SD, 112.37 ± 21.68). Scan length from 759 mm to 992 mm (mean ± SD, 855.57 ± 71.64).

The whole-body effective dose from CT scan has ranged from 10.04 mSv to 21.98 mSv (mean ± SD, 14.45 ± 2.82).

4.2.3 The correlation between patient dose and factors affecting in CT scan using Monte Carlo Simulation

Figure 4.1, 4.2 and 4.3 are scattered diagram showing the correlation between the patient effective dose and its factor affecting patient dose of CT scan. The y-axis represents the patient effective dose in mSv. The x-axis represents the factors affecting patient dose. The scattered diagram shows the linear relationship between the patient body mass index and effective dose with the correlation coefficient of 0.866 (*p-value*<0.01), the linear relationship between mAs and effective dose with the correlation coefficient of 0.980 (*p-value*<0.01), and relationship between the scan length and effective dose with correlation coefficient of -0.179.

The correlation between the body mass index and mAs is shown in figure 4.4. The scattered diagram shows the linear relationship with correlation coefficient of 0.888 (*p-value*<0.01).

Table 4.3 Patient information and the effective dose (mSv) from CT scan

Pt. No.	Gender	Age (years)	Height (cm)	Weight (kg)	Scan length (mm)	BMI (kg/m^2)	mAs	Effective dose (mSv)
1	M	28	172	55	985	18.58	93	11.344
2	F	45	152	60	759	26.00	173	21.977
3	F	28	159	47	856	18.58	101	13.393
4	F	29	160	50	856	19.53	96	12.730
5	F	60	158	53	863	21.20	116	15.398
6	F	35	160	50	873	19.53	96	12.727
7	F	52	154	62	870	26.16	153	20.274
8	F	36	154	43	870	18.14	96	12.721
9	F	30	160	50	875	19.53	92	12.199
10	M	32	169	59	875	20.63	114	13.435
11	F	44	150	50	875	22.22	116	15.482
12	F	43	156	65	759	26.42	134	17.023
13	F	49	153	53	797	22.22	133	17.264
14	M	49	177	68	992	21.73	132	16.252
15	F	58	155	56	759	23.33	120	15.248
16	F	30	159	52	759	24.51	120	15.248
17	F	60	156	47	875	19.34	109	14.566
18	F	42	150	40	759	17.78	84	10.674
19	F	59	149	47	759	20.72	101	12.835
20	M	56	168	54	875	19.15	103	12.138
21	F	57	150	47	875	21.33	113	14.986
22	M	46	164	63	875	23.42	120	14.248
23	M	49	172	51	873	17.23	92	10.830
24	F	45	154	45	875	19.00	87	11.534
25	F	47	159	40	970	15.42	75	10.036
26	F	53	162	53	980	20.23	120	16.067
27	F	47	160	47	865	18.16	91	12.137
28	M	28	178	70	990	22.40	123	15.019
29	F	43	166	63	868	23.00	132	17.485
30	F	31	149	40	759	18.02	84	10.700
31	F	48	158	56	875	22.50	116	15.293
32	F	50	164	47	875	17.10	102	13.447
33	F	35	152	65	759	28.14	142	18.087
34	F	39	155	53	759	22.08	108	13.756
35	F	43	160	65	856	25.78	146	19.225

Figure 4.1 The correlation between patient Body Mass Index (kg/m^2) and effective dose (mSv) from CT scan, r = 0.866 (*p-value*<0.01)

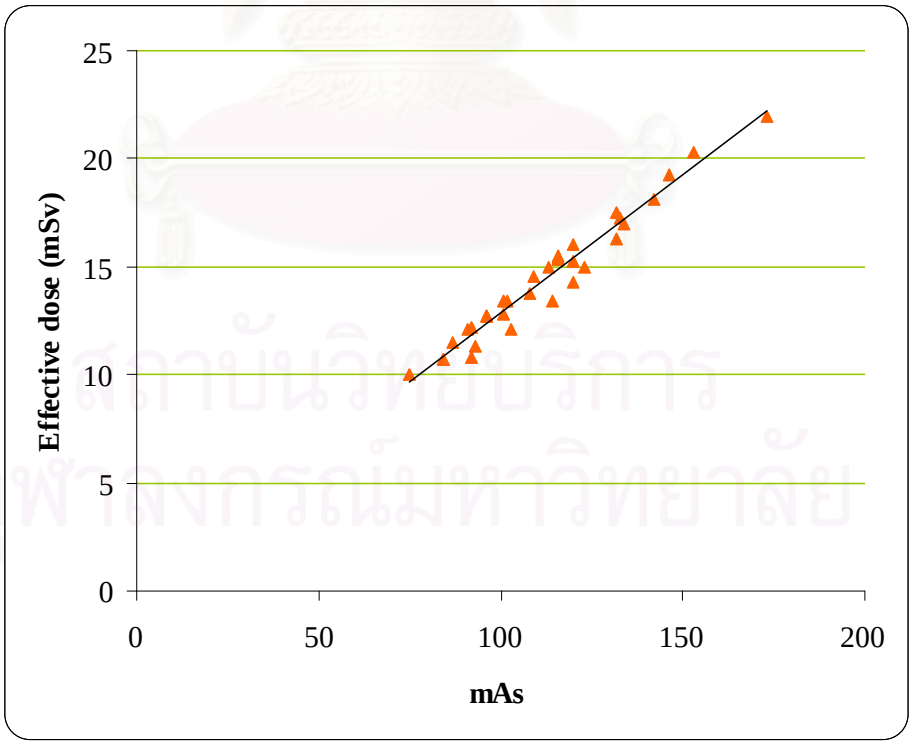

Figure 4.2 The correlation between mAs and effective dose (mSv) from CT scan, r = 0.980 (*p-value*<0.01)

Figure 4.3 The correlation between scan length (mm) and effective dose (mSv) from CT scan, r = -0.179

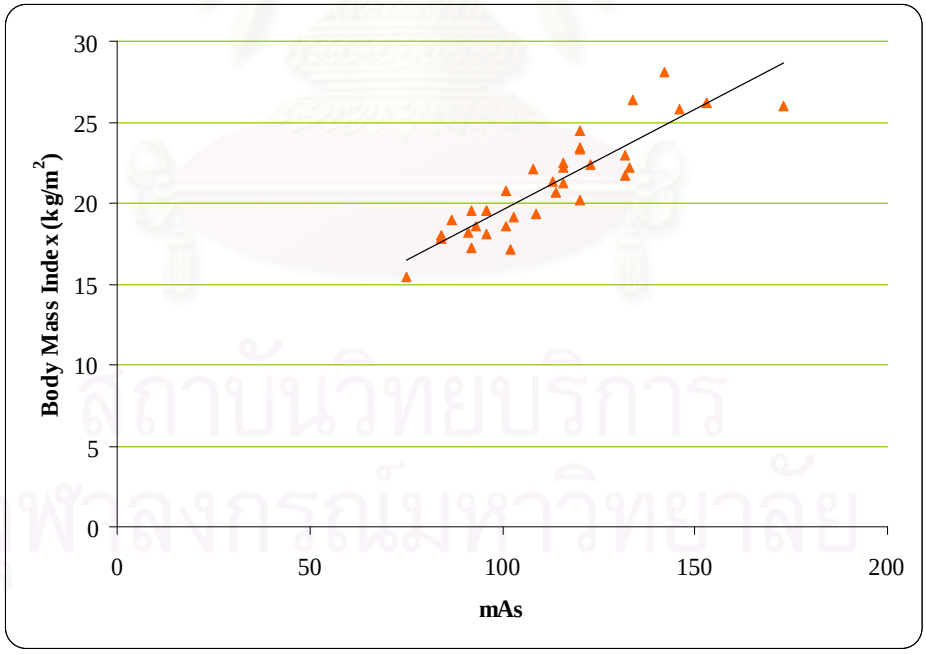

Figure 4.4 The correlation between mAs and Body Mass Index (kg/m^2), r = 0.888 (*p-value*<0.01)

4.3 Internal dose

4.3.1 Residence time (τ)

The residence time is related to the characteristics of both the physical and biological removal in target organ. The residence time in target organ calculated by the cumulative activity in target organ divided by the activity administered to patient.

In this study, 5 patients were collected to investigate mean residence time in the target organs. The mean residence time of ^{18}F-FDG in the 13 target organs, the liver, kidneys, lungs, urinary bladder, stomach, spleen, gonads, bone marrow, colon, bone surface, skin, thyroid and breast are presented in table 4.4. The standard deviation for target organs showed small number, and the highest mean residence time is 0.104 hour from liver.

Table 4.4 Mean residence time (hours) of ^{18}F-FDG

Target organ	Patient number					Mean ± SD
	1	2	3	4	5	
Liver	0.1100	0.0700	0.1000	0.1400	0.1000	0.104±0.0251
Kidneys	0.0290	0.0200	0.0250	0.0400	0.0310	0.030±0.0074
Lungs	0.0124	0.0140	0.0100	0.0160	0.0160	0.014±0.0026
Urinary bladder	0.0340	0.0400	0.0340	0.0460	0.0400	0.040±0.0050
Stomach	0.0160	0.0100	0.0100	0.0100	0.0110	0.011±0.0026
Spleen	0.0075	0.0053	0.0100	0.0120	0.0070	0.010±0.0026
Gonads	0.0037	0.0004	0.0004	0.0004	0.0004	0.001±0.0015
Bone marrow	0.0730	0.0630	0.0970	0.0710	0.0680	0.074±0.0132
Colon	0.0044	0.0130	0.0110	0.0170	0.0120	0.011±0.0046
Bone surface	0.1260	0.0790	0.0790	0.0840	0.0920	0.092±0.0197
Skin	0.0300	0.0270	0.0270	0.0260	0.0270	0.027±0.0015
Thyroid	0.0009	0.0006	0.0007	0.0010	0.0006	0.001±0.0002
Breast	0.0090	0.0090	0.0100	0.0100	0.0080	0.010±0.0008

4.3.2 Absorbed dose

The mean absorbed doses in 13 target organs were calculated in 35 patients as summarized in table 4.5, figure 4.5 and detail in table 4.6. The urinary bladder received the highest average absorbed doses of 63.72±9.41 μGy/MBq (mean ± SD), ranged from 46.21 μGy/MBq to 80.80 μGy/MBq. The skin received lowest average absorbed dose of 1.10±0.08 μGy/MBq (mean ± SD), ranged from 0.94 μGy/MBq to 1.14 μGy/MBq.

Table 4.5 Absorbed dose in 13 target organs (μGy/MBq)

Target organ	Max (μGy/MBq)	Min (μGy/MBq)	Mean ± SD (μGy/MBq)
Liver	39.50	21.50	29.83 ± 3.56
Kidneys	33.60	19.80	27.28 ± 3.53
Lungs	5.57	3.47	4.63 ± 0.59
Urinary bladder	80.80	46.21	63.72 ± 9.41
Stomach	15.36	8.84	11.57 ± 1.56
Spleen	18.50	8.72	14.79 ± 2.32
Gonads	20.98	7.71	11.46 ± 3.78
Bone marrow	24.80	14.16	18.11 ± 2.25
Colon	14.80	3.70	10.47 ± 1.97
Bone surface	26.23	16.45	21.33 ± 2.62
Skin	1.14	0.94	1.10 ± 0.08
Thyroid	13.80	6.43	10.44 ± 1.83
Breast	9.11	5.88	7.33 ± 0.90

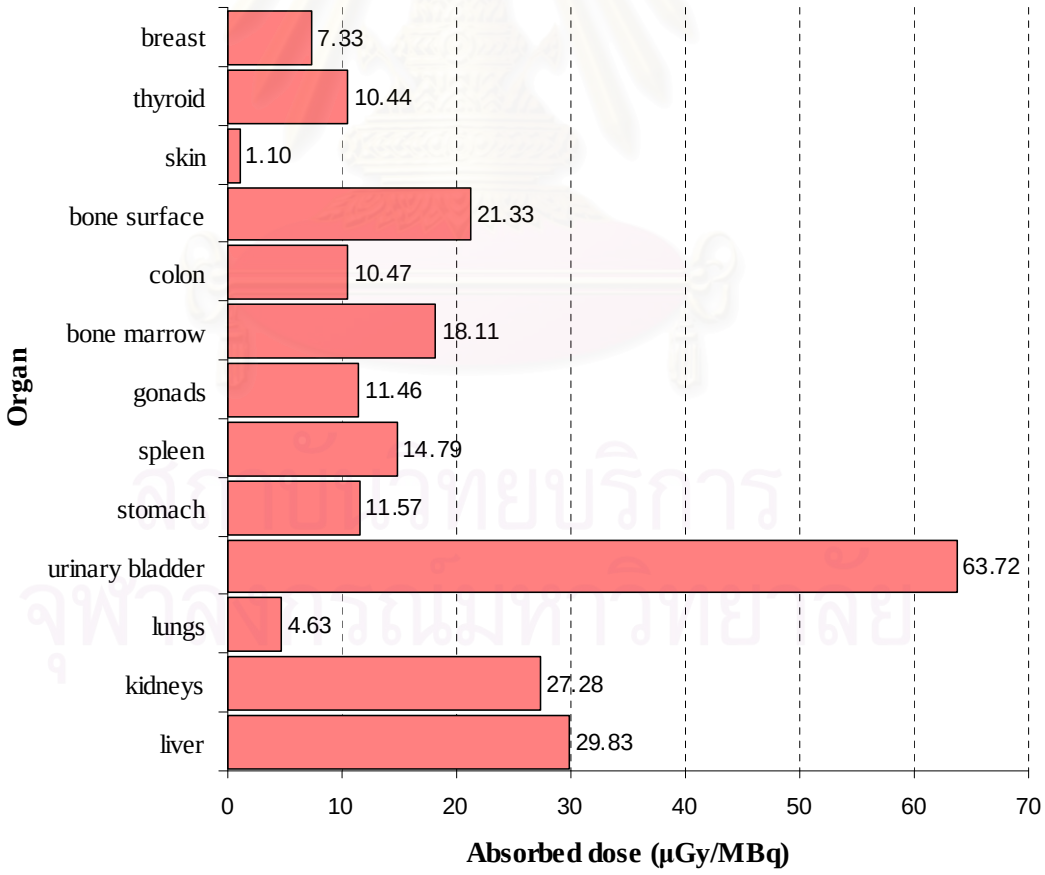

Figure 4.5 The average absorbed dose (μGy/MBq) in target organs

Table 4.6 Absorbed dose in target organs (μGy/MBq)

Target organ	Absorbed dose (μGy/MBq) Patient number																	
	1	2	3	4	5	6	7	8	9	10	11	12	13	14	15	16	17	18
Liver	27.38	21.5	30.1	39.5	29.4	31.3	29	33.2	31.3	25.17	31.3	28.6	30.06	23.86	30	30.06	32	34.2
Kidneys	25.49	19.8	23.7	33.6	28.3	28.5	24.7	31.6	28.5	24.29	28.5	24	27.4	22.11	26.4	27.4	29.7	33.4
Lungs	3.66	5.04	3.47	5.00	5.37	4.86	4.32	5.32	4.86	3.96	4.86	4.21	4.70	3.64	4.56	4.70	5.04	5.57
Urinary bladder	48.18	70.8	57.3	67.2	64.3	67.4	57	76.1	67.4	53.37	67.4	55	64.3	47.35	61.6	64.3	70.8	80.8
Stomach	15.36	11.4	10.9	9.96	11.5	12	10.3	13.5	12	10.02	12	9.97	11.5	9.02	11.1	11.5	12.6	14.2
Spleen	10.53	8.72	15.80	16.70	10.60	15.80	13.60	17.60	15.80	13.35	15.80	13.20	15.10	12.10	14.60	15.10	16.50	18.50
Gonads	19.65	10.50	9.88	8.27	9.32	9.88	8.07	11.50	9.88	18.51	9.88	7.71	9.32	16.40	8.82	9.32	10.50	12.10
Bone marrow	15.88	16.60	24.80	16.30	16.80	18.90	17.00	20.50	18.90	15.48	18.90	16.60	18.30	14.37	17.80	18.30	19.50	21.40
Colon	3.70	13.50	10.90	14.80	11.40	10.90	9.40	12.20	10.90	8.78	10.90	9.11	10.50	7.91	10.10	10.50	11.40	12.80
Bone surface	26.23	19.90	19.20	18.30	21.50	22.30	19.60	24.60	22.30	18.30	22.30	19.10	21.50	16.74	20.80	21.50	23.20	25.80
Skin	1.05	1.14	1.14	1.10	1.14	1.14	1.14	1.14	1.14	0.94	1.14	1.14	1.14	0.94	1.14	1.14	1.14	1.14
Thyroid	9.17	7.16	7.88	9.61	6.43	11.30	9.32	12.90	11.30	9.55	11.30	8.93	10.70	8.45	10.20	10.70	11.90	13.80
Breast	6.37	7.24	7.67	6.71	5.88	7.67	6.56	8.61	7.67	6.49	7.67	6.35	7.35	6.08	7.05	7.35	8.04	9.11
Pt. weight (kg)	55	47	50	60	53	50	62	43	50	59	50	65	53	68	56	53	47	40
Activity(MBq)	303	260	270	310	288	342	372	285	263	280	320	333	300	420	343	335	300	264

Table 4.6 Absorbed dose in target organs (μGy/MBq), continued.

Target organ	Absorbed dose (μGy/MBq) Patient number																
	19	20	21	22	23	24	25	26	27	28	29	30	31	32	33	34	35
Liver	32	25.89	32	24.54	26.71	32.6	34.2	30.06	32	23.62	29	34.2	30	32	28.6	30.06	28.6
Kidneys	29.7	25.49	29.7	23.24	26.87	30.7	33.4	27.4	29.7	21.69	24.7	33.4	26.4	29.7	24	27.4	24
Lungs	5.04	4.13	5.04	3.81	4.33	5.17	5.57	4.70	5.04	3.58	4.32	5.57	4.56	5.04	4.21	4.70	4.21
Urinary bladder	70.8	56.68	70.8	50.48	60.5	73.6	80.8	64.3	70.8	46.21	57	80.8	61.6	70.8	55	64.3	55
Stomach	12.6	10.56	12.6	9.54	11.2	13	14.2	11.5	12.6	8.84	10.3	14.2	11.1	12.6	9.97	11.5	9.97
Spleen	16.50	14.04	16.50	12.75	14.84	17.00	18.50	15.10	16.50	11.86	13.60	18.50	14.60	16.50	13.20	15.10	13.20
Gonads	10.50	19.65	10.50	17.50	20.98	10.20	12.10	9.32	10.50	16.02	8.07	12.10	8.82	10.50	7.71	9.32	7.71
Bone marrow	19.50	16.09	19.50	15.00	16.80	20.00	21.40	18.30	19.50	14.16	17.00	21.40	17.80	19.50	16.60	18.30	16.60
Colon	11.40	9.26	11.40	8.35	9.82	11.80	12.80	10.50	11.40	7.75	9.40	12.80	10.10	11.40	9.11	10.50	9.11
Bone surface	23.20	19.16	23.20	17.55	20.15	23.90	25.80	21.50	23.20	16.45	19.60	25.80	20.80	23.20	19.10	21.50	19.10
Skin	1.14	0.94	1.14	0.94	0.94	1.14	1.14	1.14	1.14	0.94	1.14	1.14	1.14	1.14	1.14	1.14	1.14
Thyroid	11.90	10.19	11.90	9.03	10.91	12.30	13.80	10.70	11.90	8.23	9.32	13.80	10.20	11.90	8.93	10.70	8.93
Breast	8.040	7.070	8.040	6.410	7.480	8.300	9.110	7.350	8.040	5.960	6.560	9.110	7.050	8.040	6.350	7.350	6.350
Pt. weight (kg)	47	55	47	63	51	45	40	53	47	70	62	40	56	47	65	53	65
Activity(MBq)	263	305	311	379	345	260	227	350	260	341	322	287	385	277	342	323	366

Table 4.7 The relation between mass of organ (g) and absorbed dose (μGy/MBq)

Target organ	Average mass of organ (g)	absorbed dose (μGy/MBq)	Number of patients
Liver	1371.7	29.83	35
Kidneys	236.2	27.28	35
Lungs	762.0	4.63	35
Urinary bladder	114.3	63.72	35
Stomach	190.5	11.57	35
Spleen	137.2	14.79	35
Testes	34.4	18.39	7
Ovaries	6.4	9.73	28
Bone marrow	1143.1	18.11	35
Colon	217.2	10.47	35
Bone surface	3048.2	21.33	35
Skin	2293.7	1.10	35
Thyroid	15.2	10.44	35
Breast	267.5	7.33	35

The summary of patient information, dose coefficient (μSv/MBq), the effective dose (mSv) from PET scan are shown in table 4.8 and are compared with the reported RADAR (Radiation Dose Assessment Resource) [25] dose estimates.

The Radiation Assessment Resource or the RADAR web site [25] provided information on dose assessment models and methods including the RADAR Medical Procedure Radiation Dose Calculator. This form gives radiation dose estimates for certain radiographic and nuclear medicine procedures based on literature reported values. Individual organ doses and total body effective doses are given for these specified examinations, and some combinations of examinations. In addition, a short statement is generated, which may be useful as part of a patient consent form document, explaining the radiation doses as numerical values and as equivalent days of exposure to natural background radiation.

Table 4.8 The dose coefficients (Γ_E^{FDG}) for ^{18}F-FDG and whole-body effective dose (mSv) from PET scan

Pt. No.	Gender	Age (years)	Weight (kg)	Activity (MBq)	Γ_E^{FDG} (μSv/MBq)	Effective dose (mSv)	RADAR values (mSv)
1	M	27	55	303	15.19	4.603	4.854
2	F	45	60	310	16.04	4.972	4.972
3	F	27	47	260	14.66	3.812	4.144
4	F	29	50	270	15.31	4.134	4.321
5	F	60	53	288	14.74	4.245	4.617
6	F	35	50	342	15.91	5.441	5.470
7	F	52	62	372	13.75	5.115	5.949
8	F	36	43	285	17.74	5.056	4.558
9	F	30	50	263	15.91	4.184	4.203
10	M	32	59	280	15.09	4.225	4.481
11	F	44	50	320	15.91	5.091	5.114
12	F	43	65	333	13.34	4.442	5.327
13	F	49	53	300	15.24	4.572	4.795
14	M	49	68	420	13.65	5.733	6.719
15	F	58	56	343	14.7	5.042	5.487
16	F	30	53	335	15.24	5.105	5.357
17	F	60	47	300	16.62	4.986	4.975
18	F	42	40	264	18.66	4.926	4.220
19	F	59	47	263	16.62	4.371	4.203
20	M	56	55	305	15.9	4.850	4.878
21	F	57	47	311	16.62	5.169	4.972
22	M	46	63	379	14.41	5.460	6.062
23	M	49	51	345	16.83	5.806	5.517
24	F	45	45	260	17.01	4.423	4.155
25	F	47	40	227	18.66	4.236	3.628
26	F	53	53	350	15.24	5.334	5.600
27	F	48	47	260	16.62	4.321	4.155
28	M	28	70	341	13.38	4.563	5.452
29	F	43	62	322	13.75	4.428	5.150
30	F	31	40	287	18.66	5.355	4.588
31	F	48	56	385	14.7	5.660	6.156
32	F	50	47	277	16.62	4.604	4.428
33	F	35	65	342	13.34	4.562	5.470
34	F	39	53	323	15.24	4.923	5.168
35	F	43	65	366	13.34	4.882	5.860

4.3.3 The effective dose from PET scan

The results from PET scan of calculated effective dose by two methods for 35 patients including ^{18}F-FDG injected activities are presented in table 4.9.

Table 4.9 Summary of the effective dose (mSv) and related factors from PET scan

	Min	Max	Mean ± SD
Dose coefficient (μSv/MBq)	13.34	18.66	15.56 ± 1.52
^{18}F-FDG Activity (MBq)	227	420	312 ± 43.45
Effective dose (mSv)	3.81	5.81	4.82 ± 0.5
RADAR values	3.63	6.72	5.00 ± 0.7

The average dose coefficient from administration of ^{18}F-FDG of 15.56±1.52 μSv/MBq, ranged from 13.34 μSv/MBq to 18.66 μSv/MBq. Average ^{18}F-FDG activities of 312±43.45 MBq were administered, ranged from 227 MBq to 420 MBq. The whole-body effective dose from PET scan of 4.82±0.5 mSv, ranged from 3.81 mSv to 5.81 mSv.

The result of effective dose estimates from the RADAR values of 5.00±0.7, ranged from 3.63 mSv to 6.72 mSv. The correlation between the effective dose from calculation and by RADAR dose estimates is shown in figure 4.6. The scattered diagram showed the linear relationship with correlation coefficient of 0.724 (*p-value*<0.01).

4.3.4 The correlation between patient dose and factors affecting PET scan

Figure 4.7 and 4.8 are scattered diagram showing the correlation between the patient effective dose and its factor affecting patient dose of PET scan. The y-axis represents the patient effective dose in mSv. The x-axis represents the factors affecting patient dose. The scattered diagram showed the effective dose is more depend on the activity of ^{18}F-FDG, r = 0.720 (*p-value*<0.01) than factor from patient weight, r = 0.128. The correlation coefficient between dose coefficient and patient weight has negative correlation, r = -0.906 (*p-value*<0.01) as shown in figure 4.9.

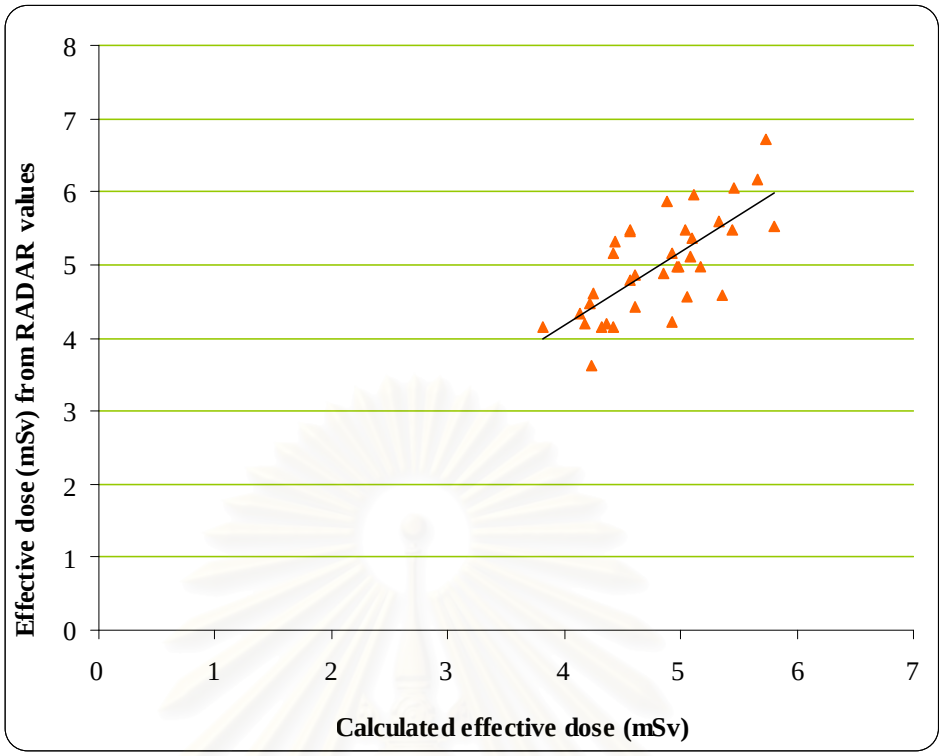

Figure 4.6 The correlation between effective dose (mSv) from calculated and RADAR values, r = 0.724 (*p-value*<0.01)

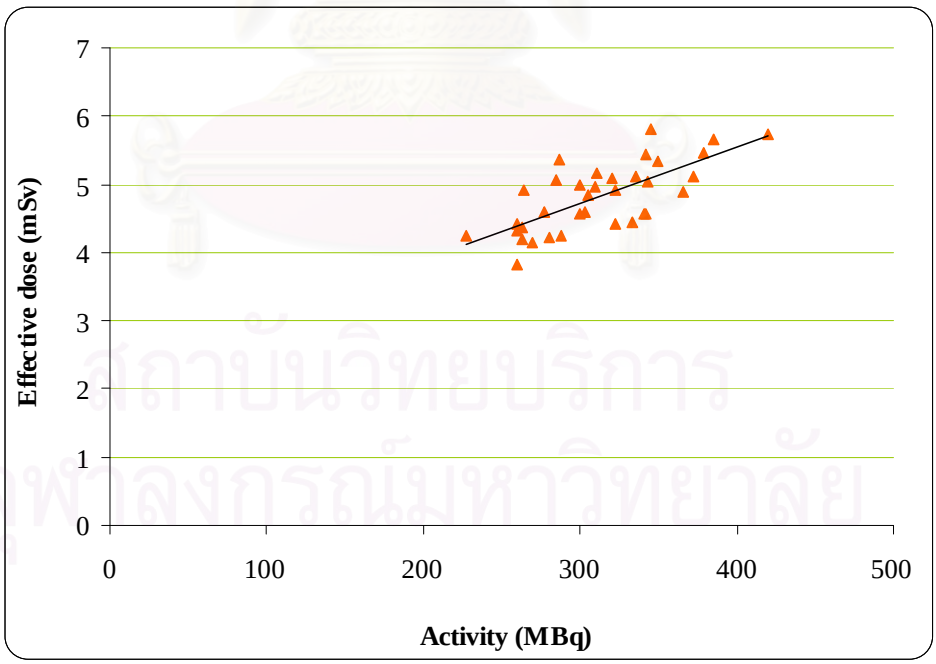

Figure 4.7 The correlation between activity of ^{18}F-FDG (MBq) and effective dose (mSv) from PET scan, r = 0.720 (*p-value*<0.01)

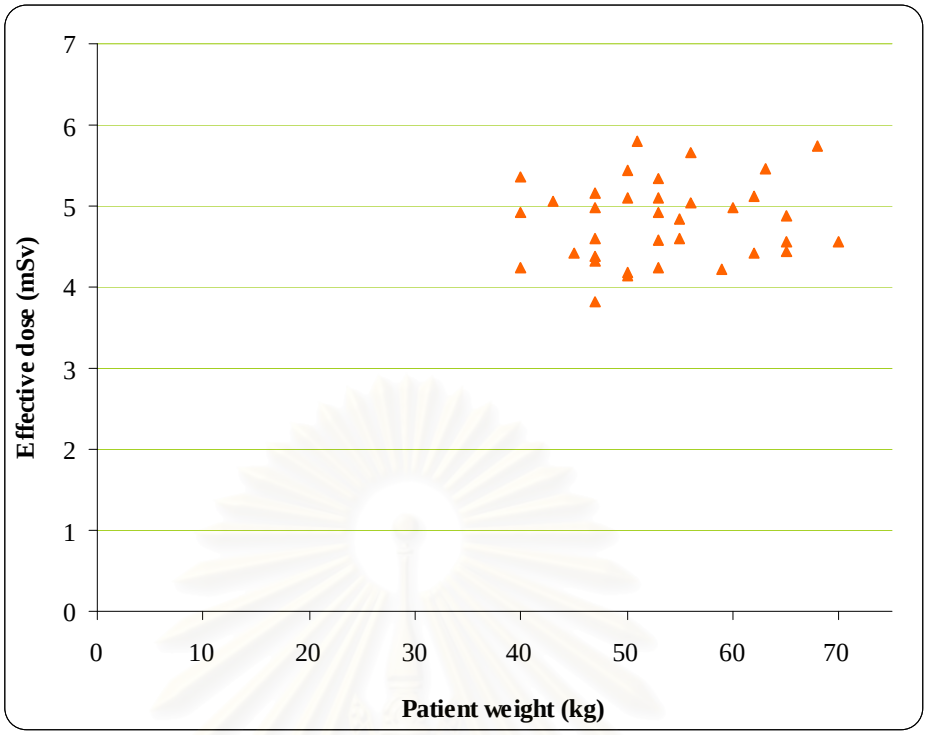

Figure 4.8 The correlation between patient weight (kg) and effective dose (mSv) from PET scan, r = 0.128

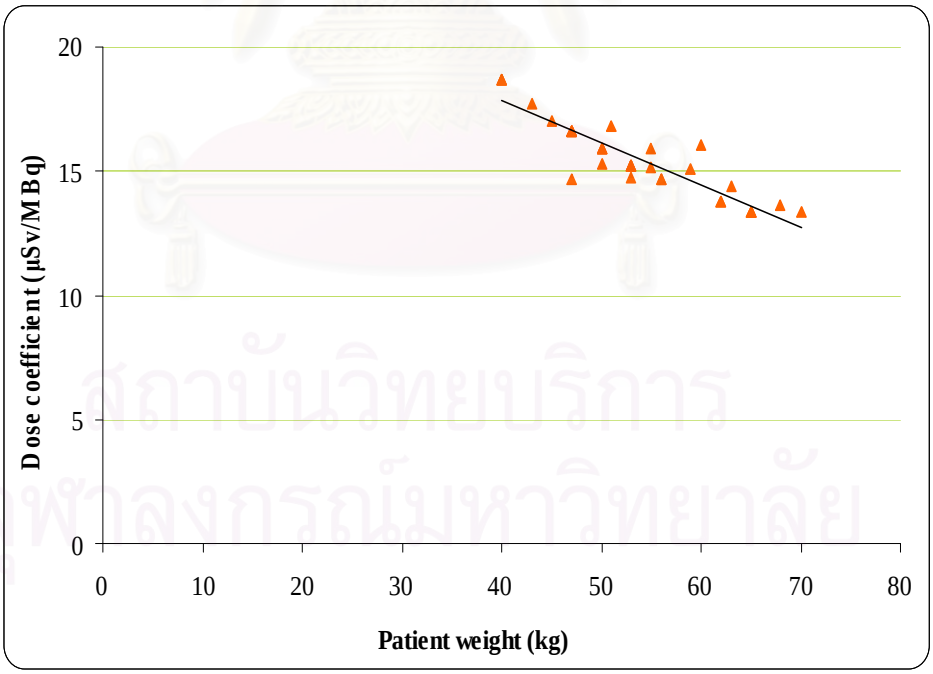

Figure 4.9 The correlation between patient weight (kg) and dose coefficient (µSv/MBq), r = -0.906 (*p-value*<0.01)

4.3.5 Patient dose from PET/CT examinations

Table 4.10 Summary data of patient dose from whole-body ^{18}F-FDG PET/CT examinations

Pt. No.	Weight (kg)	Activity (MBq)	BMI (kg/m^2)	Effective dose (mSv)		
				PET	CT	PET+CT
1	55	303	18.58	4.603	11.344	15.947
2	60	310	26.00	4.972	21.977	26.949
3	47	260	18.58	3.812	13.393	17.205
4	50	270	19.53	4.134	12.73	16.864
5	53	288	21.20	4.245	15.398	19.643
6	50	342	19.53	5.441	12.727	18.168
7	62	372	26.16	5.115	20.274	25.389
8	43	285	18.14	5.056	12.721	17.777
9	50	263	19.53	4.184	12.199	16.383
10	59	280	20.63	4.225	13.435	17.660
11	50	320	22.22	5.091	15.482	20.573
12	65	333	26.42	4.442	17.023	21.465
13	53	300	22.22	4.572	17.264	21.836
14	68	420	21.73	5.733	16.252	21.985
15	56	343	23.33	5.042	15.248	20.290
16	53	335	24.51	5.105	15.248	20.353
17	47	300	19.34	4.986	14.566	19.552
18	40	264	17.78	4.926	10.674	15.600
19	47	263	20.72	4.371	12.835	17.206
20	55	305	19.15	4.85	12.138	16.988
21	47	311	21.33	5.169	14.986	20.155
22	63	379	23.42	5.46	14.248	19.708
23	51	345	17.23	5.806	10.83	16.636
24	45	260	19.00	4.423	11.534	15.957
25	40	227	15.42	4.236	10.036	14.272
26	53	350	20.23	5.334	16.067	21.401
27	47	260	18.16	4.321	12.137	16.458
28	70	341	22.40	4.563	15.019	19.582
29	62	322	23.00	4.428	17.485	21.913
30	40	287	18.02	5.355	10.70	16.055
31	56	385	22.50	5.66	15.293	20.953
32	47	277	17.10	4.604	13.447	18.051
33	65	342	28.14	4.562	18.087	22.649
34	53	323	22.08	4.923	13.756	18.679
35	65	366	25.78	4.882	19.225	24.107

Table 4.11 Summary of effective dose (mSv) from PET/CT scan

	Min	Max	Mean ± SD
Effective dose from CT scan	10.04	21.98	14.45 ± 2.82
Effective dose from PET scan	3.81	5.81	4.82 ± 0.5
Effective dose from PET/CT scan	14.27	26.95	19.27 ± 2.92

The summary of effective dose from PET/CT examinations is presented in table 4.10 and table 4.11. The results shows that the average effective dose from CT scan was 14.45±2.82 mSv, ranged from 10.04 mSv to 21.98 mSv, the average whole-body effective dose from PET scan was 4.82±0.5 mSv, ranged from 3.81 mSv to 5.81 mSv. The average whole-body effective dose from PET/CT examination was 19.27±2.92 mSv, ranged from 14.27 mSv to 26.95 mSv.

CHAPTER 5

DISCUSSION AND CONCLUSION

5.1 Discussion

As PET/CT scan using ^{18}F-FDG has been widely used for metabolic studies it is necessary to determine the patient radiation absorbed dose. Some studies provide the type of human kinetic data needed for dosimetry such as International Commission on Radiological Protection (ICRP), publication 53 and 80 [26], present table of ^{18}F-FDG doses derived from a model assuming. In this study, the absorbed dose in target organ was calculated based on biokinetic data obtained in humans, Thai patient, after a bolus intravenous injection.

5.1.1 Comparison of measured and calculated CTDI

The calculated CTDI was higher than the measured CTDI in air 3.70 percent. These would make the effective dose calculated by these values less than the effective dose calculated using default values.

5.1.2 Comparison of patient dose to published data

The mean absorbed dose in target organs in this work was compared to other works as presented in table 5.1. All of the absorbed doses in target organ in this work except the lungs and skin, agree with other authors. The mean absorbed dose to each organ was less than the others according to the method of measurement. The absorbed dose in urinary bladder wall agrees with other studies.

The absorbed dose at target organs is comparable to Mejia el al [19], as the similar size of Japanese and Thai and estimated from data in humans. They used S tables derived for Japanese adults and based on a model of Japanese reference man.

The results in table 4.7 show that the absorbed dose is independent of the mass of the target organ. The size of the target organ affects the total amount of energy absorbed by the organ, but has little effects on the concentration [13]. Although the injected activity of ^{18}F-FDG was 4.75 MBq per kilogram, it is adequate in image quality. In addition, the PET/CT scan was acquired at 1 hour after injection which was correlated a maximum accumulation of FDG in tumors at about 45 minutes after injection.

The dose coefficient listed in table 4.8 can be used to estimate whole-body effective dose from PET scan, using the patient specific such as the age, sex and body weight. The dose coefficient and patient weight is inversely correlated with $r = -0.906$ (p-*value*<0.01). The S values for the European and American adult reference man are lower than the corresponding values for Thai. Thus, an underestimation of the absorbed dose to Thai patient would occur if the absorbed dose was calculated using European and American reference man.

The average effective dose for patients undergoing whole-body ^{18}F-FDG PET/CT examinations was 19.27 mSv, and the range was between 14.27 and 26.95 mSv. This is in comparable to Brix et al [3] study of average dose of 25 mSv for PET/CT. The average effective dose from CT scan using WinDose program was 14.45 mSv, and the range was between 10.04 and 21.98 mSv, these results agree with the effective dose determined by Brix et al. using thermoluminescent dosimeters (TLDs).

Table 5.1 Comparison of the absorbed dose in target organ of this study to other published data.

Target organ	Absorbed dose (µGy/MBq)			
	This study	MIRD 19 [2]	Mejia et al [20]	Brix et al [3]
Liver	29.83	24	23	11
Kidneys	27.28	21	30	
Lungs	4.63	15	10	10
Urinary bladder	63.72	73	66	160
Stomach	11.57			11
Spleen	14.79	15	22	
Gonads	11.46	11	15	13.5
Bone marrow	18.11	11	12	11
Colon	10.47			13
Bone surface	21.33			11
Skin	1.1			8
Thyroid	10.44			10
Breast	7.33			6.8

5.1.3 Comparison of the residence time to published data

The cumulative activity in target organ can be calculated by measure the organ activity at 1, 2, and 3 hours after injection, and interpolate to injected time using exponential equation to fit the time activity curve. The calculation includes physical and biological half-lives. The results agree with Mejia et al. They calculated the cumulative activity in some source organs by used only physical decay of the activity remaining in the organ after last measurement, indicated the residence time in some organs, such as liver, kidneys and spleen of this study with minimal difference. The comparison of residence time in target organs with other studies is presented in table 5.2.

Table 5.2 Comparison of the residence time (hour) in target organ of this study to other published data.

Target organs	This study	Mejia et al	Jones et al	Hays and Segall
Liver	0.11	0.11		0.15
Kidneys	0.029	0.03		
Lungs	0.012	0.02		0.07
Urinary bladder	0.034	0.12	0.2	0.09
Stomach	0.016			
Spleen	0.0075	0.01		
Gonads	0.004			
Bone marrow	0.073			
Colon	0.0044			
Bone surface	0.126			
Skin	0.03			
Thyroid	0.0009			
Breast	0.0006			

5.1.4 Factors affecting patient dose

The patient effective dose increases with increasing the patient BMI for CT scan. The correlation between patient BMI and patient dose were good, r = 0.866 (*p-value*<0.01). The patient BMI is directly affecting the mAs when using Automatic Exposure Control (AEC) for CT scan. The maximum BMI was 26 kg/m^2 as shown in table 4.3. The mAs and the patient dose increase with BMI. This means that the patient size is important predictor of patient dose. Whereas, the average scan length from CT scan was 855.57 ± 71.64 mm ranged from 759 mm to 992 mm. The correlation between patient dose and scan length were very poor with r = -0.179, as shown in figure 4.3. For PET scan, the patient dose increases with the activity of ^{18}F-FDG. The effective dose depends on the activity of ^{18}F-FDG rather than patient weight with correlation coefficient = 0.720 (*p-value*<0.01).

Although the MIRD method provides reasonable organ doses, the typical application of this technique includes several significant assumptions, limitation, and simplifications that, taken together, could result in differences between the true and calculated doses. These include the following:

1. The radioactivity is assumed to be uniform distributed in each source organ. This is rarely the case and, in fact, significant pathology or characteristics of the radiopharmaceutical may result in a highly nonuniform activity distribution.
2. The organ sizes and geometries are idealized into simplified shapes on aid mathematical computation.
3. Each organ is assumed to be homogeneous in density and composition.

4. The phantom for the reference is only approximations of the physical dimension of any given individual.

5. Dose contributions from minor radiation sources are ignored.

6. With a few exceptions, low energy photons and all particulate radiation are assumed to be absorbed locally.

5.2 Conclusion

Combined PET/CT scan are more than just a convenient diagnostic tool for acquiring perfectly registered functional and anatomic images. They represent a new generation of clinical imaging tools that highlight the complexity of multidisciplinary clinical decision making. In addition, they emphasize the crucial role of adequate workflow management when combined with appropriate technology and computer systems in providing efficient and cost-effective patient management.

As nuclear medicine has grown to include a substantial therapeutic component, the importance of radionuclide dosimetry has also grown. Radiation dosimetry is primarily of interest because radiation dose quantities serve as indices of the risk of biologic damage to the patient. The Medical Internal Radiation Dosimetry (MIRD) Committee of the Society of Nuclear Medicine has developed a methodology for calculating the radiation dose to selected organs and the whole body from internally administered radionuclides. The MIRD formalism takes into account variables associated with the deposition of ionizing radiation energy and those associated with the biologic system for which the dose is being calculated.

The average effective dose of patients undergoing whole-body ^{18}F-FDG PET/CT examinations at King Chulalongkorn Memorial Hospital, Thailand, was 19.27 mSv and the range between 14.27 and 26.95 mSv. The effective dose obtained from CT scan based on the Monte Carlo simulation and it is greater than the effective dose obtained from PET scan about 3 times. For WinDose Monte Carlo simulation program, when all parameters were fixed, the patient dose depends on mAs and patient gender rather than patient scan length. The PET/CT acquisition protocols examined in this study reflect the range of patient dose. The reduction of patient dose can be done by adjusting the protocol of PET/CT systems such as, kV, mAs, and optimization of activities of radiopharmaceutical administered to the patient. Using AEC mode in CT scan had benefit when used with small patient size such as Thai people. The benefits of this study are the records of patient dose and related information for ^{18}F-FDG PET/CT in the future.

REFERENCES

[1] Townsend DW, Carney JPJ, Yap JT, Hall NC. PET/CT Today and Tomorrow. Journal of Nuclear Medicine 2004; 45: 4S-14S.

[2] Hays MT, Watson EE, Thomas SR, Stabin MG. MIRD Dose Estimate Report No.19: Radiation Absorbed Dose Estimates from ^{18}F-FDG. Journal of Nuclear Medicine 2002; 43: 210-14.

[3] Brix G, Lechel U, Glatting G, Ziegler SI, Munzing W, Muller SP, et al. Radiation Exposure of Patients Undergoing Whole-Body Dual Modality ^{18}F-FDG PET/CT Examinations. Journal of Nuclear Medicine 2005; 46: 608-13.

[4] Health Physics Society. Radiation term and definitions. Available at : *http://hps.org/publicinformation/radterms.*

[5] Mettler FA, Guiberteau MJ. Positron Emission Tomography (PET) Imaging. Essentials of Nuclear Medicine Imaging 2005; 5: 359-80.

[6] Tarantola G, Zito F, Gerundini P. PET Instrumentation and Reconstruction Algorithms in Whole-Body Applications. Journal of Nuclear Medicine 2003; 44: 756–69.

[7] NEMA Standards Publication NU 2-2001. Performance Measurements of Positron Emission Tomographs; 2001.

[8] McNitt-Gray MF.The AAPM/RSNA Physic Tutorial for Residents: radiation dose in CT. Radiographics 2002; 22 :1541-53.

[9] Toohey RE, Stabin MG, Watson EE. The AAPM/RSNA Physics Tutorial for Residents: Internal Radiation Dosimetry: Principles and Applications. Radiographics 2000; 20: 533-46.

[10] Stabin MG, Siegel JA. Physical models and dose factors for use in internal assessment. Health Physics 2003; 85: 294-310.

[11] International Commission on Radiological Protection. 1990 Recommendations of the International Commission on Radiological Protection. ICRP Publication 60; Pergamon Press; New York 1991.

[12] Sgouros G. Dosimetry of internal emitters. Journal of Nuclear Medicine 2005; suppl: 18-27.

[13] Sprawls P. Radionuclide Dosimetry. Physical Principle of Medical Imaging 1995; 2: 579-606.

[14] Loevinger R, Budinger T, Watson E. MIRD Prime for Absorbed Dose Calculations. Society of Nuclear Medicine: 1998.

[15] Bushberg JT, Seibert JA, Leidholdt EM, Boone JM. Radiopharmaceutical Dosimetry: MIRD Method. The essential physics of medical imaging 2002; 2: 805-12.

[16] Snyder WS, Ford MR, Warner GG, Watson SB. "S" Absorbed dose per unit cumulated activity for selected radionuclides and organs. MIRD Pamphlet No 11. Society of Nuclear Medicine 1975; 1-10.

[17] Stabin MG. MIRDOSE: personal computer software for internal dose assessment in nuclear medicine. Journal of Nuclear Medicine. 1996; 37: 538-46.

[18] Kim JH, Whang JH, Kim CS. Radiation Protection Dosimetry. Oxford journal 2006; 118: 395–401.

[19] Mejia AA, Nakamura T, Masatoshi I, Hatazawa J, Mazaki M, Watanuki S. Estimation of absorbed doses in humans due to intravenous administration of fluorine-18-fluorodeoxyglucose in PET studies. Journal of Nuclear Medicine 1991; 32: 699–706.

[20] Siemens Medical solutions. LSO PET/CT HI-REZ 16 Product Specification Manual; 2004.

[21] Kalender WA, Schmidt B, Zankl M, Schmidt M. A PC program for estimating organ dose and effective dose values in computed tomography. European Radiology 1999; 9:555-62.

[22] Scanditronix Wellhofer. Calibration protocol for chamber DCT10-RS manual.

[23] International Commission on Radiological Protection: Report of the Task Group on Reference Man, ICRP Publication 23, Pergamon Press, New York, NY, 1975.

[24] ICRP Publication 26.Recommendations of the International Commission on Radiological Protection 1977. Oxford: Pergamon Press.

[25] RADAR Medical Procedure Radiation Dose Calculator and Consent Language Generator. Available at : *www.doseinfo-radar.com/RADAROver.html*.

[26] Radiation Dose to Patients from Radiopharmaceuticals. Oxford: U.K.: Pergamon Press; 1999; 76. ICRP Publication 80, Addendum 2 to ICRP Publication 53.

APPENDICES

APPENDIX A

Table I. Masses of the organs and tissues (unit:g) [23]

Organ	Reference man ICRP 23
Adrenal glands	20
Blood	5,400
Brain	1,500
Breast	26
Eyes	30
Esophagus	40
Fat	10,000
Gall bladder	10
Gastrointestinal tract	2,000
Heart	330
Kidneys	310
Liver	1,800
Lymphoid tissue	700
Lung	1,000
Miscellaneous(blood vessels, cartilage, nerves, etc.)	390
Muscle	30,000
Pancreas	70
Prostate gland	20
Salivary glands	50
Skeleton	10,000
Skin and subcutaneous tissue	6,100
Spinal cord	30
Spleen	150
Stomach	250
Teeth	20
Testes	40
Thymus	10
Thyroid gland	20
Urinary bladder	150
Total body	70,000

APPENDIX B

Case Record Form ^{18}F-FDG PET/CT Examinations

Date of exam …..……

Patient no ……

Sex…….. Age……(years)

Patient height……..(cm) Patient weight…….(kg)

Patient BMI ……(kg/m^2)Activity ^{18}F-FDG…….(MBq)

Injection time…….Start scan time……

Finish scan time……..Scan length……..(cm)

CTDI$_{vol}$ ……..(mGy)DLP…….(mGy.cm)

APPENDIX C

Patient consent form

ข้อมูลสำหรับผู้เข้าร่วมวิจัย

การวิจัย เรื่อง การหาปริมาณรังสีในผู้ป่วยจากการตรวจ PET/CT ด้วย ^{18}F-FDG

เรียน ผู้เข้าร่วมวิจัยทุกท่าน

ท่านเป็นผู้ที่ได้รับเชิญให้เข้าร่วมการศึกษาวิจัยการหาปริมาณรังสีในผู้ป่วยจากการตรวจ PET/CT ด้วย ^{18}F-FDG และปัจจัยที่ส่งผลต่อปริมาณรังสีที่ผู้ป่วยได้รับจากการตรวจ PET/CT โดยก่อนที่ท่านจะตกลงเข้าร่วมการศึกษาดังที่ได้กล่าว ขอเรียนให้ท่านทราบถึงเหตุผลและรายละเอียดของการศึกษาวิจัยในครั้งนี้

เนื่องจากการตรวจด้วย PET/CT ผู้ป่วยจะได้รับรังสีจากภายในและภายนอกร่างกาย โดยที่รังสีภายนอกได้จากเอกซเรย์คอมพิวเตอร์และภายในร่างกายได้จากสารเภสัชรังสีที่ฉีดเข้าสู่เส้นเลือดดำ ซึ่งในประเทศไทยยังไม่มีรายงานเกี่ยวกับเรื่องดังกล่าว

ดังนั้นการศึกษาวิจัยในครั้งนี้ มีวัตถุประสงค์เพื่อ หาปริมาณรังสีที่ผู้ป่วยได้รับจากการตรวจ PET/CT ด้วยการฉีดสารเภสัชรังสี (^{18}F-FDG)ในการตรวจแต่ละครั้งว่ามีปริมาณรังสีเป็นเท่าไร เกินมาตรฐานที่กำหนดไว้หรือไม่ และยังเป็นการศึกษาถึงปัจจัยที่มีผลต่อปริมาณรังสีที่ผู้ป่วยจะรับจากการตรวจดังกล่าว

ประโยชน์ของการวิจัยในครั้งนี้ คือ ทำให้ได้ซึ่งข้อมูลขั้นพื้นฐานของปริมาณรังสีที่ผู้ป่วยได้รับจากการตรวจ PET/CT ในประเทศไทย เพื่อเป็นข้อมูลอ้างอิงและประโยชน์ต่อผู้ป่วยที่เข้ารับการตรวจในอนาคตข้างหน้า โดยเฉพาะผู้ป่วยที่อยู่ในช่วงวัยเจริญพันธุ์ และท่านยังจะได้ทราบถึงปริมาณรังสีที่ท่านได้รับจากการตรวจในครั้งนี้ ซึ่งเราจะแจ้งให้ท่านทราบภายหลังจากที่การวิจัยเสร็จสิ้นแล้ว

หากท่านตกลงที่จะเข้าร่วมการศึกษาวิจัยนี้จะมีข้อปฏิบัติร่วมกันดังต่อไปนี้

1. ท่านจะต้องดื่มน้ำ 1 ลิตร ในระหว่างการตรวจ
2. หลังจากฉีดสารเภสัชรังสีแล้ว ต้องนอนพักโดยไม่ทำกิจกรรมใดๆประมาณ 1 ชั่วโมง ในห้องที่จัดเตรียมไว้ให้ เพื่อให้สารเภสัชรังสีจับรอยโรคได้ดี
3. ท่านต้องปัสสาวะให้เรียบร้อยก่อนเข้าห้องตรวจ
4. หลังจากที่ทำการตรวจตามปกติแล้ว จะทำการตรวจเพิ่มเติมอีก 2 ครั้ง ซึ่งเป็นการตรวจเหมือนการตรวจตามปกติ โดยไม่ฉีดสารเภสัชรังสีเพิ่มเติม รวมระยะเวลาในการเข้าร่วมงานวิจัยประมาณ 3-4 ชั่วโมง

การเข้าร่วมวิจัยนี้ เป็นไปโดยสมัครใจ และไม่มีค่าตอบแทนใดๆ ท่านอาจปฏิเสธที่จะเข้าร่วมหรือถอนตัวจากการวิจัยนี้ได้ทุกเมื่อ ซึ่งผลการศึกษาวิจัยในครั้งนี้ จะใช้สำหรับวัตถุประสงค์ทางวิชาการเท่านั้น โดยข้อมูลต่างๆจะไม่มีการเปิดเผยสู่สาธารณชนและจะไม่มีการเปิดเผยชื่อของท่านตามกฎหมาย

หากท่านมีปัญหาหรือข้อสงสัยประการใด กรุณาติดต่อ นายกิติวัฒน์ คำวัน ผู้วิจัย เบอร์โทรศัพท์ 086-7068301 ซึ่งยินดีให้คำตอบแก่ท่านทุกเมื่อ

ขอขอบคุณในความร่วมมือของท่านมา ณ โอกาสนี้

.....

ใบยินยอมเข้าร่วมการวิจัย (Consent form)

การวิจัยเรื่อง การหาปริมาณรังสีในผู้ป่วยจากการตรวจ PET/CT ด้วย ^{18}F-FDG

วันให้คำยินยอม วันที่ .....เดือน.....พ.ศ. .....

ก่อนที่จะลงนามในใบยินยอมให้ทำการวิจัยนี้ ข้าพเจ้าได้รับการอธิบายจากผู้วิจัยถึงวัตถุประสงค์ของการทำวิจัย วิธีการวิจัย อันตรายหรืออาการที่อาจจะเกิดขึ้นจากการทำวิจัย รวมถึงประโยชน์ที่ได้รับจากการทำวิจัยอย่างละเอียดและมีความเข้าใจดีแล้ว

ผู้วิจัยรับรองว่าจะตอบคำถามต่างๆที่ข้าพเจ้าสงสัยด้วยความเต็มใจไม่ปิดบังซ่อนเร้นจนข้าพเจ้าพอใจ

ข้าพเจ้ามีสิทธิ์ที่จะบอกเลิกการเข้าร่วมในโครงการวิจัยนี้เมื่อใดก็ได้และเข้าร่วมโครงการวิจัยนี้โดยสมัครใจ และการบอกเลิกการเข้าร่วมการวิจัยนี้จะไม่มีผลใดๆต่อข้าพเจ้า

ผู้วิจัยรับรองว่าจะเก็บข้อมูลเกี่ยวกับตัวข้าพเจ้าไว้เป็นความลับ และจะเปิดเผยได้เฉพาะในรูปที่เป็นสรุปผลการวิจัย และการเปิดเผยข้อมูลเกี่ยวกับตัวข้าพเจ้าต่อหน่วยงานต่างที่เกี่ยวข้องจะทำได้ในเฉพาะกรณีที่จำเป็นด้วยเหตุผลทางวิชาการเท่านั้น

ข้าพเจ้าได้อ่านข้อความข้างต้นแล้ว และมีความเข้าใจดีทุกประการ และได้ลงนามในใบยินยอมนี้ด้วยความเต็มใจ

ลงนาม ..... ผู้ยินยอม
( )

ลงนาม ..... พยาน
( )

ลงนาม ..... พยาน
( )

ลงนาม ..... ผู้ทำวิจัย
( )

APPENDIX D

PET/CT daily QC

The daily quality control program for CT and PET is regularly performed using water phantom for the study of CT image quality, kVp calibration, pixel noise and CT number values. The Ge/Ga-68 phantom is used for PET daily QC, to check chi-square value, for detector for response, or performance of detectors. Two-bed test is checking the match-registration between PET and CT scan, as displayed in the output screen as in figure I (A) and I (B).

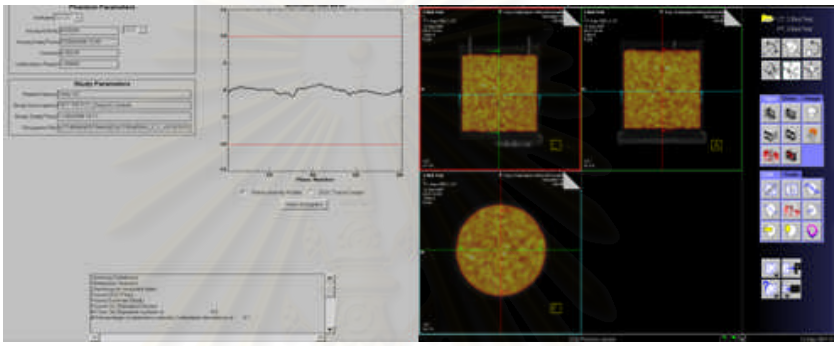

Figure I Chi-square values output screen (A) and two-bed test output screen (B)

1. Ge/Ga-68 phantom

The cylindrical uniform phantom as shown in figure II is Ge/Ga-68 phantom, Model CS-20-1, activity 54 MBq, with diameter 20 cm and 20 cm length cylinder. Ge/Ga-68 phantom used for PET calibration as daily test. ^{68}Ga decays to stable ^{68}Ge by positron emission with a half-life of 288 days.

Figure II Ge/Ga-68 phantom

Table II. The results of quality control of PET/CT system.

July 2007

Date	CT			PET				
	Check up	Quality	Chi-square	2 bed test	trues (cps)	random (cps)	single (cps)	Temp. (°C)
2/07/07	√	√	0.9	√	78.9k	7.8k	2850k	20
3/07/07	√	√	0.9	√	78.6k	7.8k	2850k	20
4/07/07	√	√	0.9	√	78.3k	7.8k	2844k	20
5/07/07	√	√	0.9	√	78.3k	7.7k	2843k	20
6/07/07	√	√	1.0	√	77.9k	7.7k	2833k	20
9/07/07	√	√	0.9	√	77.2k	7.6k	2815k	20
10/07/07	√	√	1.0	√	76.9k	7.6k	2809k	20
11/07/07	√	√	1.1	√	76.3k	7.6k	2810k	21
12/07/07	√	√	1.0	√	77.4k	7.5k	2801k	21
13/07/07	√	√	1.0	√	77.0k	7.5k	2798k	20
16/07/07	√	√	1.0	√	76.8k	7.4k	2786k	20
17/07/07	√	√	0.9	√	76.1k	7.3k	2776k	20
18/07/07	√	√	0.8	√	75.9k	7.4k	2772k	20
19/07/07	√	√	0.8	√	75.9k	7.3k	2768k	20
20/07/07	√	√	0.8	√	76.1k	7.3k	2763k	20
23/07/07	√	√	0.9	√	75.7k	7.2k	2742k	20
24/07/07	√	√	0.9	√	75.1k	7.2k	2738k	20
25/07/07	√	√	0.8	√	75.1k	7.1k	2735k	20
26/07/07	√	√	0.9	√	74.6k	7.1k	2726k	20
27/07/07	√	√	0.9	√	74.5k	7.1k	2722k	20

August 2007

Date	CT			PET				
	Check up	Quality	Chi-square	2 bed test	trues (cps)	random (cps)	single (cps)	Temp. (°C)
1/08/07	√	√	0.9	√	73.8k	7.0k	2694k	20
3/08/07	√	√	0.9	√	73.5k	6.9k	2690k	20
6/08/07	√	√	0.9	√	72.5k	6.8k	2677k	20
7/08/07	√	√	0.9	√	72.5k	6.8k	2663k	20
8/08/07	√	√	0.9	√	72.3k	6.8k	2659k	20
10/08/07	√	√	0.9	√	72.0k	6.7k	2660k	20
15/08/07	√	√	0.9	√	71.2k	6.6k	2628k	20
16/08/07	√	√	0.9	√	70.6k	6.5k	2625k	20
21/08/07	√	√	0.9	√	69.7k	6.5k	2599k	20
22/08/07	√	√	0.9	√	69.7k	6.5k	2599k	20
23/08/07	√	√	0.9	√	68.9k	6.4k	2590k	20
24/08/07	√	√	0.9	√	69.1k	6.4k	2587k	20
27/08/07	√	√	0.9	√	68.9k	6.4k	2579k	20
28/08/07	√	√	0.9	√	68.5k	6.3k	2572k	20
29/08/07	√	√	0.9	√	68.2k	6.3k	2562k	20
30/08/07	√	√	0.9	√	67.9k	6.3k	2559k	20
31/08/07	√	√	0.9	√	67.9k	6.2k	2552k	20

September 2007

Date	CT				PET			
	Check up	Quality	Chi-square	2 bed test	trues (cps)	random (cps)	single (cps)	Temp. (°C)
3/09/07	√	√	0.9	√	67.5k	6.26k	2544k	21
4/09/07	√	√	0.9	√	67.2k	6.20k	2532k	20
5/09/07	√	√	0.9	√	67.0k	6.20k	2532k	20
6/09/07	√	√	0.9	√	66.4k	6.10k	2532k	20
7/09/07	√	√	0.9	√	66.7k	6.10k	2520k	20
10/09/07	√	√	0.9	√	66.4k	6.10k	2513k	20
11/09/07	√	√	0.9	√	65.8k	6.00k	2509k	20
12/09/07	√	√	0.9	√	65.6k	6.00k	2504k	20
13/09/07	√	√	0.9	√	65.3k	6.10k	2502k	20
14/09/07	√	√	0.9	√	65.4k	6.00k	2498k	20
17/09/07	√	√	0.9	√	64.6k	5.90k	2484k	20
19/09/07	√	√	0.9	√	64.5k	5.80k	2474k	20
20/09/07	√	√	0.8	√	64.1k	5.80k	2467k	20
21/09/07	√	√	0.9	√	64.0k	5.80k	2458k	20
24/09/07	√	√	0.9	√	63.7k	5.70k	2452k	20
25/09/07	√	√	0.9	√	63.6k	5.70k	2448k	20
26/09/07	√	√	0.9	√	63.3k	5.70k	2443k	20
27/09/07	√	√	0.9	√	63.0k	5.70k	2436k	20
28/09/07	√	√	0.9	√	63.0k	5.70k	2437k	20

October 2007

Date	CT				PET			
	Check up	Quality	Chi-square	2 bed test	trues (cps)	random (cps)	single (cps)	Temp. (°C)
1/10/07	√	√	0.9	√	62.3k	5.6k	2419k	20
2/10/07	√	√	0.9	√	61.6k	5.6k	2419k	20
3/10/07	√	√	0.9	√	62.4k	5.6k	2420k	20
4/10/07	√	√	0.9	√	61.5k	5.6k	2404k	20
5/10/07	√	√	0.9	√	61.6k	5.4k	2401k	20
8/10/07	√	√	0.9	√	61.4k	5.4k	2390k	20
9/10/07	√	√	0.9	√	60.5k	5.5k	2387k	20
10/10/07	√	√	0.9	√	60.9k	5.4k	2385k	20
11/10/07	√	√	0.9	√	60.7k	5.4k	2383k	20
12/10/07	√	√	0.9	√	60.3k	5.4k	2374k	20
22/10/07	√	√	1.2	√	58.5k	5.2k	2326k	20
25/10/07	√	√	1.2	√	59.0k	5.1k	2316k	20
26/10/07	√	√	1.2	√	59.4k	5.1k	2315k	20
29/10/07	√	√	1.2	√	58.3k	5.0k	2299k	21
30/10/07	√	√	1.2	√	58.7k	5.1k	2298k	20
31/10/07	√	√	1.2	√	58.4k	5.1k	2295k	20

November 2007

Date	CT				PET			
	Check up	Quality	Chi-square	2 bed test	trues (cps)	random (cps)	single (cps)	Temp. (°C)
1/11/07	√	√	1.2	√	58.1k	5.0k	2291k	20
2/11/07	√	√	0.9	√	58.1k	5.0k	2285k	20
5/11/07	√	√	1.0	√	57.4k	5.0k	2273k	20
6/11/07	√	√	0.9	√	56.6k	4.9k	2268k	20
7/11/07	√	√	1.2	√	57.3k	5.0k	2267k	20
8/11/07	√	√	1.2	√	56.9k	5.0k	2265k	20
9/11/07	√	√	1.2	√	56.5k	5.0k	2253k	21
16/11/07	√	√	1.2	√	56.1k	4.8k	2233k	20
19/11/07	√	√	1.2	√	55.7k	4.8k	2219k	20
21/11/07	√	√	1.2	√	55.3k	4.7k	2216k	20
23/11/07	√	√	1.2	√	54.3k	4.7k	2213k	20
26/11/07	√	√	1.2	√	54.7k	4.6k	2195k	20
29/11/07	√	√	0.9	√	54.6k	4.6k	2187k	21

December 2007

Date	CT				PET			
	Check up	Quality	Chi-square	2 bed test	trues (cps)	random (cps)	single (cps)	Temp. (°C)
3/12/07	√	√	0.9	√	54.16k	4.54k	2171k	20
4/12/07	√	√	0.9	√	53.95k	4.56k	2161k	21
6/12/07	√	√	0.9	√	53.90k	4.49k	2161k	20
7/12/07	√	√	0.9	√	53.59k	4.49k	2150k	20
11/12/07	√	√	0.9	√	55.38k	4.90k	2141k	20
12/12/07	√	√	0.9	√	52.90k	4.42k	2138k	20
13/12/07	√	√	0.9	√	53.43k	4.50k	2131k	20
14/12/07	√	√	0.9	√	54.10k	4.83k	2135k	20
15/12/07	√	√	0.9	√	54.00k	4.83k	2121k	20
18/12/07	√	√	0.9	√	54.00k	4.75k	2112k	20
19/12/07	√	√	0.9	√	54.00k	4.80k	2110k	20
20/12/07	√	√	0.9	√	51.30k	4.30k	2114k	20
21/12/07	√	√	0.9	√	51.30k	4.30k	2106k	21
25/12/07	√	√	0.9	√	52.80k	4.79k	2097k	20
26/12/07	√	√	0.9	√	50.90k	4.10k	2090k	20
27/12/07	√	√	0.9	√	50.60k	4.20k	2087k	20
28/12/07	√	√	0.9	√	50.50k	4.16k	2085k	20

cps – count per second
k – 10^3
Temp – temperature
°C – degree Celsius

NEMA Standards Publication NU 2-2001 [7]

Performance Measurements of Positron Emission Tomographs

PET phantom for test performance characteristic of PET scan

The requirement of NEMA NU2-2001 for test performance characteristic of PET scan was introduced PET phantom set, consist of torso phantom IEC/2001, scatter phantom and sensitivity phantom.

1. Total performance phantom [7]

The phantom as show in figure III, is an International Electric Commission (IEC) body phantom set, used for evaluated image quality in PET scan, which consists of a torso cavity, removable lung insert, and 6 fillable spheres with inner diameter of 10, 13, 17, 22, 28 and 37 mm and wall thickness of 1 mm. A cylindrical insert filled to simulate the attenuation of lung with outside dimension 51 mm diameter and 180 mm length and wall thickness less than 4 mm, it was centered inside the body phantom.

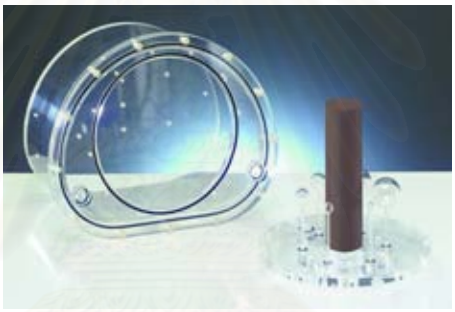

Figure III Torso phantom

2. Scatter phantom [7]

The phantom as shown in figure IV, is a scatter phantom set, used for evaluated the scatter fraction and noise equivalent count rate. This phantom including a solid circular cylinder composed of polyethylene with a specific gravity of 0.96, an outside diameter of 203 mm, an overall length of 700 mm, and a plastic tube that is 800 mm long and has an inner diameter of 3.2 mm to hold the source activity.

Figure IV Scatter phantom

3. Sensitivity phantom [7]

The phantom as shown in figure V, is a sensitivity phantom set. These phantom used for evaluated sensitivity of detector of PET scan, consists of 5 concentric aluminum tubes, each long 700 mm, and a 1.8 mL fillable polyethylene tube inserted into the center sleeve.

Figure V Sensitivity phantom

The performance tests are consisting of:

A. Spatial resolution
B. Scatter fraction
C. Sensitivity
D. Image quality

A. Spatial resolution

The purpose of this measurement is to characterize the widths of the reconstructed image point spread functions (PSF) of compact radioactive sources. The width of the spread function is measured by its full width at half-maximum amplitude (FWHM) and full width at tenth-maximum amplitude (FWTM).

Method

The spatial resolution is measured in the transverse slice in 2 directions, radially and tangentially, and in the axial direction. Point sources of ^{18}F are imaged in air. The point source consists of a small quantity of concentrated radioactivity inside a glass capillary. The resolution is measured with the sources at 6 locations. Two axial positions are selected, the center of the axial FOV and a position one fourth of the axial FOV from the center. For both axial locations, the source is imaged at 3 positions, (a) $x = 0$ and $y = 1$ cm, (b) $x = 0$ and $y = 10$ cm, and (c) $x = 10$ and $y = 0$ cm. The source arrangement is shown diagrammatically in Figure VI.

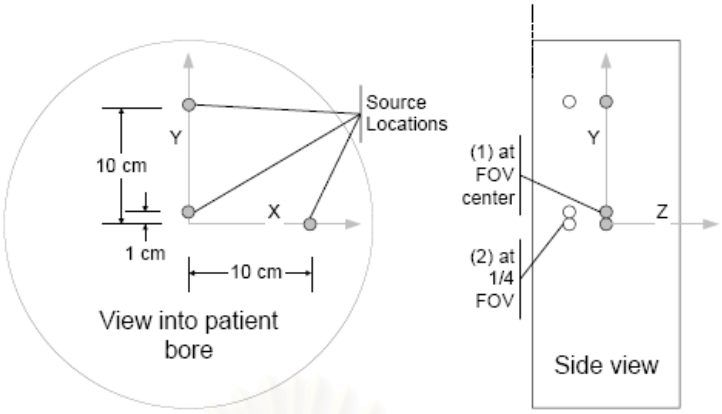

Figure VI Positions of source for resolution measurement

B. Scatter fraction

The purpose of this procedure is to measure the relative system sensitivity to scattered radiation.

Method

The phantom in this measurement comprises a 20-cm-diameter solid polyethylene cylinder with an overall length of 70 cm. The data for the measurement of intrinsic scatter fraction are taken from the low activity scans of the measurement of counting rate performance, when the count loss and randoms rates are both <1% of the true rate. Activity is placed in a line source that is threaded through a hole in the cylinder at a radius of 4.5 cm and parallel to the central axis. For consistency, the phantom is rotated such that the line source is at the lowest position, because the measured result will depend on the relative orientation of the line source and the bed.

C. Sensitivity

The purpose of this procedure is to measure the sensitivity or ability of the scanner to detect positrons.

Method

A 70-cm-long plastic tube is filled with a radioactivity, sufficiently low that count losses and randoms are negligible. The tubing is encased in metal sleeves of varying thickness and imaged, suspended in the center of the transverse FOV. Alternatively, the radioactivity can be placed in the smallest metal sleeve, as long as it is well sealed.

D. Image quality

The purpose of this measurement is to produce images simulating those obtained in a whole-body study with both hot and cold lesions. Spheres of different diameters are imaged in a simulated body phantom with non-uniform attenuation. Activity is also present outside the scanner.

Method

The phantom consists of a torso phantom, containing hot and cold spheres in a warm background. The hot spheres have inner diameters of 1.0, 1.3, 1.7, and 2.2 cm, the cold spheres have inner diameters of 2.8 and 3.7 cm. A 5-cm-diameter insert with an attenuation coefficient approximately equal to the average value in lung is also placed in the center of the phantom, and measured attenuation correction is performed. The background is filled with ^{18}F at an activity concentration typical of what is seen in patient FDG studies, 370 MBq/70-kg patient, or 5.3 kBq/mL. The hot spheres are sequentially filled with activity concentrations of 8 and 4 times that of the background, 2 sequential acquisitions. The line source of the 70-cm-long phantom is filled with sufficient activity to yield an effective activity concentration equal to that of the background in the torso phantom. The arrangement of radionuclide distribution is illustrated in figure V.

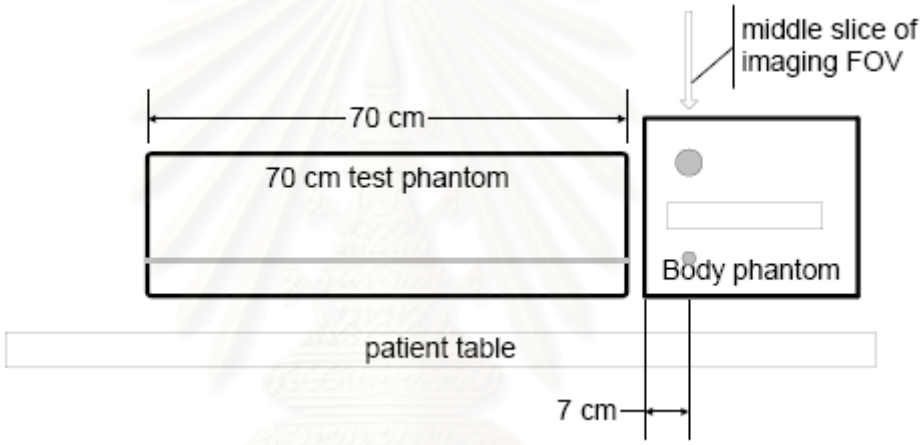

Figure VII The arrangement of radionuclide distribution

APPENDIX E

Table III. Specific absorbed fractions (per gram) for the adult male [25]

Source Organ	Target Organ	0.5 MeV
Adrenals	Breasts	2.90E-06
Adrenals	Stomach	1.10E-05
Adrenals	Upper Large Intestine Wall	4.30E-06
Adrenals	Kidneys	3.30E-05
Adrenals	Liver	1.90E-05
Adrenals	Lungs	1.10E-05
Adrenals	Red Marrow	1.20E-05
Adrenals	Bone Surfaces	6.70E-06
Adrenals	Skin	2.00E-06
Adrenals	Spleen	2.00E-05
Adrenals	Testes	2.00E-07
Adrenals	Thyroid	5.60E-07
Adrenals	Urinary Bladder Wall	6.50E-07
Adrenals	Total Body	6.10E-06
Brain	Breasts	2.50E-07
Brain	Stomach	5.70E-08
Brain	Upper Large Intestine Wall	1.30E-08
Brain	Kidneys	3.00E-08
Brain	Liver	1.10E-07
Brain	Lungs	6.10E-07
Brain	Red Marrow	4.40E-06
Brain	Bone Surfaces	7.60E-06
Brain	Skin	2.40E-06
Brain	Spleen	1.20E-07
Brain	Testes	9.90E-10
Brain	Thyroid	7.00E-06
Brain	Urinary Bladder Wall	2.80E-09
Brain	Total Body	4.10E-06
Breasts	Breasts	2.30E-04
Breasts	Stomach	3.30E-06
Breasts	Upper Large Intestine Wall	6.00E-07
Breasts	Kidneys	1.30E-06
Breasts	Liver	3.70E-06
Breasts	Lungs	1.10E-05
Breasts	Red Marrow	3.10E-06
Breasts	Bone Surfaces	2.20E-06
Breasts	Skin	4.20E-06
Breasts	Spleen	2.60E-06
Breasts	Testes	0.00E+00
Breasts	Thyroid	1.80E-06
Breasts	Urinary Bladder Wall	1.80E-07
Breasts	Total Body	3.60E-06
Gall Bladder Contents	Breasts	1.90E-06
Gall Bladder Contents	Stomach	1.20E-05
Gall Bladder Contents	Upper Large Intestine Wall	3.30E-05

Source Organ	Target Organ	0.5 MeV
Gall Bladder Contents	Kidneys	1.70E-05
Gall Bladder Contents	Liver	3.50E-05
Gall Bladder Contents	Lungs	3.10E-06
Gall Bladder Contents	Red Marrow	5.00E-06
Gall Bladder Contents	Bone Surfaces	2.50E-06
Gall Bladder Contents	Skin	1.70E-06
Gall Bladder Contents	Spleen	5.20E-06
Gall Bladder Contents	Testes	6.10E-07
Gall Bladder Contents	Thyroid	2.90E-07
Gall Bladder Contents	Urinary Bladder Wall	2.80E-06
Gall Bladder Contents	Total Body	5.80E-06
Lower Large Intestine Contents	Breasts	2.70E-07
Lower Large Intestine Contents	Stomach	5.90E-06
Lower Large Intestine Contents	Upper Large Intestine Wall	1.40E-05
Lower Large Intestine Contents	Kidneys	3.70E-06
Lower Large Intestine Contents	Liver	1.10E-06
Lower Large Intestine Contents	Lungs	4.00E-07
Lower Large Intestine Contents	Red Marrow	1.00E-05
Lower Large Intestine Contents	Bone Surfaces	4.20E-06
Lower Large Intestine Contents	Skin	1.90E-06
Lower Large Intestine Contents	Spleen	2.90E-06
Lower Large Intestine Contents	Testes	7.50E-06
Lower Large Intestine Contents	Thyroid	4.90E-08
Lower Large Intestine Contents	Urinary Bladder Wall	2.00E-05
Lower Large Intestine Contents	Total Body	5.70E-06
Small Intestine Contents	Breasts	6.00E-07
Small Intestine Contents	Stomach	9.60E-06
Small Intestine Contents	Upper Large Intestine Wall	6.10E-05
Small Intestine Contents	Kidneys	9.50E-06
Small Intestine Contents	Liver	5.30E-06
Small Intestine Contents	Lungs	8.80E-07
Small Intestine Contents	Red Marrow	8.30E-06
Small Intestine Contents	Bone Surfaces	3.30E-06
Small Intestine Contents	Skin	1.70E-06
Small Intestine Contents	Spleen	4.80E-06
Small Intestine Contents	Testes	1.60E-06
Small Intestine Contents	Thyroid	5.90E-08
Small Intestine Contents	Urinary Bladder Wall	9.10E-06
Small Intestine Contents	Total Body	5.80E-06
Stomach Contents	Breasts	3.10E-06
Stomach Contents	Stomach	1.80E-04
Stomach Contents	Upper Large Intestine Wall	1.10E-05
Stomach Contents	Kidneys	1.10E-05
Stomach Contents	Liver	6.60E-06
Stomach Contents	Lungs	5.00E-06
Stomach Contents	Red Marrow	4.00E-06
Stomach Contents	Bone Surfaces	2.40E-06
Stomach Contents	Skin	2.00E-06
Stomach Contents	Spleen	3.30E-05

Source Organ	Target Organ	0.5 MeV
Stomach Contents	Testes	3.60E-07
Stomach Contents	Thyroid	3.00E-07
Stomach Contents	Urinary Bladder Wall	1.30E-06
Stomach Contents	Total Body	4.80E-06
Upper Large Intestine Contents	Breasts	7.10E-07
Upper Large Intestine Contents	Stomach	1.30E-05
Upper Large Intestine Contents	Upper Large Intestine Wall	1.50E-04
Upper Large Intestine Contents	Kidneys	9.30E-06
Upper Large Intestine Contents	Liver	8.60E-06
Upper Large Intestine Contents	Lungs	1.10E-06
Upper Large Intestine Contents	Red Marrow	7.10E-06
Upper Large Intestine Contents	Bone Surfaces	2.90E-06
Upper Large Intestine Contents	Skin	1.70E-06
Upper Large Intestine Contents	Spleen	4.40E-06
Upper Large Intestine Contents	Testes	1.30E-06
Upper Large Intestine Contents	Thyroid	1.20E-07
Upper Large Intestine Contents	Urinary Bladder Wall	7.40E-06
Upper Large Intestine Contents	Total Body	5.60E-06
Heart Contents	Breasts	1.20E-05
Heart Contents	Stomach	7.30E-06
Heart Contents	Upper Large Intestine Wall	1.30E-06
Heart Contents	Kidneys	3.40E-06
Heart Contents	Liver	9.20E-06
Heart Contents	Lungs	2.00E-05
Heart Contents	Red Marrow	5.60E-06
Heart Contents	Bone Surfaces	3.70E-06
Heart Contents	Skin	2.00E-06
Heart Contents	Spleen	5.10E-06
Heart Contents	Testes	8.70E-08
Heart Contents	Thyroid	2.30E-06
Heart Contents	Urinary Bladder Wall	2.50E-07
Heart Contents	Total Body	4.60E-06
Heart Wall	Breasts	1.30E-05
Heart Wall	Stomach	1.10E-05
Heart Wall	Upper Large Intestine Wall	1.50E-06
Heart Wall	Kidneys	3.70E-06
Heart Wall	Liver	1.00E-05
Heart Wall	Lungs	1.90E-05
Heart Wall	Red Marrow	5.60E-06
Heart Wall	Bone Surfaces	3.70E-06
Heart Wall	Skin	2.00E-06
Heart Wall	Spleen	7.00E-06
Heart Wall	Testes	9.90E-08
Heart Wall	Thyroid	2.30E-06
Heart Wall	Urinary Bladder Wall	1.70E-07
Heart Wall	Total Body	5.90E-06
Kidneys	Breasts	1.30E-06
Kidneys	Stomach	1.10E-05
Kidneys	Upper Large Intestine Wall	9.30E-06

Source Organ	Target Organ	0.5 MeV
Kidneys	Kidneys	2.50E-04
Kidneys	Liver	1.30E-05
Kidneys	Lungs	3.20E-06
Kidneys	Red Marrow	8.50E-06
Kidneys	Bone Surfaces	3.90E-06
Kidneys	Skin	2.30E-06
Kidneys	Spleen	3.00E-05
Kidneys	Testes	3.70E-07
Kidneys	Thyroid	3.70E-07
Kidneys	Urinary Bladder Wall	1.30E-06
Kidneys	Total Body	5.70E-06
Liver	Breasts	3.70E-06
Liver	Stomach	7.00E-06
Liver	Upper Large Intestine Wall	8.30E-06
Liver	Kidneys	1.30E-05
Liver	Liver	8.70E-05
Liver	Lungs	8.70E-06
Liver	Red Marrow	4.40E-06
Liver	Bone Surfaces	3.00E-06
Liver	Skin	2.00E-06
Liver	Spleen	3.50E-06
Liver	Testes	2.00E-07
Liver	Thyroid	6.10E-07
Liver	Urinary Bladder Wall	9.00E-07
Liver	Total Body	5.70E-06
Lungs	Breasts	1.10E-05
Lungs	Stomach	5.20E-06
Lungs	Upper Large Intestine Wall	1.10E-06
Lungs	Kidneys	3.20E-06
Lungs	Liver	8.70E-06
Lungs	Lungs	5.20E-05
Lungs	Red Marrow	5.60E-06
Lungs	Bone Surfaces	4.20E-06
Lungs	Skin	2.20E-06
Lungs	Spleen	7.20E-06
Lungs	Testes	6.40E-08
Lungs	Thyroid	4.20E-06
Lungs	Urinary Bladder Wall	1.70E-07
Lungs	Total Body	4.90E-06
Muscle	Breasts	2.30E-06
Muscle	Stomach	5.10E-06
Muscle	Upper Large Intestine Wall	5.00E-06
Muscle	Kidneys	4.70E-06
Muscle	Liver	3.60E-06
Muscle	Lungs	4.30E-06
Muscle	Red Marrow	4.50E-06
Muscle	Bone Surfaces	4.60E-06
Muscle	Skin	3.20E-06
Muscle	Spleen	4.90E-06

Source Organ	Target Organ	0.5 MeV
Muscle	Testes	5.00E-06
Muscle	Thyroid	5.50E-06
Muscle	Urinary Bladder Wall	6.40E-06
Muscle	Total Body	4.80E-06
Pancreas	Breasts	3.30E-06
Pancreas	Stomach	5.50E-05
Pancreas	Upper Large Intestine Wall	6.90E-06
Pancreas	Kidneys	2.30E-05
Pancreas	Liver	1.60E-05
Pancreas	Lungs	7.80E-06
Pancreas	Red Marrow	7.30E-06
Pancreas	Bone Surfaces	4.00E-06
Pancreas	Skin	1.70E-06
Pancreas	Spleen	5.80E-05
Pancreas	Testes	2.90E-07
Pancreas	Thyroid	5.60E-07
Pancreas	Urinary Bladder Wall	1.00E-06
Pancreas	Total Body	6.60E-06
Active Marrow	Breasts	3.10E-06
Active Marrow	Stomach	4.00E-06
Active Marrow	Upper Large Intestine Wall	7.00E-06
Active Marrow	Kidneys	8.50E-06
Active Marrow	Liver	4.40E-06
Active Marrow	Lungs	5.60E-06
Active Marrow	Red Marrow	2.30E-05
Active Marrow	Bone Surfaces	1.20E-05
Active Marrow	Skin	2.50E-06
Active Marrow	Spleen	4.60E-06
Active Marrow	Testes	1.70E-06
Active Marrow	Thyroid	3.90E-06
Active Marrow	Urinary Bladder Wall	4.10E-06
Active Marrow	Total Body	5.30E-06
Trabecular Bone	Breasts	1.90E-06
Trabecular Bone	Stomach	2.00E-06
Trabecular Bone	Upper Large Intestine Wall	2.40E-06
Trabecular Bone	Kidneys	3.20E-06
Trabecular Bone	Liver	2.50E-06
Trabecular Bone	Lungs	3.50E-06
Trabecular Bone	Red Marrow	1.00E-05
Trabecular Bone	Bone Surfaces	1.40E-05
Trabecular Bone	Skin	3.00E-06
Trabecular Bone	Spleen	2.50E-06
Trabecular Bone	Testes	2.20E-06
Trabecular Bone	Thyroid	4.00E-06
Trabecular Bone	Urinary Bladder Wall	2.00E-06
Trabecular Bone	Total Body	4.80E-06
Cortical Bone	Breasts	1.90E-06
Cortical Bone	Stomach	2.00E-06
Cortical Bone	Kidneys	3.20E-06

Source Organ	Target Organ	0.5 MeV
Cortical Bone	Liver	2.50E-06
Cortical Bone	Lungs	3.50E-06
Cortical Bone	Red Marrow	1.00E-05
Cortical Bone	Bone Surfaces	1.40E-05
Cortical Bone	Skin	3.00E-06
Cortical Bone	Spleen	2.50E-06
Cortical Bone	Testes	2.20E-06
Cortical Bone	Thyroid	4.00E-06
Cortical Bone	Urinary Bladder Wall	2.00E-06
Cortical Bone	Total Body	4.80E-06
Spleen	Breasts	2.60E-06
Spleen	Stomach	3.20E-05
Spleen	Upper Large Intestine Wall	4.40E-06
Spleen	Kidneys	3.00E-05
Spleen	Liver	3.50E-06
Spleen	Lungs	7.20E-06
Spleen	Red Marrow	4.60E-06
Spleen	Bone Surfaces	3.00E-06
Spleen	Skin	2.10E-06
Spleen	Spleen	4.50E-04
Spleen	Testes	2.50E-07
Spleen	Thyroid	5.50E-07
Spleen	Urinary Bladder Wall	7.50E-07
Spleen	Total Body	5.70E-06
Testes	Breasts	0.00E+00
Testes	Stomach	4.10E-07
Testes	Upper Large Intestine Wall	1.20E-06
Testes	Kidneys	3.70E-07
Testes	Liver	2.00E-07
Testes	Lungs	6.40E-08
Testes	Red Marrow	1.70E-06
Testes	Bone Surfaces	2.60E-06
Testes	Skin	5.50E-06
Testes	Spleen	2.50E-07
Testes	Testes	1.20E-03
Testes	Thyroid	8.90E-09
Testes	Urinary Bladder Wall	1.60E-05
Testes	Total Body	4.80E-06
Thymus	Breasts	1.40E-05
Thymus	Stomach	2.30E-06
Thymus	Upper Large Intestine Wall	5.70E-07
Thymus	Kidneys	1.20E-06
Thymus	Liver	2.90E-06
Thymus	Lungs	1.30E-05
Thymus	Red Marrow	4.20E-06
Thymus	Bone Surfaces	3.00E-06
Thymus	Skin	2.60E-06
Thymus	Spleen	1.70E-06
Thymus	Testes	4.20E-08

Source Organ	Target Organ	0.5 MeV
Thymus	Thyroid	7.00E-06
Thymus	Urinary Bladder Wall	1.20E-07
Thymus	Total Body	5.20E-06
Thyroid	Breasts	1.80E-06
Thyroid	Stomach	4.00E-07
Thyroid	Upper Large Intestine Wall	1.20E-07
Thyroid	Kidneys	3.70E-07
Thyroid	Liver	6.10E-07
Thyroid	Lungs	4.20E-06
Thyroid	Red Marrow	3.90E-06
Thyroid	Bone Surfaces	4.80E-06
Thyroid	Skin	2.40E-06
Thyroid	Spleen	5.50E-07
Thyroid	Testes	8.90E-09
Thyroid	Thyroid	1.70E-03
Thyroid	Urinary Bladder Wall	2.50E-08
Thyroid	Total Body	5.20E-06
Urinary Bladder Contents	Breasts	1.40E-07
Urinary Bladder Contents	Stomach	1.20E-06
Urinary Bladder Contents	Upper Large Intestine Wall	6.90E-06
Urinary Bladder Contents	Kidneys	1.40E-06
Urinary Bladder Contents	Liver	8.50E-07
Urinary Bladder Contents	Lungs	1.20E-07
Urinary Bladder Contents	Red Marrow	3.90E-06
Urinary Bladder Contents	Bone Surfaces	2.30E-06
Urinary Bladder Contents	Skin	2.10E-06
Urinary Bladder Contents	Spleen	8.00E-07
Urinary Bladder Contents	Testes	1.60E-05
Urinary Bladder Contents	Thyroid	2.50E-08
Urinary Bladder Contents	Urinary Bladder Wall	2.50E-04
Urinary Bladder Contents	Total Body	5.10E-06
Total Body	Breasts	3.60E-06
Total Body	Stomach	6.00E-06
Total Body	Upper Large Intestine Wall	6.40E-06
Total Body	Kidneys	5.70E-06
Total Body	Liver	5.70E-06
Total Body	Lungs	4.90E-06
Total Body	Red Marrow	5.40E-06
Total Body	Bone Surfaces	5.80E-06
Total Body	Skin	3.20E-06
Total Body	Spleen	5.70E-06
Total Body	Testes	4.80E-06
Total Body	Thyroid	5.20E-06
Total Body	Urinary Bladder Wall	6.30E-06
Total Body	Total Body	4.80E-06

Table IV. Specific absorbed fractions (per gram) for the adult female [25]

Source organ	Target Organ	0.5 MeV
Adrenals	Breasts	3.36E-06
Adrenals	Stomach	1.42E-05
Adrenals	Upper Large Intestine Wall	5.71E-06
Adrenals	Kidneys	4.42E-05
Adrenals	Liver	2.33E-05
Adrenals	Lungs	1.35E-05
Adrenals	Red Marrow	1.37E-05
Adrenals	Bone Surfaces	8.76E-06
Adrenals	Skin	2.37E-06
Adrenals	Spleen	2.78E-05
Adrenals	Thyroid	8.12E-07
Adrenals	Urinary Bladder Wall	9.32E-07
Adrenals	Ovaries	2.13E-06
Adrenals	Total Body	7.78E-06
Brain	Breasts	3.39E-07
Brain	Stomach	9.00E-08
Brain	Upper Large Intestine Wall	2.23E-08
Brain	Kidneys	5.29E-08
Brain	Liver	1.40E-07
Brain	Lungs	6.28E-07
Brain	Red Marrow	6.28E-06
Brain	Bone Surfaces	9.69E-06
Brain	Skin	2.82E-06
Brain	Spleen	1.27E-07
Brain	Thyroid	3.67E-06
Brain	Urinary Bladder Wall	4.82E-09
Brain	Ovaries	9.42E-09
Brain	Total Body	4.79E-06
Breasts	Breasts	2.24E-04
Breasts	Stomach	4.39E-06
Breasts	Upper Large Intestine Wall	9.87E-07
Breasts	Kidneys	1.59E-06
Breasts	Liver	4.59E-06
Breasts	Lungs	1.26E-05
Breasts	Red Marrow	3.31E-06
Breasts	Bone Surfaces	2.83E-06
Breasts	Skin	4.99E-06
Breasts	Spleen	2.86E-06
Breasts	Thyroid	2.43E-06
Breasts	Urinary Bladder Wall	2.83E-07
Breasts	Ovaries	4.08E-07
Breasts	Total Body	4.47E-06
Gall Bladder Contents	Breasts	2.40E-06
Gall Bladder Contents	Stomach	1.78E-05
Gall Bladder Contents	Upper Large Intestine Wall	4.02E-05
Gall Bladder Contents	Kidneys	1.90E-05
Gall Bladder Contents	Liver	4.36E-05

Source organ	Target Organ	0.5 MeV
Gall Bladder Contents	Lungs	4.41E-06
Gall Bladder Contents	Red Marrow	5.46E-06
Gall Bladder Contents	Bone Surfaces	3.22E-06
Gall Bladder Contents	Skin	2.08E-06
Gall Bladder Contents	Spleen	8.01E-06
Gall Bladder Contents	Thyroid	4.65E-07
Gall Bladder Contents	Urinary Bladder Wall	3.08E-06
Gall Bladder Contents	Ovaries	7.68E-06
Gall Bladder Contents	Total Body	7.07E-06
Lower Large Intestine Contents	Breasts	3.80E-07
Lower Large Intestine Contents	Stomach	7.19E-06
Lower Large Intestine Contents	Upper Large Intestine Wall	1.77E-05
Lower Large Intestine Contents	Kidneys	4.24E-06
Lower Large Intestine Contents	Liver	1.62E-06
Lower Large Intestine Contents	Lungs	5.36E-07
Lower Large Intestine Contents	Red Marrow	1.22E-05
Lower Large Intestine Contents	Bone Surfaces	5.36E-06
Lower Large Intestine Contents	Skin	2.31E-06
Lower Large Intestine Contents	Spleen	3.42E-06
Lower Large Intestine Contents	Thyroid	8.79E-08
Lower Large Intestine Contents	Urinary Bladder Wall	2.32E-05
Lower Large Intestine Contents	Ovaries	8.01E-05
Lower Large Intestine Contents	Total Body	7.04E-06
Small Intestine Contents	Breasts	8.63E-07
Small Intestine Contents	Stomach	1.16E-05
Small Intestine Contents	Upper Large Intestine Wall	7.41E-05
Small Intestine Contents	Kidneys	1.24E-05
Small Intestine Contents	Liver	6.62E-06
Small Intestine Contents	Lungs	1.22E-06
Small Intestine Contents	Red Marrow	1.00E-05
Small Intestine Contents	Bone Surfaces	4.15E-06
Small Intestine Contents	Skin	2.10E-06
Small Intestine Contents	Spleen	6.48E-06
Small Intestine Contents	Thyroid	1.18E-07
Small Intestine Contents	Urinary Bladder Wall	1.21E-05
Small Intestine Contents	Ovaries	4.83E-05
Small Intestine Contents	Total Body	6.91E-06
Stomach Contents	Breasts	4.12E-06
Stomach Contents	Stomach	2.20E-04
Stomach Contents	Upper Large Intestine Wall	1.48E-05
Stomach Contents	Kidneys	1.28E-05
Stomach Contents	Liver	9.45E-06
Stomach Contents	Lungs	6.91E-06
Stomach Contents	Red Marrow	4.29E-06
Stomach Contents	Bone Surfaces	3.32E-06
Stomach Contents	Skin	2.47E-06
Stomach Contents	Spleen	3.45E-05
Stomach Contents	Thyroid	5.73E-07
Stomach Contents	Urinary Bladder Wall	1.70E-06

Source organ	Target Organ	0.5 MeV
Stomach Contents	Ovaries	3.80E-06
Stomach Contents	Total Body	6.08E-06
Upper Large Intestine Contents	Breasts	8.88E-07
Upper Large Intestine Contents	Stomach	1.68E-05
Upper Large Intestine Contents	Upper Large Intestine Wall	1.82E-04
Upper Large Intestine Contents	Kidneys	1.11E-05
Upper Large Intestine Contents	Liver	1.10E-05
Upper Large Intestine Contents	Lungs	1.66E-06
Upper Large Intestine Contents	Red Marrow	8.14E-06
Upper Large Intestine Contents	Bone Surfaces	3.67E-06
Upper Large Intestine Contents	Skin	2.15E-06
Upper Large Intestine Contents	Spleen	5.88E-06
Upper Large Intestine Contents	Thyroid	1.97E-07
Upper Large Intestine Contents	Urinary Bladder Wall	9.37E-06
Upper Large Intestine Contents	Ovaries	4.10E-05
Upper Large Intestine Contents	Total Body	6.83E-06
Heart Contents	Breasts	1.51E-05
Heart Contents	Stomach	1.02E-05
Heart Contents	Upper Large Intestine Wall	1.90E-06
Heart Contents	Kidneys	4.50E-06
Heart Contents	Liver	1.27E-05
Heart Contents	Lungs	2.59E-05
Heart Contents	Red Marrow	5.51E-06
Heart Contents	Bone Surfaces	4.49E-06
Heart Contents	Skin	2.45E-06
Heart Contents	Spleen	6.82E-06
Heart Contents	Thyroid	3.13E-06
Heart Contents	Urinary Bladder Wall	4.61E-07
Heart Contents	Ovaries	7.09E-07
Heart Contents	Total Body	5.90E-06
Heart Wall	Breasts	1.75E-05
Heart Wall	Stomach	1.56E-05
Heart Wall	Upper Large Intestine Wall	2.07E-06
Heart Wall	Kidneys	4.73E-06
Heart Wall	Liver	1.37E-05
Heart Wall	Lungs	2.48E-05
Heart Wall	Red Marrow	5.30E-06
Heart Wall	Bone Surfaces	4.33E-06
Heart Wall	Skin	2.56E-06
Heart Wall	Spleen	8.80E-06
Heart Wall	Thyroid	2.82E-06
Heart Wall	Urinary Bladder Wall	4.62E-07
Heart Wall	Ovaries	8.72E-07
Heart Wall	Total Body	6.52E-06
Kidneys	Breasts	1.59E-06
Kidneys	Stomach	1.19E-05
Kidneys	Upper Large Intestine Wall	1.13E-05
Kidneys	Kidneys	2.67E-04
Kidneys	Liver	1.55E-05

Source organ	Target Organ	0.5 MeV
Kidneys	Lungs	4.58E-06
Kidneys	Red Marrow	9.87E-06
Kidneys	Bone Surfaces	5.34E-06
Kidneys	Skin	2.64E-06
Kidneys	Spleen	3.66E-05
Kidneys	Thyroid	3.20E-07
Kidneys	Urinary Bladder Wall	1.83E-06
Kidneys	Ovaries	4.89E-06
Kidneys	Total Body	7.11E-06
Liver	Breasts	4.59E-06
Liver	Stomach	9.67E-06
Liver	Upper Large Intestine Wall	1.04E-05
Liver	Kidneys	1.55E-05
Liver	Liver	1.07E-04
Liver	Lungs	1.19E-05
Liver	Red Marrow	4.89E-06
Liver	Bone Surfaces	4.10E-06
Liver	Skin	2.53E-06
Liver	Spleen	5.22E-06
Liver	Thyroid	8.78E-07
Liver	Urinary Bladder Wall	1.34E-06
Liver	Ovaries	2.74E-06
Liver	Total Body	7.09E-06
Lungs	Breasts	1.26E-05
Lungs	Stomach	7.30E-06
Lungs	Upper Large Intestine Wall	1.49E-06
Lungs	Kidneys	4.58E-06
Lungs	Liver	1.19E-05
Lungs	Lungs	6.98E-05
Lungs	Red Marrow	6.25E-06
Lungs	Bone Surfaces	5.40E-06
Lungs	Skin	2.82E-06
Lungs	Spleen	9.93E-06
Lungs	Thyroid	5.23E-06
Lungs	Urinary Bladder Wall	3.17E-07
Lungs	Ovaries	6.13E-07
Lungs	Total Body	6.29E-06
Muscle	Breasts	2.91E-06
Muscle	Stomach	6.26E-06
Muscle	Upper Large Intestine Wall	5.68E-06
Muscle	Kidneys	5.82E-06
Muscle	Liver	4.58E-06
Muscle	Lungs	5.70E-06
Muscle	Red Marrow	5.56E-06
Muscle	Bone Surfaces	5.63E-06
Muscle	Skin	3.79E-06
Muscle	Spleen	6.20E-06
Muscle	Thyroid	5.62E-06
Muscle	Urinary Bladder Wall	6.80E-06

Source organ	Target Organ	0.5 MeV
Muscle	Ovaries	7.88E-06
Muscle	Total Body	5.10E-06
Ovaries	Breasts	4.08E-07
Ovaries	Stomach	4.32E-06
Ovaries	Upper Large Intestine Wall	4.57E-05
Ovaries	Kidneys	4.89E-06
Ovaries	Liver	2.50E-06
Ovaries	Lungs	6.10E-07
Ovaries	Red Marrow	1.17E-05
Ovaries	Bone Surfaces	4.72E-06
Ovaries	Skin	2.07E-06
Ovaries	Spleen	2.79E-06
Ovaries	Thyroid	6.37E-08
Ovaries	Urinary Bladder Wall	3.07E-05
Ovaries	Ovaries	2.16E-03
Ovaries	Total Body	7.93E-06
Pancreas	Breasts	3.98E-06
Pancreas	Stomach	6.64E-05
Pancreas	Upper Large Intestine Wall	8.91E-06
Pancreas	Kidneys	2.63E-05
Pancreas	Liver	2.04E-05
Pancreas	Lungs	1.02E-05
Pancreas	Red Marrow	7.30E-06
Pancreas	Bone Surfaces	4.86E-06
Pancreas	Skin	2.03E-06
Pancreas	Spleen	6.81E-05
Pancreas	Thyroid	6.99E-07
Pancreas	Urinary Bladder Wall	1.35E-06
Pancreas	Ovaries	3.41E-06
Pancreas	Total Body	8.21E-06
Active Marrow	Breasts	3.31E-06
Active Marrow	Stomach	4.43E-06
Active Marrow	Upper Large Intestine Wall	7.78E-06
Active Marrow	Kidneys	9.87E-06
Active Marrow	Liver	4.89E-06
Active Marrow	Lungs	6.25E-06
Active Marrow	Red Marrow	2.59E-05
Active Marrow	Bone Surfaces	1.50E-05
Active Marrow	Skin	3.02E-06
Active Marrow	Spleen	5.20E-06
Active Marrow	Thyroid	4.65E-06
Active Marrow	Urinary Bladder Wall	5.28E-06
Active Marrow	Ovaries	1.17E-05
Active Marrow	Total Body	6.52E-06
Trabecular Bone	Breasts	2.15E-06
Trabecular Bone	Stomach	2.59E-06
Trabecular Bone	Upper Large Intestine Wall	2.93E-06
Trabecular Bone	Kidneys	4.26E-06
Trabecular Bone	Liver	3.21E-06

Source organ	Target Organ	0.5 MeV
Trabecular Bone	Lungs	4.41E-06
Trabecular Bone	Red Marrow	1.26E-05
Trabecular Bone	Bone Surfaces	1.65E-05
Trabecular Bone	Skin	3.55E-06
Trabecular Bone	Spleen	3.18E-06
Trabecular Bone	Thyroid	4.67E-06
Trabecular Bone	Urinary Bladder Wall	2.41E-06
Trabecular Bone	Ovaries	3.86E-06
Trabecular Bone	Total Body	5.82E-06
Cortical Bone	Breasts	2.15E-06
Cortical Bone	Stomach	2.59E-06
Cortical Bone	Upper Large Intestine Wall	2.93E-06
Cortical Bone	Kidneys	4.26E-06
Cortical Bone	Liver	3.21E-06
Cortical Bone	Lungs	4.41E-06
Cortical Bone	Red Marrow	1.26E-05
Cortical Bone	Bone Surfaces	1.65E-05
Cortical Bone	Skin	3.55E-06
Cortical Bone	Spleen	3.18E-06
Cortical Bone	Thyroid	4.67E-06
Cortical Bone	Urinary Bladder Wall	2.41E-06
Cortical Bone	Ovaries	3.86E-06
Cortical Bone	Total Body	5.82E-06
Spleen	Breasts	2.86E-06
Spleen	Stomach	3.72E-05
Spleen	Upper Large Intestine Wall	6.08E-06
Spleen	Kidneys	3.66E-05
Spleen	Liver	5.22E-06
Spleen	Lungs	9.93E-06
Spleen	Red Marrow	5.20E-06
Spleen	Bone Surfaces	4.15E-06
Spleen	Skin	2.45E-06
Spleen	Spleen	5.16E-04
Spleen	Thyroid	7.74E-07
Spleen	Urinary Bladder Wall	1.16E-06
Spleen	Ovaries	2.79E-06
Spleen	Total Body	7.27E-06
Thymus	Breasts	1.55E-05
Thymus	Stomach	2.85E-06
Thymus	Upper Large Intestine Wall	7.35E-07
Thymus	Kidneys	1.42E-06
Thymus	Liver	3.80E-06
Thymus	Lungs	1.55E-05
Thymus	Red Marrow	4.53E-06
Thymus	Bone Surfaces	3.93E-06
Thymus	Skin	3.21E-06
Thymus	Spleen	2.28E-06
Thymus	Thyroid	1.05E-05
Thymus	Urinary Bladder Wall	1.91E-07

Source organ	Target Organ	0.5 MeV
Thymus	Ovaries	3.38E-07
Thymus	Total Body	6.38E-06
Thyroid	Breasts	2.43E-06
Thyroid	Stomach	6.51E-07
Thyroid	Upper Large Intestine Wall	1.94E-07
Thyroid	Kidneys	3.20E-07
Thyroid	Liver	8.78E-07
Thyroid	Lungs	5.23E-06
Thyroid	Red Marrow	4.65E-06
Thyroid	Bone Surfaces	6.01E-06
Thyroid	Skin	5.54E-06
Thyroid	Spleen	7.74E-07
Thyroid	Thyroid	1.97E-03
Thyroid	Urinary Bladder Wall	4.59E-08
Thyroid	Ovaries	8.35E-08
Thyroid	Total Body	5.68E-06
Urinary Bladder Contents	Breasts	2.78E-07
Urinary Bladder Contents	Stomach	1.48E-06
Urinary Bladder Contents	Upper Large Intestine Wall	9.72E-06
Urinary Bladder Contents	Kidneys	1.88E-06
Urinary Bladder Contents	Liver	1.09E-06
Urinary Bladder Contents	Lungs	3.04E-07
Urinary Bladder Contents	Red Marrow	5.28E-06
Urinary Bladder Contents	Bone Surfaces	2.96E-06
Urinary Bladder Contents	Skin	2.52E-06
Urinary Bladder Contents	Spleen	1.19E-06
Urinary Bladder Contents	Thyroid	4.53E-08
Urinary Bladder Contents	Urinary Bladder Wall	4.03E-04
Urinary Bladder Contents	Ovaries	6.06E-05
Urinary Bladder Contents	Total Body	6.38E-06
Uterus	Breasts	3.98E-07
Uterus	Stomach	3.35E-06
Uterus	Upper Large Intestine Wall	2.21E-05
Uterus	Kidneys	3.83E-06
Uterus	Liver	2.74E-06
Uterus	Lungs	5.40E-07
Uterus	Red Marrow	8.27E-06
Uterus	Bone Surfaces	3.52E-06
Uterus	Skin	2.22E-06
Uterus	Spleen	2.45E-06
Uterus	Thyroid	8.35E-08
Uterus	Urinary Bladder Wall	6.53E-05
Uterus	Ovaries	8.64E-05
Uterus	Total Body	8.12E-06
Total Body	Breasts	4.50E-06
Total Body	Stomach	7.34E-06
Total Body	Upper Large Intestine Wall	7.87E-06
Total Body	Kidneys	6.98E-06
Total Body	Liver	7.08E-06

Source organ	Target Organ	0.5 MeV
Total Body	Lungs	6.30E-06
Total Body	Red Marrow	6.68E-06
Total Body	Bone Surfaces	7.03E-06
Total Body	Skin	3.80E-06
Total Body	Spleen	7.09E-06
Total Body	Thyroid	5.65E-06
Total Body	Urinary Bladder Wall	5.88E-06
Total Body	Ovaries	7.97E-06
Total Body	Total Body	5.82E-06

VITAE

NAME	Mr.Kitiwat Khamwan
SEX	Male
NATIONALITY	Thai
DATE OF BIRTH	15 December 1980
PLACE OF BIRTH	Nakhonpanom, Thailand
INSTITUTIONS ATTENDED	Naresuan University, 2003: Bachelor of Science (Radiological Technology) Chulalongkorn University, 2008: Master of Science (Medical Imaging)
POSITION HELD & OFFICE	Radiological Technologist, 2003 to present Department of Radiology Saint Louis Hospital, Bangkok, Thailand 10120
HOME ADDRESS	94 Moo 3, T. Koksawang, A. Plapak, Nakhonpanom, Thailand 48160